UNIVERSITY OF CRETE

Department of Medicine

Laboratory of Basic Sciences

and

INSTITUTE OF MOLECULAR BIOLOGY AND BIOTECHNOLOGY

–

FOUNDATION OF RESEARCH AND TECHNOLOGY (IMBB - FoRTH)

Heraklion

January 2016

PhD thesis

"Investigation of the role of the glial isoform of TAG-1 protein in the organization of mammalian myelinated fibers"

«Διερεύνηση του ρόλου της γλοιακής μορφής της πρωτεΐνης TAG-1 στην οργάνωση των εμμύελων ινών στα θηλαστικά»

Kastriti Maria-Eleni

ΠΑΝΕΠΙΣΤΗΜΙΟ ΚΡΗΤΗΣ

Τμήμα Ιατρικής

Εργαστήριο Βασικών Επιστημών

και

ΙΝΣΤΙΤΟΥΤΟ ΜΟΡΙΑΚΗΣ ΒΙΟΛΟΓΙΑΣ ΚΑΙ ΒΙΟΤΕΧΝΟΛΟΓΙΑΣ

–

ΙΔΡΥΜΑ ΤΕΧΝΟΛΟΓΙΑΣ ΚΑΙ ΕΡΕΥΝΑΣ

(IMBB - FoRTH)

Ηράκλειο

Ιανουάριος 2016

Διδακτορική Διατριβή

«Διερεύνηση του ρόλου της γλοιακής μορφής της πρωτεΐνης TAG-1 στην οργάνωση των εμμύελων ινών στα θηλαστικά»

Καστρίτη Μαρία-Ελένη

Ευχαριστίες

Αν και η συγκεκριμένη διατριβή είναι γραμμένη στα Αγγλικά, διάλεξα να απευθύνω την ευγνωμοσύνη μου στα Ελληνικά. Είμαι σίγουρη ότι η μικρή μου Giulia πλέον μπορεί να διαβάσει και να καταλάβει άψογα!

Λένε πώς για τους άντρες ο στρατός είναι το μέρος που ωριμάζουν και κάνουν διαχρονικές φιλίες. Λοιπόν, για κάθε υποψήφιο διδάκτορα θεωρώ πως ακριβώς το ίδιο είναι η «θητεία» του στο εργαστήριο. Και μιλάω για στιγμές τόσο εντός του «στρατοπέδου» όσο και στις εξόδους!

Θα ήθελα να απευθύνω το μεγαλύτερο ευχαριστώ στην καθηγήτρια μου, την κα Καραγωγέως, για τη συνεχή της παρουσία και στήριξη, καθώς και την εμπιστοσύνη που έδειξε στο πρόσωπό μου εξαρχής. Δε θα ξεχάσω ποτέ πόσες φορές παρέβλεψε αναποδιές και δυσκολίες και συνέχισε να με κινητοποιεί και να συμβάλλει συνεχώς στην βελτίωση μου ως επιστήμονα. Επίσης η στήριξή της πρακτικά κατά τη διάρκεια των τελευταίων μηνών (και όχι μόνο), οι οποίοι ήταν οι πιο δύσκολοι για τη πορεία του διδακτορικού αλλά και της επιλογής των μελλοντικών μου βημάτων, ήταν κρίσιμη.

Ένας ακόμη από τους ανθρώπους που με στήριξαν στη συγκεκριμένη εργασία είναι ο αγαπητός Δρ. Κλεόπας. Μαέστρο επί της Κύπρου σας ευχαριστώ για την στήριξη και τη βοήθεια κατά τη διάρκεια της συνεργασίας μας. Ακόμη θέλω να ευχαριστήσω την μαμά Ειρήνη και όλα τα κορίτσια του ορόφου. Ειδικά όμως την Αλεξία και την Νατάσα, θέλω να τις ευχαριστήσω που με απάλλαξαν από αρκετά εγκεφαλικά κύτταρα. Μια που τα έχω σε εξαιρετική περίσσεια, δυσκολεύουν πολλές φορές τη ζωή μου. Οι κοπελούες μου κατάλαβαν αμέσως ποια ήταν η ρίζα του προβλήματος και φρόντισαν με την κατάλληλη δόση γλυκανίσου να το αντιμετωπίσουν. Κάνει θαύματα ο γλυκάνισος!

Όσο για τα παιδιά στο εργαστήριο της καθ. Καραγωγέως, δε μπορώ να σκεφτώ κανέναν χωρίς να χαμογελάω. Μου φαίνεται αδιανόητο που πρέπει πλέον να φύγω, αλλά οι καθημερινές αναμνήσεις που έχω με όλους είναι ικανές να με κάνουν να συνεχίσω να μειδιάζω (Κώστα αυτό ήταν για σένα!). Ξεκινώντας από τον πρώην γείτονα στον πάγκο, ποτέ δεν φανταζόμουν πώς θα μπορούσε να είναι η μίξη Κρητικής διαλέκτου – επιστήμης, αλλά στο πρόσωπο του φανταστικού GGB είναι απολαυστικότατη!! Καλή σταδιοδρομία και ό,τι καλύτερο για την οικογένειά σου! Συνεχίζοντας στα γνήσια Κρητικά παιδιά, μικιό μου Κατερινάκι, είσαι ένα πλάσμα με ενδιαφέροντα και πολλά ταλέντα! Να τα αναπτύξεις όλα και να είσαι ευτυχισμένη όπου και να βρεθείς τελικά! Και φυσικά, αγαπητέ Κώστα, σίγουρα οι συζητήσεις μας γύρω από επιστημονικά (και μη) θέματα θα μου μείνουν αξέχαστες, όπως και οι πολλές συμβουλές που μου έδινες επί καθημερινής βάσεως. Μαρία μου, η σταθερή αξία του εργαστηρίου (φυσικά μαζί με τον Κώστα) και στήριγμα όλων! Το συνεχές σου ενδιαφέρον στη δουλειά είναι κίνητρο για όλους και είσαι από τα καλύτερα παιδιά!!! Μη ξεχνάς, Skype!!! Ειρηνάκι μου, αν και έχουμε συνεργαστεί λίγο καιρό, έχω χαρεί πολύ που σε συναναστράφηκα. Να μη το βάλεις κάτω και ελπίζω να βρεις σύντομα αυτό που θα ήθελες να κάνεις. Αγαπητέ Λιάκο, ψηλέ, θα μου λείψεις ρε… Ποιος θα τραγουδάει (δε λέω τι, ξέρεις εσύ) κάθε μέρα; Καλή συνέχεια στο διδακτορικό σου και πολλές επιτυχίες! Giuletάκι, να

είσαι πάντα χαμογελαστή και χαρούμενη!!! Και να αποκτήσεις ό,τι επιθυμείς στη ζωή σου! Δε περίμενα ποτέ ότι θα έχω όλη τη Κρητική κουζίνα και οινογνωσία συνδεδεμένη με μια Ιταλίδα στο μυαλό μου! Μικρές Νούμερο 2, Ζουζάνα και Κατερίνα, σας εύχομαι οι αναποδιές που έτυχαν τελευταία να μη σας αποκαρδιώσουν και να συνεχίσετε απτόητες!! Και ελπίζω να μου στέλνετε κάθε χρονιά φωτογραφίες από τις ευρηματικότατες στολές σας τις Απόκριες! Ληδάκι, ευελπιστώ ότι θα σε συναντήσω σύντομα κάπου στην Ευρώπη. Και μην ξεχνάμε ότι όταν γίνεις και γνωστή κιθαρίστας, πέρα από γνωστή επιστήμονας, θα έχω χαρτάκια με το γραφικό σου χαρακτήρα και θα κομπάζω ότι σε ξέρω. Πέρα από την βοήθειά σου στα επαγγελματικά, δε θα ξεχάσω και όσα έκανες για μένα εκτός εργαστηρίου. Γλυκιά μου Simona, είσαι από τους ανθρώπους που δε θα ξεχάσω ποτέ και νοιώθω απεριόριστα τυχερή που σε γνώρισα. Να είσαι πάντα ευτυχισμένη με το γλυκό σου κοριτσάκι και τον καλό σου! Γεωργία μου, αν και δε σε έβλεπα τόσο όσο τους άλλους στο εργαστήριο, κάναμε ουσιαστικές συζητήσεις και πριν έρθω Κρήτη και από ό,τι φαίνεται θα τις συνεχίσουμε στη Σουηδία! Ανυπομονώ να τα πούμε από κοντά. Παίδες, ολοκληρώνοντας την σκέψη μου, θα ήθελα να σας ευχαριστήσω για όλες τις στιγμές που μοιραστήκαμε, όλα τα lab meeting που βασανιζόσασταν για να με ακούσετε και ελπίζω να μη με ξεχάσετε πολύ γρήγορα.

Μία φανταστική γείτονάς μου στη δουλειά ήταν επίσης στήριγμα και φίλη τον τελευταίο καιρό. Ίσως να έπαιξε ρόλο βέβαια ότι στην προηγούμενή της ζωή ήταν αρκουδάκι… Ελενάκι μου σε ευχαριστώ πολύ για όσα μοιραστήκαμε και για την υπομονή μου έκανες μαζί μου. Με στήριξες σε μια πολύ δύσκολη περίοδο και πάντα με έκανες να το νοιώθω αυτό χωρίς πολλά λόγια και φρου φρου. Να είσαι πάντα το αισιόδοξο, τσαμπουκαλίδικο και τέρμα συναισθηματικό πλάσμα που ξέρω και να με θυμάσαι που και που!

Αν και είχα φανταστικούς συνεργάτες, πολλοί άνθρωποι με στήριξαν όλα αυτά τα χρόνια και εκτός εργαστηρίου. Είμαι τόσο τυχερή που ένα καταπληκτικό πλάσμα που γνώρισα στο πανεπιστήμιο είναι ακόμη δίπλα μου.. Χριστινάκι, σε ευχαριστώ για όλες τις φορές που ήρθες να με δεις, που μου σκούπισες τις μύξες μου, που προσπάθησες (πάντα με επιτυχία) να με κάνεις να χαμογελάσω και που πλέον με θεωρείς οικογένεια (ελπίζω). Και φυσικά η αγάπη μου για σένα επεκτείνεται και στον Γιώργο και στην γλυκιά μου Κλεονίκη. Θα είστε πάντα οι άνθρωποι που θεωρώ ως σταθερή αξία στη ζωή μου.

My dear Ruth, I am so lucky to have you as my flat mate, even if it was just for some months. I am wishing all the luck and happiness to you and Carlos and I am expecting to see you soon!

Μια αναπάντεχη έκπληξη τους τελευταίους μήνες ήταν τα γλυκά μου παιδιά Βάσω, Γιώργος και Κωστής (αλφαβητικά και όχι με αύξουσα σημαντικότητα, σας λατρεύω και τους τρεις). Χαίρομαι τόσο πολύ που οι συμπτώσεις και η τύχη με έφερε στο μαγαζί και που διασταυρώθηκαν οι δρόμοι μας. Θέλω λοιπόν να σας πω ένα τεράστιο ευχαριστώ που υπομείνατε τη γκρίνια μου, την κυκλοθυμία και τα ξεσπάσματά μου. Ελπίζω να σας προσέφερα και από την μεριά μου κάτι. Σας αγαπώ πολύ και ελπίζω να σας βλέπω συχνά από

εδώ και πέρα. Προφανώς σε γάμους, βαφτίσεις και λοιπά event περιμένω πρόσκληση (νωρίτερα και όχι μισή ώρα πριν όπως όταν βρισκόμασταν στο Ηράκλειο).

Τέλος, θα ήθελα να πω χίλια ευχαριστώ στους γλυκύτατους και υπομονετικούς γονείς μου, οι οποίοι με στηρίζουν ηθικά, συναισθηματικά και πρακτικά για τόσα πολλά χρόνια, που δυστυχώς μερικές στιγμές το θεωρούσα δεδομένο. Θέλω να σας πω ότι είμαι πάρα πολύ τυχερή που είστε εσείς οι γονείς μου και χωρίς εσάς δε θα είχα καταφέρει να επιτύχω κανέναν από τους στόχους μου. Σας αγαπώ πολύ και ας μη το δείχνω συνεχώς.

Table of Contents

ABSTRACT 10

ΠΕΡΙΛΗΨΗ 12

A. INTRODUCTION 14

A.1. The evolution and functional importance of myelination 14

A.2 Myelin origin and composition 15

A.3. OL origin and CNS myelination in the developing nervous system 16

A.4. OL plasticity and myelination during adulthood in the insulted CNS 20

A.5. The pathology of Multiple Sclerosis 22

A.6. Organization of subdomains of myelinated fibers 25

A.7. TAG-1 structure and functional importance in myelinated fibers 29

A.8. Disruption of perinodal domains in demyelination and MS 29

A.9. Experimental models of MS in mice 31

A.10. Goal of the study 33

B. MATERIALS AND METHODS I 34

B.1. Laboratory Animals 34

B.2 Genotyping 34

B.2.1 Genomic DNA extraction from tail pieces 35

B.2.2. Genotyping PCR 35

B.2.3. Agarose gel electrophoresis 37

B.3. Demyelinating Protocols 37

B.3.1. Focal injection of lysophosphatidylcholine or lysolecithin (LPC) 38

B.3.2. Induction of Experimental Autoimmune Encephalomyelitis (EAE) 39

B.4. Histological Methods 41

B.4.1. CNS tissue collection and preparation 41

B.4.1.1. Tissue fixation, dissection and isolation 41

B.4.1.2. Cryoprotection 41
B.4.1.3. Embedding, freezing and cryosectioning 42
B.4.2. Immunohistochemistry on cryosections derived from adult mice 42
B.5. Quantification of signal in immunohistochemical experiments 43
B.5.1. Quantification of demyelination 43
B.5.2. Quantification of autoimmune infiltrates 44
B.5.3. Quantification of axonal density 45
B.5.4. Quantification of axonal loss 45
B.5.5. Quantification of clustering 46
B.5.6. Quantification of oligodendrocyte precursor cells and mature oligodendrocytes 46
B.6. Fluorescence Activated Cell Sorting (FACS) 47
B.6.1. Isolation of mononuclear cells from total spinal cords 47
B.6.2. Fluorescent staining of isolated cells and sample analysis 48
B.7. Morphological stainings 48
B.7.1. Hematoxylin & Eosin (H&E) morphological stain 48
C. MATERIALS AND METHODS II 49
C.1. Human brain tissue samples 49
C.2. Characterization and classification of MS lesions 49
C.2.1. Neuropathological analysis of MS lesions 49
C.2.2. Classification of lesions 50
C.3. Analysis of mRNA 50
C.3.1. RNA extraction 51
C.3.2. Reverse transcription 52
C.3.3. Real-time PCR and analysis 54
C.4. Immunoblot analysis 55
C.4.1. Tissue lysis and sample preparation 55
C.4.2. Protein separation with SDS-polyacrylamide gel electrophoresis (SDS-PAGE) 56

C.4.3. Western Blotting 57

C.4.4. Immunoblotting 58

C.4.5. Quantification of results obtained by Western Blot 59

C.5. Immunohistochemistry on cryosections 59

C.5.1. Quantification of juxtaparanodal length and perinodal clustering 60

D. RESULTS I 62

D.1. Introduction of the *Tag-1-/-* genotype in the C57BL/6 background 62

D.1.1. Analysis of the *Tag-1-/-* juxtaparanodal phenotype in the C57BL/6 background 63

D.2. Characterization of the stages and clinical picture of MOG_{35-55}-induced Experimental Autoimmune Encephalomyelitis (EAE) 64

D.3. EAE induction on *Tag-1+/+* versus *Tag-1-/-* mice 69

D.3.1. Analysis of susceptibility and disease course and duration in the absence of TAG-1 69

D.3.2. Analysis of the profile of inflammatory infiltrates in the absence of TAG-1 72

D.4. Study of the role of TAG-1 in the demyelination and remyelination following LPC insult 75

E. RESULTS II 81

E.1. Analysis of the pattern of TAG-1+ juxtaparanodes 81

E.1.1.Analysis of the pattern of TAG-1+ juxtaparanodes in control white matter 81

E.1.2. Analysis of the localization of juxtaparanodal molecules in chronic Multiple Sclerosis normal appearing white matter 82

E.2. Analysis of the localization of juxtaparanodal molecules in perilesions and chronic Multiple Sclerosis plaques 86

E.3. Quantification of juxtaparanodal clustering in perilesions and MS NAWM 87

E.4. TAG-1 and Caspr2 diffusion in MS NAWM and chronic perilesions 89

E.5 Analysis of the protein levels of juxtaparanodal molecules in MS NAWM and chronic lesions 90

F. DISCUSSION I 95

F.1. Characterization of the juxtaparanodal *Tag-1-/-* phenotype in the C57BL/6 background 95

F.2. The EAE model 96

F.2.1. Study of neuropathology and tissue damage during EAE in wild type mice 96

F.2.2. Study of EAE in wild type versus *Tag-1-/-* mice 98

F.3. Study of LPC focal de- and remyelination in wild type versus *Tag-1-/-* mice 102

Outlook and Future Directions 105

G. DISCUSSION II 107

G.1. Juxtaparanodal changes in the chronic MS NAWM 107

G.2. Juxtaparanodal changes in the perilesions of chronic lesions 108

G.3. Disruption of voltage-gated potassium channel clustering and clinical significance for MS 111

G.4. Paranodal and juxtaparanodal molecules in the chronic lesion areas 111

Outlook and Future Directions 112

BIBLIOGRAPHY 115

APPENDIX 130

ABSTRACT

Myelinated fibers are divided in discrete subdomains around the Na_v-enriched nodes of Ranvier: the paranodes, where axoglial interactions occur, the juxtaparanodes, where voltage-gated potassium channels (VGKCs) are aggregated, and the internode. The integrity of these domains is crucial for the function of the axon and the propagation of axon potentials along its length. Perinodal changes have been reported in Multiple Sclerosis (MS) with functional consequences for the axon. TAG-1 (Transient Axonal Glycoprotein-1 or Contactin2 – Cntn2), both an axonal and glial protein, is also found enriched at juxtaparanodes and is responsible for the recruitment and maintenance of VGKC and Caspr2 at these sites, while it was also identified as an autoantigen in a subset of MS patients. Furthermore, the protein has been assigned with crucial roles in mediating processes such as migration, fasciculation and maturation in a variety of neuronal subtypes in the developing central nervous system (CNS).

In the first part of the study, in an effort to further study its role in myelination, we focused on the role of TAG-1 in demyelination and remyelination in two different murine models. In the first one, the EAE (Experimental Autoimmune Encephalomyelitis) model, we induced demyelination after activation of the immune system directed against a myelin component, driving autoimmunity which results in spinal cord white matter (WM) pathology and associated clinical symptoms. TAG-1 absence resulted in a delay in the development of neurological symptoms, linked to a reduced recruitment of Tregs in the spinal cord. The second model utilizes a toxin (lysophospatidylocholine - LPC) to induce focal demyelination in the corpus callosum (cc). Following demyelination, TAG-1 affects microglial and astroglial recruitment to the lesioned area, driving also OPC differentiation. Last but not least, in the absence of TAG-1 another mechanism is driven to cluster VGKCs at JXPs during remyelination.

In the second part of our study, we report on alterations of the juxtaparanodal proteins TAG-1, Caspr2 and VGKCs in normal appearing white matter (NAWM), perilesion and chronic lesion areas in post-mortem white matter tissue from MS patients compared to control white matter. We show that the molecular organization and maintenance of JXPs is affected in lesions, perilesions and NAWM in chronic MS through protein and mRNA expression as well as immunohistochemistry. The three molecules analyzed were differentially altered.

TAG-1 clustering at JXPs was reduced in NAWM; TAG-1 and Caspr2 are diffused in perilesions and absent in lesion areas. VGKCs were no longer enriched at juxtaparanodes either at the NAWM or the perilesion and demyelinated plaques. While the protein levels of the three molecules showed only a tendency of reduction in the plaques, there was a significant upregulation of Caspr2 mRNA in the lesions accompanied by a transcriptional increase of paranodal Caspr, indicating an axonal homeostatic mechanism.

Overall, our study points to novel roles of TAG-1 in demyelination and remyelination in mice, such as a pivotal role in driving autoimmunity, microglial and astroglial recruitment, as well as differentiation of oligodendrocyte precursor cells (OPCs) to mature, myelin-producing, oligodendrocytes (OLs). In chronic MS tissue, the comparative analysis of the juxtaparanodal complex revealed for the first time differential alterations of the three components and a juxtaparanodal vulnerability in NAWM, an area of diffuse pathology lacking demyelination.

ΠΕΡΙΛΗΨΗ

Οι εμμύελες ίνες των θηλαστικών διαιρούνται σε διακριτές υποπεριοχές, οι οποίες πλαισιώνουν τους κόμβους του Ranvier, στους οποίους βρίσκονται τα τασεοελεγχόμενα κανάλια νατρίου (voltage gated Na channels - Na_v). Δίπλα από τον κόμβο του Ranvier βρίσκονται σε διαδοχή οι λεγόμενες παρακομβικές περιοχές (paranodes - PNs), στις οποίες λαμβάνουν χώρα φυσικές αλληλεπιδράσεις των γλοιακών και αξονικών μεμβρανών, οι εγγύς των παρακομβικών περιοχές (juxtaparanodes - JPXs), στις οποίες γίνεται η συσσώρευση των τασεοελεγχόμενων διαύλων καλίου (voltage-gated K channels - VGKCs) και στη συνέχεια το μεσοκομβικό διάστημα (internode). Η συνοχή των παραπάνω υποπεριοχών είναι υψίστης σημασίας για τη λειτουργία του νευράξονα και την επαγωγή του δυναμικού ενεργείας κατά μήκος του. Ισχυρές αλλαγές επί των περιοχών αυτών έχουν αναφερθεί στη Σκλήρυνση κατά Πλάκας (Multiple Sclerosis - MS), συνοδευόμενες από λειτουργικές συνέπειες για την νευρική λειτουργία. Η πρωτεΐνη TAG-1 (Transient Axonal Glycoprotein-1 ή Contactin2 – Cntn2), η οποία εκφράζεται από τον άξονα και το γλοιακό κύτταρο, εντοπίζεται και αυτή στα JXPs και είναι υπεύθυνη για την μοριακή στρατολόγηση και συγκράτηση των VGKCs και της αξονικής πρωτείνης Caspr2 σε αυτές. Επίσης, η TAG-1 έχει ταυτοποιηθεί ως πιθανό αυτοαντιγόνο σε μια υποκατηγορία ασθενών οι οποίοι πάσχουν από MS και η νευρωνική της μορφή έχει βρεθεί να συμμετέχει σε πολλές διεργασίες όπως η κυτταρική μετανάστευση και διαφοροποίηση, η αξονική δεσμίδωση σε διάφορους τύπους νευρικών κυττάρων στο αναπτυσσόμενο κεντρικό νευρικό σύστημα (Central Nervous System - CNS).

Στο πρώτο μέρος της παρούσας μελέτης προσπαθήσαμε να προσεγγίσουμε το ρόλο της TAG-1 στη μυελίνωση, χρησιμοποιώντας δύο μοντέλα απομυελίνωσης σε μύες. Στο πρώτο μοντέλο, αυτό της Αυτοάνοσης Πειραματικής Εγκεφαλομυελίτιδας (Experimental Autoimmune Encephalomyelitis - EAE), έγινε η επαγωγή της απομυελίνωσης μετά από την ενεργοποίηση του ανοσοποιητικού συστήματος έναντι μια δομικής πρωτεΐνης της μυελίνης, καταλήγοντας σε παθολογία της λευκής ουσίας του νωτιαίου μυελού και σχετιζόμενα κλινικά συμπτώματα. Απουσία της TAG-1 παρατηρήθηκε καθυστερημένη ανάπτυξη των νευρολογικών συμπτωμάτων, συνδεδεμένη με μειωμένη στρατολόγηση των ανοσορρυθμιστικών Τ λεμφοκυττάρων (regulatory T cells - Tregs) στο νωτιαίο μυελό. Στο δεύτερο απομυελινωτικό μοντέλο γίνεται χρήση μιας τοξίνης (λυσοφωσφατιδυλοχολίνη – lysophosphatidylocholine - LPC) για να επαχθεί τοπική απομυελίνωση του μεσολοβίου (corpus callosum - cc). Μετά την επαγωγή, η TAG-1 εμπλέκεται στην μοριακή

στρατολόγηση των μικρογλοιακών και αστρογλοιακών κυττάρων στη περιοχή της απομυελίνωσης, επάγωντας και τη διαφοροποίηση των πρόδρομων κυττάρων των ολιγοδενδροκυττάρων (Oligodendrocyte Precursor Cells – OPCs). Επιπροσθέτως, απουσία της TAG-1 τα VGKCs συσσωρεύονται στα JXPs μέσω ενός εναλλάκτικού μηχανισμού κατά την επαναμυελίνωση.

Στο δεύτερο μέρος της μελέτης, αναφέρουμε αλλαγές επί των πρωτεινών των JXPs TAG-1, Caspr2 και VGKCs στην φαινομενικά υγιή λευκή ουσία (normal appearing white matter - NAWM), στις περιοχές γύρω από τις απομυελινωτικές πλάκες (perilesions) και στις απομυελινωμένες περιοχές (lesions or plaques) σε ιστό post-mortem από ασθενείς πάσχοντες από MS σε σχέση με λευκή ουσία ελέγχου. Δείχνουμε ότι η μοριακή οργάνωση και διατήρηση των JXPs βρίσκεται επηρεασμένη σε όλες τις παραπάνω περιοχές μέσω ανάλυσης της πρωτεινικής έκφρασης και των επιπέδων mRNA, αλλά και μέσω πειραμάτων ανοσοϊστοχημείας. Τα τρία μόρια βρέθηκαν να επηρεάζονται σε διαφορετικό βαθμό. Η συσσώρευση της TAG-1 στα JXPs ήταν μειωμένη στη NAWM, ενώ παρατηρήθηκε η διάχυση των TAG-1 και Caspr2 στις περιοχές γύρω και επί των απομυελινωτικών πλακών. Τα VGKCs δεν βρίσκονταν στα JXP σε καμία από τις περιοχές υπό μελέτη. Στο πρωτεϊνικό επίπεδο, αποκαλύψαμε μόνο μια τάση μείωσης των τριών μορίων στις πλάκες, ενώ τα επίπεδα του αξονικού μορίου των PNs, Caspr, βρέθηκαν αυξημένα, πιθανώς λόγω ενός μηχανισμού ομοιόστασης του νευράξονα.

Εν κατακλείδι, από τα αποτελέσματα της μελέτης μας προκύπτει η συμμετοχή της TAG-1 σε καινοτόμες βιολογικές διεργασίες κατά την απομυελίνωση και επαναμυελίνωση σε μύες, όπως στην προώθηση της αυτοανοσίας, της μοριακής στρατολόγησης της μικρογλοίας και αστρογλοίας, καθώς και της διαφοροποιήσης των OPCs σε ώριμα ολιγοδενδροκύτταρα (oligodendrocytes - OLs), ικανά να παράξουν ώριμη μυελίνη. Στην χρόνια MS, αποκαλύψαμε για πρώτη φορά την διαφορική διάχυση και ρύθμιση των τριών πρωτεϊνών που καθιστούν το μοριακό σύμπλοκο των JXPs και την ευαισθησία τους στη NAWM, η οποία χαρακτηρίζεται από διάχυτη παθολογία αλλά όχι από απομυελίνωση.

A. INTRODUCTION

A.1. The evolution and functional importance of myelination

Concurrently with the evolution of vertebrates came an increase in body size, which corresponded to the need of action potential propagation along bigger distances. The propagation of the signal could be facilitated by two possible mechanisms: either the increase in axonal diameter, observed in many invertebrates like cephalopods (e.g. in squids) (Zalc and Colman 2000) or a decrease in axonal capacitance and increase in axial resistance by means of physical insulation. The first adaptation was not possible in vertebrates due to the restricted area that the nerves could occupy, since they are enclosed by a bonny encasing, another innovation of this animal group (Zalc, Goujet et al. 2008). Furthermore, the increase in axonal diameter would be sufficient for increased signal propagation only in animals with relatively small size (body length of 0.1-30 cm). Consequently, the emergence of insulation was seen in jaw-bearing vertebrates (gnathostomes) and was accomplished by axonal enwrapment by the membrane of specialized cells, termed glial cells, in a process called myelination.

Thus, myelination resulted in improved signal conduction in larger and more complex species. As an example, the velocity of action potential propagation along a non-myelinated fiber with a diameter of 10 μm is less or equal to 1 m/sec, while in a myelinated axon of the same caliber it increases to 50-100 m/sec (Zalc, Goujet et al. 2008). In addition to the increased signal propagation, myelin has been proposed to have two additional functions:

- It protects the axons mechanically by creating an additional layer around them and thus isolates the electrical signal from the surrounding tissue (Virchow, 1854; Ranvier, 1878),

- It supports the axons by providing energy metabolites (i.e. lactate, which is produced by mature glial cells) (Funfschilling, Supplie et al. 2012, Lee, Leach et al. 2012, Lee, Morrison et al. 2012, Morrison, Lee et al. 2013). There are two mechanisms of transport from the soma to the axons: active (or fast) transport by means of motor proteins, such in the case of vesicles, and passive (or slow) transport via diffusion of soluble molecules. In the latter case, the speed of transport is so slow that it would require several days for metabolites to reach the axon. Glial cells have been shown to transport lactate from their cell bodies to axons through the monocarboxylate transporter 1 (MCT1) (Morrison, Lee et

al. 2013). Taking into account the vulnerability of the axons to nutrient and energy deprivation the importance of the neighboring glial cells in this context is highlighted.

In conclusion, myelin emergence favored the evolutionary success of vertebrates that possess myelinated axons by allowing increased brain and body size and the evolution of complex and sophisticated behavioral traits.

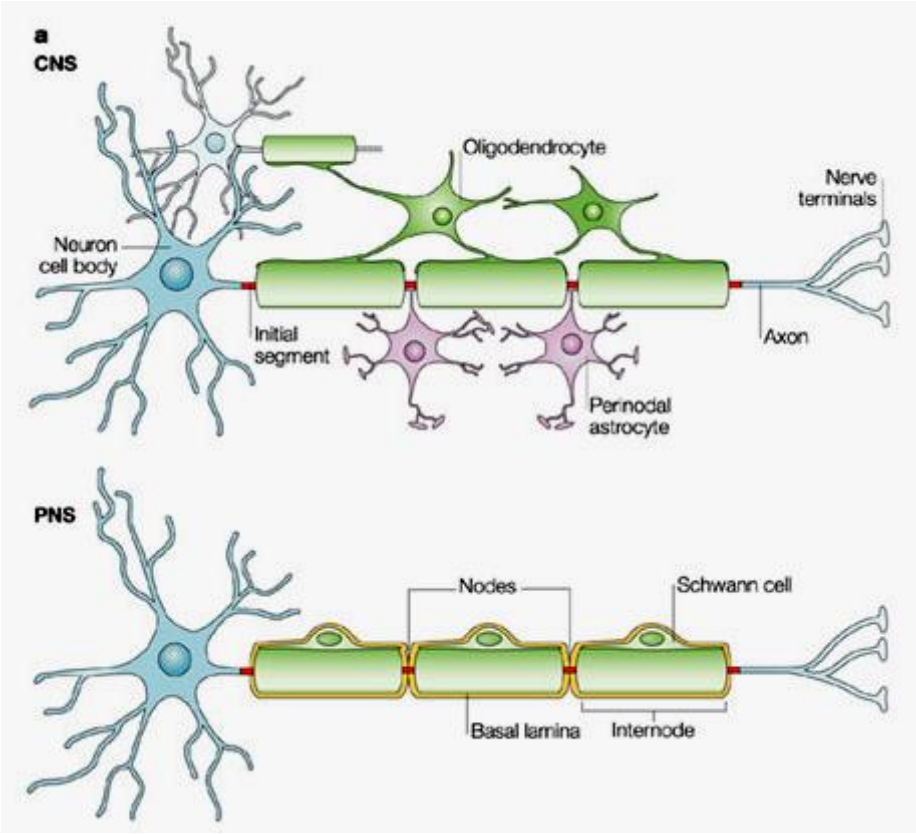

Figure 1. Myelinating cells of the nervous system and overall organization of myelinated axons. Glial cells wrap their plasma membrane several times around axons, thereby creating myelinated segments, the internodes, and domains called nodes of Ranvier where myelin is absent in period distances along the axon. In the CNS, oligodendrocytes myelinate up to 40 axonal segments while in the PNS, Schwann cells are capable of myelinating only one axon. From (Poliak and Peles 2003).

A.2 Myelin origin and composition

Myelin is formed by glial cells, which expand their plasma membrane around the axon and wrap it several times. In the central nervous system (CNS) the cells that perform this task are the oligodendrocytes (OLs), while in the peripheral nervous system (PNS) the Schwann cells (Figure 1). Myelin is composed of 70-80% lipids (mainly galactosylceramide or cerebroside) and 15-30% myelin-specific proteins. The increased composition of myelin in

lipids is opposed to other biological membranes, which have a bigger protein-to-lipid ratio (Morell and Quarles 1999). The distinct composition of the cell membrane of the two glial types results in unique myelin proteins in the CNS and the PNS. CNS myelin is composed of the myelin basic protein (MBP), proteolipid protein (PLP), 2′:3′-Cyclic nucleotide-3′-phosphodiesterase (CNP) and myelin-associated glycoprotein (MAG). In the PNS, myelin shares some common proteins with the CNS, such as MBP and MAG, while others such as P_0 and peripheral myelin protein-22 (PMP-22).

OLs and Schwann cells have a different origin but in both cases myelination is a dynamic procedure throughout development and adult life, which depends on constant cell-cell interactions between axons and glial cells. However, a striking difference between the two is the constant need of the Schwann cell to receive contact-dependent signaling from the axons (Mirsky, Winter et al. 1980). Even to be cultured *in vitro*, Schwann cells require cAMP, which mimics the presence of neurons (Morgan, Jessen et al. 1991, Bacallao and Monje 2015). On the other hand, OLs are able to myelinate even when a simulation of an axon is present, like a fixed axon or a nanofiber with a diameter within the range of that of axons (Rosenberg, Kelland et al. 2008, Lee, Leach et al. 2012, Lee, Chong et al. 2013). Furthermore, while one OL myelinates up to 40 axonal segments (Pfeiffer, Warrington et al. 1993), each Schwann cell wraps only a single axon. In conclusion, the differences in cell biology and origin of the two types of glial cells may account for the functional differences as well. We will not discuss further the biology of Schwann cells as this study focused on the CNS and OLs.

A.3. OL origin and CNS myelination in the developing nervous system

Mouse oligodendrocyte precursor cells (OPCs) are generated in discrete waves during embryogenesis from neuroepithelial precursors situated in or adjacent to the ventricular zone (VZ) of the nervous system and are characterized by the expression of the proteoglycan NG2´the platelet-derived growth factor receptor alpha (Pdgfrα) and the oligodendrocyte lineage transcription factor Olig2 (Rowitch 2004, Richardson, Kessaris et al. 2006, Tomassy and Fossati 2014).

In the spinal cord, the majority of OPCs (Olig2, Pdgfrα and Sox10-expressing cells) are generated at embryonic day 12.5 (E12.5) in the ventral domain, known as pMN (since it

generates also motoneurons) in a Sonic Hedgehog (Shh)-dependent manner (Warf, Fok-Seang et al. 1991, Pringle and Richardson 1993, Sun, Pringle et al. 1998, Orentas, Hayes et al. 1999, Richardson, Smith et al. 2000, Rowitch 2004) (Figure 2a). Nevertheless, recent work has shown that 20% of all spinal cord-derived OPCs arise from the dorsal domain at E15.5 and preferentially myelinate axons of the rubrospinal and corticothalamic tract (Cai, Qi et al. 2005, Fogarty, Richardson et al. 2005, Vallstedt, Klos et al. 2005, Tripathi, Clarke et al. 2011).

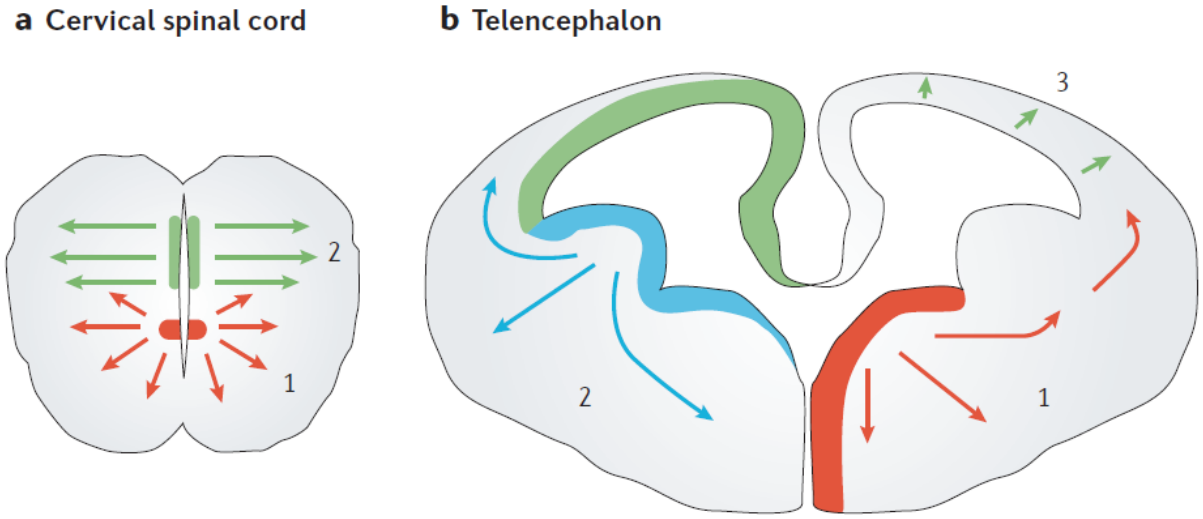

Figure 2. Waves of oligodendrogenesis in the mouse CNS. (a) In the spinal cord, the ventrally-derived OPCs are generated first (1), followed by the dorsally-derived (2) approximately two days later during early embryogenesis. **(b)** Similarly, oligodendrogenesis in the forebrain initiates at ventral structures (1, AEP and MGE) and progresses towards dorsal (2, embryonically: CGE and LGE; 3, postnatally: cortex) **(**From (Kessaris, Fogarty et al. 2006)).

Similarly, in the forebrain OPCs are generated in multiple waves from dorsal and ventral locations, following a course from ventral to dorsal areas (Figure 3b). The first one takes place at E14.5 in ventral areas, the anterior entopeduncular area (AEP) and the medial ganglionic eminence (MGE) followed by their migration to the whole embryonic telencephalon (Spassky, Goujet-Zalc et al. 1998, Olivier, Cobos et al. 2001, Spassky, Heydon et al. 2001, Tekki-Kessaris, Woodruff et al. 2001). At E15.5, the second population of OPCs arises from the caudal and lateral ganglionic eminences (CGE and LGE), while the third and last wave of oligodendrogenesis occurs postnatally (Kessaris, Fogarty et al. 2006). Interestingly, the late-born OPCs take over while the early-born that originate from the first wave almost disappear in the adult nervous system.

After their specification, OPCs migrate while still in a proliferative state to populate the spinal cord and forebrain. This migration is controlled by various morphogens and extracellular matrix (ECM) proteins as well as the corresponding receptors (de Castro and Bribian 2005, Colognato and Tzvetanova 2011, Mitew, Hay et al. 2014, Ackerman, Garcia et al. 2015). When they reach their destination, OPCs become post-mitotic and acquire a pre-myelinating identity as Nkx2.2+ cells, mainly in white matter regions (Figure 3). Pre-myelinating OPCs are able to wrap axons with their plasma membrane but do not form mature myelin (Kirby, Takada et al. 2006, Kucenas, Snell et al. 2008, Mitew, Hay et al. 2014, Snaidero, Mobius et al. 2014, Zhu, Zhao et al. 2014). In mice, this state is highly transient and the cells either progress to become myelinating OLs or proceed to apoptosis (Barres, Hart et al. 1992, Trapp, Nishiyama et al. 1997).

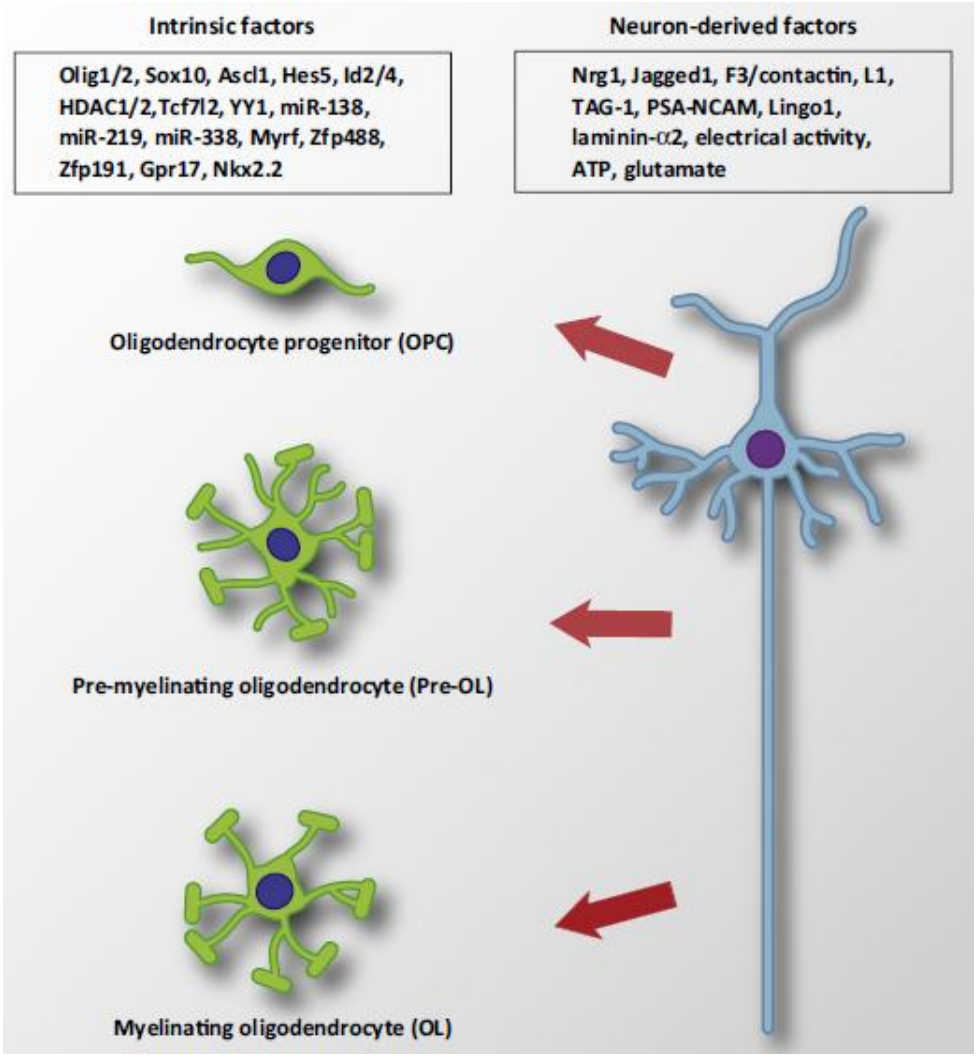

Figure 3. Known cell-autonomous and non-cell-autonomous factors controlling the specification and development of oligodendrocytes (OLs). Oligodendrocyte precursor cells (OPCs) are specified at precise

domains of the CNS. Next, they proceed to migrate and become pre-myelinating OLs at their final targets and wrap axons. Finally, they produce mature myelin and form the myelin sheath (From (Tomassy, Dershowitz et al. 2015)).

Each of the steps in OL development described above is controlled by a variety of extrinsic and intrinsic factors, with a high degree of complexity, since there are crucial regional differences between various areas of the CNS (Figure 3). Among these signals are transcription factors, chromatin remodeling and post-transcriptional modifications.

An example is that of Olig2, a transcription factor which is necessary both for OPC specification and differentiation (Zhou, Choi et al. 2001, Rowitch 2004, Wang, Dulin et al. 2006). In specified OPCs, Olig2 recruits the chromatin-remodeller Brg1 (Brahma-related gene 1) to regulatory elements of genes coding for myelin and myelin-associated proteins and differentiation factors, such as MBP, Ugt8a (UDP glycosyltransferase 8), the transcriptional activator Sox10 [SRY (sex determining region Y)-box10] and Myrf (myelin regulatory factor) (Yu, Chen et al. 2013). Myrf, a membrane protein specific for post-mitotic OLs, is indispensable for the maturation of OLs and the expression of MBP (Cahoy, Emery et al. 2008, Emery, Agalliu et al. 2009). Interestingly, Sox10, in collaboration with Olig2, induces the expression of Myrf and then bith Sox10 and Myrf synergistically promote the myelination program in OLs (Hornig, Frob et al. 2013).

Chromatin remodeling has also been shown to be crucial for OL development, as the activity of total histone deacetylases (HDACs), a class of enzymes that compact chromatin, is fundamental for terminal differentiation of OPCs to OLs and expression of myelin genes (Marin-Husstege, Muggironi et al. 2002). Prior to oligodendrocyte differentiation, β-catenin is found in the nucleus in a complex bound to TCF7L2, a member of TCF (T-cell factor)/LEF (lymphoid enhancer family) transcription factor family, thus inhibiting its function. HDAC1 and HDAC2 bind to β-catenin, dissociate it from the complex and TCF7L2 eventually drives OL differentiation (Ye, Chen et al. 2009). Another chromatin modification, histone methylation resulting in the repression of gene transcription, was recently shown to be critical for the conversion of OPCs to mature myelin forming cells (Liu, Magri et al. 2015).

Post-transcriptional modifications are mediated by non-coding microRNAs (miRs) in a variety of tissues. Similarly, miR-138, miR-219 and miR-338 exert repression on negative regulators of differentiation such as Sox6 and Pdgfrα in developing OPCs (Lau, Verrier et al. 2008, Dugas, Cuellar et al. 2010, Zhao, He et al. 2010, Svaren 2014).

Signals originating from axons result in the control of the myelin formation, thickness and distribution of the myelin sheath (Barres and Raff 1993, Barres, Schmid et al. 1993, Taveggia, Feltri et al. 2010). Most of the identified mechanisms, however, have been identified in the PNS and seem not to apply in the CNS. For instance, in the PNS the myelination and the thickness of the myelin depend on axonal caliber, with a threshold of caliber of axons that become myelinated of 1 μm (Duncan 1934, Friede and Samorajski 1967, Voyvodic 1989). In the CNS, there is no specific range of axonal diameter that characterizes myelinated axons and even axons with as little a diameter as 0.2 μm become myelinated (Hildebrand, Remahl et al. 1993). Additionally, while several molecules have been shown to mediate axonal-glial communication in the PNS, only a few from those implicated in the CNS myelination have been discovered. Among these are some membrane-associated factors and ECM constituents, such as laminin-α2, Notch ligands (Jagged1 and F3/contactin), PSA-NCAM (polysialylated neuronal cell adhesion molecule), and Lingo1 (Nave and Werner 2014) (Figure 3). Lastly, neuronal activity also promotes OL differentiation and maturation, as shown by the increase in the number and stability of myelin loops after artificial increase of neuronal excitability with a γ-aminobutyric acid (GABA)-antagonist (Hines, Ravanelli et al. 2015, Mensch, Baraban et al. 2015). Researchers propose that electrical activity induces the expression of surface proteins (e.g. L1) and synaptic vesicle release, which in turn stimulates myelin synthesis and distribution (Itoh, Stevens et al. 1995, Wake, Lee et al. 2011).

A.4. OL plasticity and myelination during adulthood in the insulted CNS

Although the majority of OPCs differentiate during the first weeks of postnatal life, a total of 5-8% glial cells of the CNS remain as an undifferentiated pool of cells. Myelin continues to be generated in the healthy adult nervous system as a result of neuronal activity, both in mice and humans (Giedd 2004, Miller, Duka et al. 2012) (Giedd 2004; Miller et al. 2012). While in humans this is performed by OLs that have already differentiated during development, in mice new myelin during adulthood is formed by newly differentiated OLs (Young, Psachoulia et al. 2013, Yeung, Zdunek et al. 2014).

Demyelination is defined as the loss of myelin around axons and can either be due to a congenital condition affecting glial cells (leukodystrophies) or an acquired inflammatory pathology, such as Multiple Sclerosis (MS). Following damage, however, remyelination occurs thanks to adult OPCs and neural stem cells (NSCs). Adult OPCs are NG2+;Pdgfrα+

cells and can be found not only in healthy brain parenchyma but also in and around demyelinating Multiple Sclerosis lesions (Scolding, Franklin et al. 1998). These cells are not capable of migrating along long distances but rather differentiate locally (Gensert and Goldman 1997, Zawadzka, Rivers et al. 2010). On the other hand, NSCs express glial fibrillary acidic protein (GFAP) and Nestin and are located in the subventricular zone (SVZ) of the brain. Under normal circumstances NSCs are quiescent but after a demyelinating incidence they can give rise to OLs as response to local increase to Shh and induction of the effector molecule Gli1 (Menn, Garcia-Verdugo et al. 2006, Samanta, Grund et al. 2015).

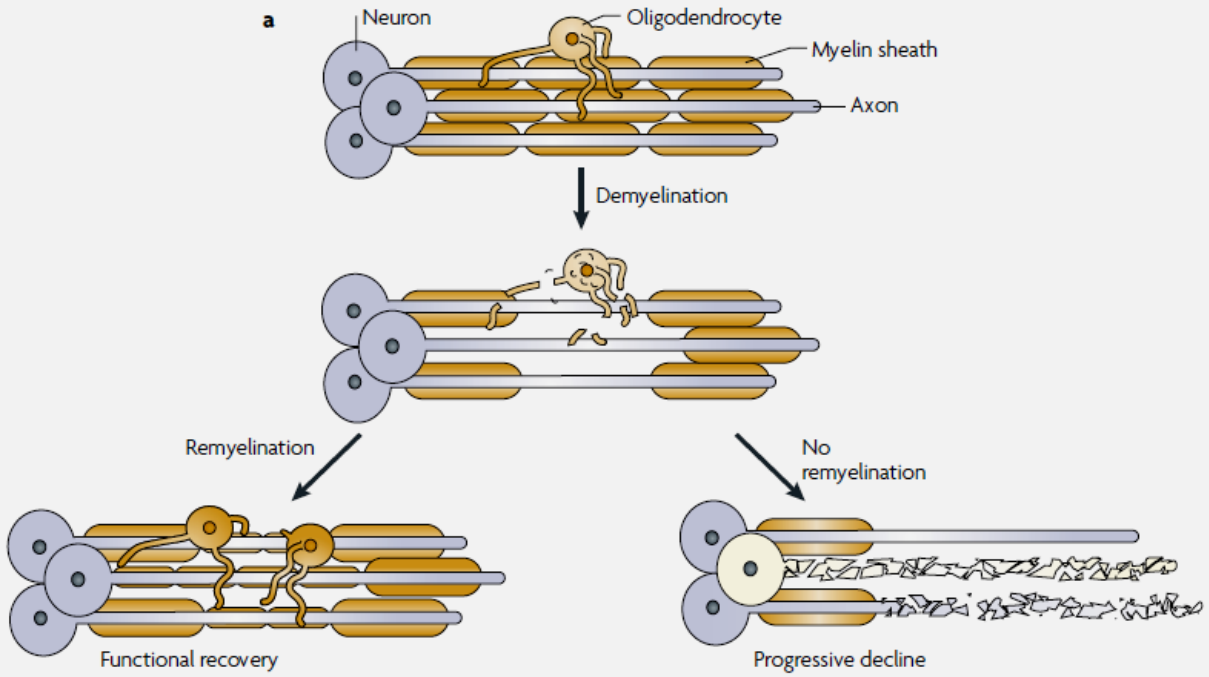

Figure 4. The outcome of demyelination in the CNS. Following demyelination in the CNS, regardless the cause, there are two possibilities. The first one is often seen in experimental models of demyelination and involves the remyelination from newly differentiated OLs, resulting in the formation of thinner, but still sufficient myelin sheaths and functional recovery of the axons. Nevertheless, in other cases, especially in demyelinating conditions like MS, remyelination is not successful and axons eventually degenerate due to loss of trophic support. From (Franklin and Ffrench-Constant 2008).

However, in the adult CNS, axons do not always become properly remyelinated following an insult, as opposed to the PNS and small caliber axons are mostly favored (Mason, Langaman et al. 2001) (Figure 4). This is believed to be due to the formation of a glial scar surrounding the damaged area and/or faulty re-ensheathment of axons by the OLs (Huebner and Strittmatter 2009). This failure in remyelination stands true not only for mice, but also for human inflammatory demyelinating pathologies such as Multiple Sclerosis, especially during later stages of the disease (Prineas and Connell 1979, Franklin and Ffrench-

Constant 2008, Franklin and Goldman 2015). During early disease progression remyelination proceeds successfully and correlates with increased OPC proliferation, while later on remyelination attempts are fruitless and lead to degeneration of the denuded axons (Raine, Scheinberg et al. 1981, Franklin and Ffrench-Constant 2008) (Figure 4). Although it remains unclear why this happens, increased numbers of NG2+ OPCs are found in and around MS lesions during early and chronic disease stages but they do not have the capacity to differentiate to OLs (Wolswijk 1998, Wolswijk 1998, Kuhlmann, Miron et al. 2008, Huang, Fancy et al. 2011).

A.5. The pathology of Multiple Sclerosis

MS is a chronic autoimmune disease of the CNS characterized by foci of inflammation accompanied by demyelination, axonal loss and glial scar formation (Lassmann 1998, Prineas, Kwon et al. 2001). Although the primary etiology of the disease is unknown, the neurological decline that is observed is attributed to the neuronal and axonal loss caused by chronic local inflammation and generalized immune system activation in the CNS (Frischer, Bramow et al. 2009, Weiner 2009, Lassmann, van Horssen et al. 2012). This view is supported by the fact that patients suffering chronically from MS are refractory to treatments that suppress the peripheral immune system (Zamvil and Steinman 2003, Compston and Coles 2008).

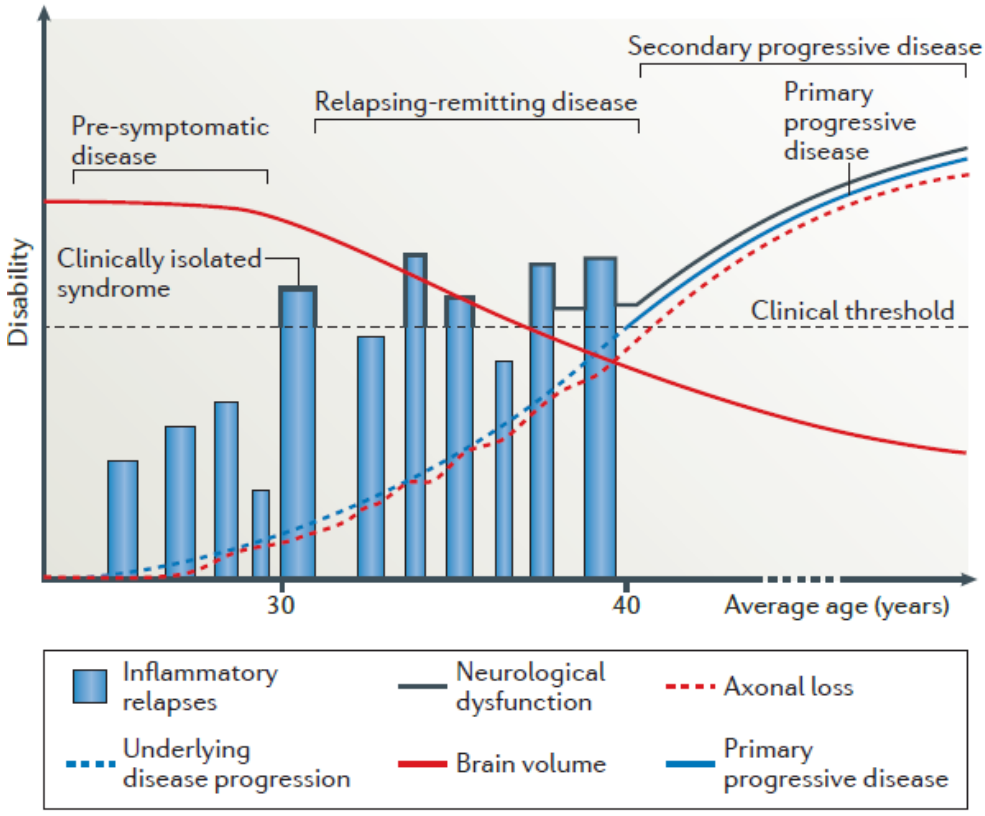

Figure 5. Clinical course and correlation of disability with stages of Multiple Sclerosis. The most common form of the disease is relapsing-remitting multiple sclerosis. It is characterized by an initial isolated episode of neurological dysfunction, followed by recovery (remission) and alternating periods of relapse and remission. Relapses correspond to peak of inflammation and demyelination of white matter areas. Over time, each remission is milder and disability accumulates, leading to development of secondary progressive multiple sclerosis. In secondary progressive disease, inflammatory lesions are almost absent, and progressive neurological decline is accompanied by CNS atrophy. Approximately 10% of patients with multiple sclerosis are affected by the primary progressive disease form, which features progressive decline without relapses. From (Dendrou, Fugger et al. 2015).

Despite the heterogeneity of the disease, the forms of MS can be classified into three broad categories based on the symptomatology of the patients: relapsing-remitting (RRMS), primary progressive (PPMS) and secondary progressive (SPMS) (Figure 5). RRMS represents 85% of all cases and is characterized by repetitive incidents of increasing neurological symptoms accompanied by periods of partial or complete recovery. The majority of RRMS patients usually progress to SPMS in 6-10 years from disease onset, where symptom severity becomes gradually greater and there are no more remissions (Weinshenker, Bass et al. 1989, Runmarker and Andersen 1993). PPMS is the most aggressive form of MS, with initial occurrence of symptoms that lead to gradually progressive disability (Figure 5).

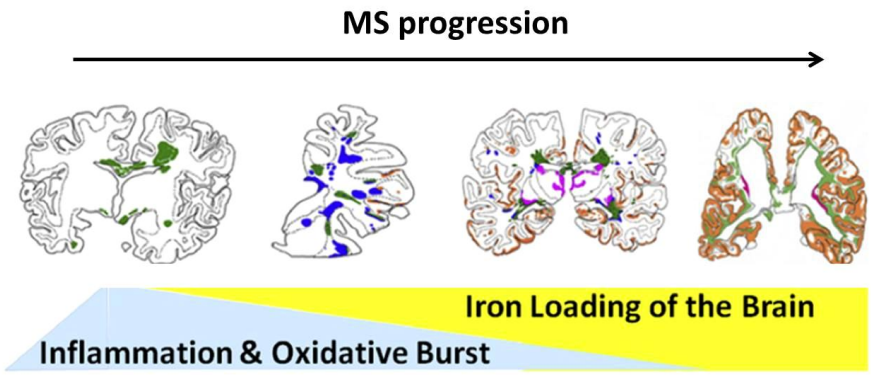

Figure 6. Overview of Multiple Sclerosis pathology over time. At initial stages white matter (WM) lesions are evident and become remyelinated. Later on, gray matter lesions are most common, while inflammation levels drop but there is continuous tissue damage due to oxidative stress and almost absent remyelination. Additionally, extracellular iron accumulation and brain atrophy are seen. Green: demyelinated WM lesions, blue: remyelinated WM lesions; brown: gray matter lesions. Adapted from (Lassmann and van Horssen 2011).

One of the most common pathological hallmarks is, as mentioned, the presence of demyelinating lesions (plaques or lesions) characterized by axonal loss which greatly correlates with patient disability and astroglial scaring (Bjartmar, Kidd et al. 2001, Lassmann, Bruck et al. 2007). In addition to the demyelinating plaques that are seen both in the white and grey matter, the normal appearing white matter (NAWM) has recently been recognized as an area of diffuse pathology (Filippi, Tortorella et al. 1999, Ciccarelli, Werring et al. 2001). Among the pathological hallmarks observed are the presence of activated microglia, neurodegeneration, a compromised blood-brain barrier (BBB) and increased glutamate concentration (Plumb, McQuaid et al. 2002, Kutzelnigg, Lucchinetti et al. 2005, Srinivasan, Sailasuta et al. 2005, Howell, Rundle et al. 2010, Tisell, Leinhard et al. 2013).

The main cause of tissue injury is inflammation, even though infiltrates are most prominent during RRMS and progressively decline with disease duration to the point that they reach the levels of age-matched healthy controls, both in the NAWM and lesion areas in progressive stages (the so-called burn out stage) (Frischer, Bramow et al. 2009) (Figure 6). At the same time, an increasing amount of free iron accumulation is seen, which also takes place normally in aged brain and increases the levels of neurodegeneration (Hallgren and Sourander 1958). In the human brain, age-related iron accumulation takes place in OLs of the cortex and white matter, while injury or death of OLs during demyelination in active lesions leads to the release of iron in the extracellular space and may lead to toxicity (Hametner, Wimmer et al. 2013, Lassmann 2014).

Multiple sclerosis is considered a T-cell-driven disease characterized by high complexity. Infiltrates detected in lesions are mainly composed of CD8+ T-cells while CD4+ T-cells and B-cells are found, albeit in smaller numbers, in the perivascular space and the meningues (Esiri 1980, Ozawa, Suchanek et al. 1994, Babbe, Roers et al. 2000, Serafini, Rosicarelli et al. 2004). Furthermore, in actively demyelinating lesions a high degree of microglial activation and macrophage accumulation is seen (Lassmann 2011).

As already mentioned, remyelination in the majority of MS patient fails irrespectively of the disease stage or type, but there are cases where remyelinated areas with thinner myelin sheaths (or shadow plaques) reach even 90% of total white matter lesions (Patrikios, Stadelmann et al. 2006, Patani, Balaratnam et al. 2007). One factor that seems to affect positively the efficiency of remyelination is the proximity to the cortical gray matter while mouse studies have shown that the inability of the present OPCs to mature and remyelinate the lesions is not explained by the continuous cycles of demyelination (Patrikios, Stadelmann et al. 2006, Albert, Antel et al. 2007, Rodriguez, Wegner et al. 2014).

A.6. Organization of subdomains of myelinated fibers

Under normal conditions in the adult CNS, a myelinated fiber is characterized by the presence of specialized areas at periodic intervals, the so-called nodes of Ranvier, flanked by the paranodes (PNs). At the distal side of the PNs another specialized domain is formed, named the juxtaparanode (JXP). Along a myelinated fiber, the segment from one JXP to the next is called the internode (Figure 7A). Each of these domains is characterized by the presence of specific proteins.

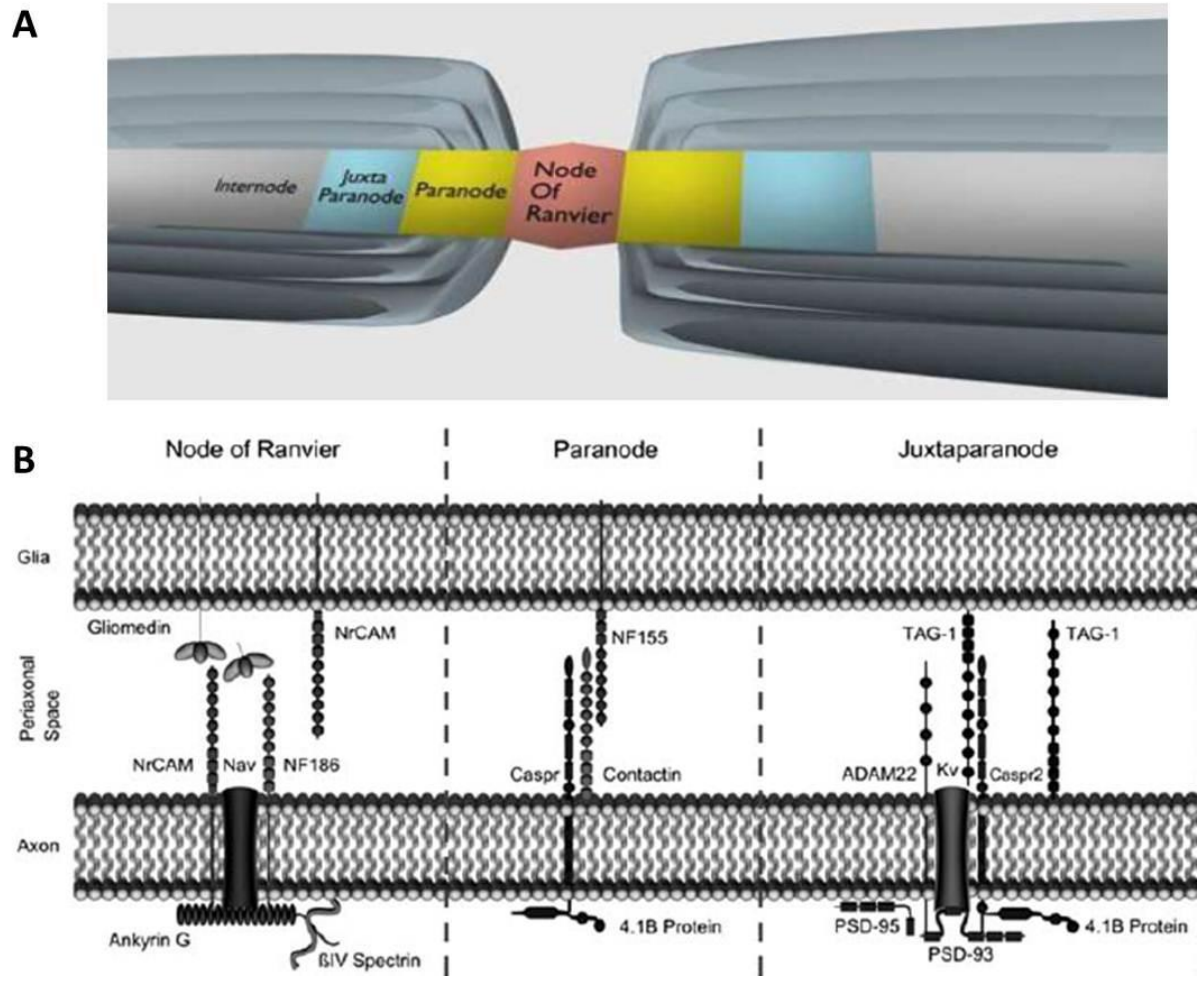

Figure 7. Organization of domains of myelinated fibers of the CNS. (A) Scheme depicting the general subdivisions found on a myelinated fiber. **(B)** Molecules found at each domain either on the axonal or the glial side in a PNS fiber, with some of the molecules absent in the CNS. From Zoupi et al 2011.

Nodes of Ranvier are 1 μm-long membrane stretches which occur in between the myelinated domains of the axon and are enriched in voltage-gated sodium channels (Na_v), which are responsible for the saltatory conduction of the action potential and are retained at the node through interaction with the scaffold protein ankyrin-G (AnkG) (Pan, Kao et al. 2006) (Figure 7B). During development the subtype Nav1.2 is expressed while during maturation of the nodes it is replaced by the Nav1.6 (Boiko, Rasband et al. 2001, Kaplan, Cho et al. 2001). Interestingly, under demyelinating conditions the immature Nav1.2 type takes over (Craner, Lo et al. 2003, Rasband, Kagawa et al. 2003). Sodium channel accumulation and maintenance depends on two proteins of the immunoglobulin superfamily (IgSF); NrCAM, expressed by both axons and glia and the 186 kDa isoform of Neurofascin (NF186), found on the axon (Davis, Lambert et al. 1996, Feinberg, Eshed-Eisenbach et al. 2010).

PNs are the sites where the glial and axonal membranes are in close proximity and are connected with septate-like junctions, thus forming the axo-glial junctions. Paranodal complexes are formed through the interactions between two axonal surface proteins, contactin-associated protein-1 (Caspr) and Contactin-1 (Cntn-1) as well as the 155-kDa isoform of Neurofascin (NF155) on the glial surface (Menegoz, Gaspar et al. 1997, Peles, Nativ et al. 1997, Rios, Melendez-Vasquez et al. 2000, Charles, Tait et al. 2002, Sherman, Tait et al. 2005, Susuki and Rasband 2008, Labasque and Faivre-Sarrailh 2010). In mice which lack any of these molecules, PNs and axoglial contact are eventually disrupted and the proteins that are normally found at JXPs diffuse towards the nodes (Figure 8, lower left panel). Caspr bears a 4.1-binding motif, with which it tethers to the corresponding cytoskeletal adaptor protein 4.1B, also found at JXPs (Denisenko-Nehrbass, Oguievetskaia et al. 2003). Even though PNs constitute a physical and molecular barrier against the diffusion of the nodal components, these domains alone are not sufficient for preserving the nodal complexes at place. A study in which the nodal NF186 was conditionally ablated from the CNS and PNS showed that the presence of normal PNs was not enough to keep nodal components in place when the tethering proteins are absent from these domains (Thaxton, Pillai et al. 2011).

Proper formation of the JXPs depends firstly on the presence of the PNs, that act as a barrier against molecular diffusion and secondly on several intracellular scaffold proteins that cluster and maintain the juxtaparanodal components at place (Susuki and Rasband 2008) (Figure 8). At these domains, a tripartite complex is formed by the voltage-gated potassium channels (VGKCs) and the Neurexin family protein contactin-associated protein-2 (Caspr2) on the axonal membrane and the glycophosphatidylinositol (GPI)-anchored protein Transient Axonal Glycoprotein-1/Contactin-2 (TAG-1/Cntn-2, from now on referred to as TAG-1), present in both the neuronal and the glial membrane (Traka, Dupree et al. 2002, Poliak and Peles 2003, Poliak, Salomon et al. 2003, Traka, Goutebroze et al. 2003, Labasque and Faivre-Sarrailh 2010, Savvaki, Theodorakis et al. 2010). The absence of either TAG-1 or Caspr2 results in the disruption of the complex and the diffusion of the VGKCs towards the internodal area (Poliak, Salomon et al. 2003, Traka, Goutebroze et al. 2003, Savvaki, Panagiotaropoulos et al. 2008) (Figure 8). The juxtaparanodal complex is connected to the actin cytoskeleton by means of the association of the cytoplasmic tail of Caspr2 with the adaptor protein 4.1B (Denisenko-Nehrbass, Oguievetskaia et al. 2003, Horresh, Bar et al.

2010). Furthermore, the adaptor proteins post-synaptic density-93 and 95 (PSD-93 and PSD-95), also found at juxtaparanodal domains, interact with Caspr2 and VGKCs through their PDZ-binding domain, but their absence does not affect the formation of the juxtaparanodal complex (Rasband, Park et al. 2002, Horresh, Poliak et al. 2008, Horresh, Bar et al. 2010, Ogawa, Oses-Prieto et al. 2010). VGKCs that are found at JXPs are of the subtypes Kv1.1, Kv1.2 and 1.4 and their proposed role is the regulation of action potential propagation and the reduction of repetitive axonal firing in development, injury and remyelination (Rasband, Trimmer et al. 1998, Rasband 2004).

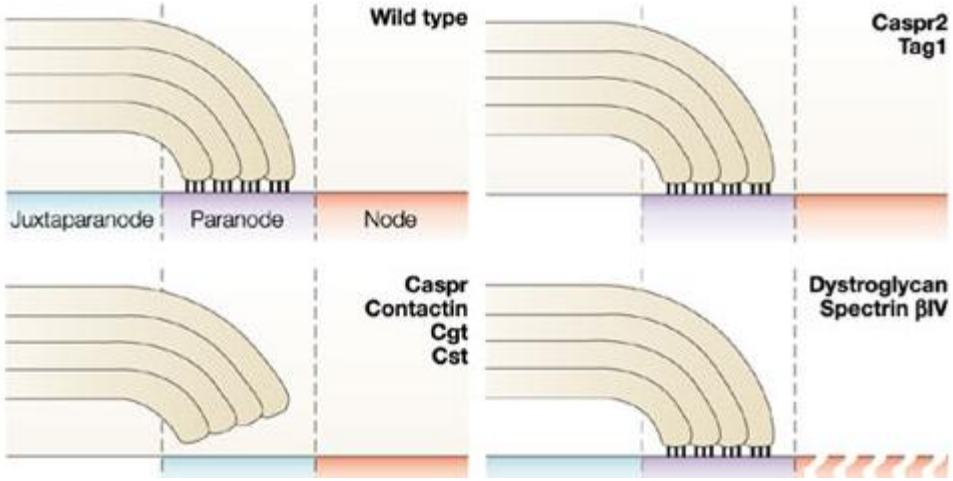

Figure 8 Schematic representation of perinodal changes reported in various mouse mutants. In the absence of either TAG-1 or Caspr2, the juxtaparanodal complex fails to form and VGKCs diffuse in the internode, while paranodes remain unaffected (upper right case). When paranodes are disrupted, as observed in null mice for either Caspr, Contactin, galactosyltransferase (Cgt) or cerebroside sulfotransferase (Cst) the juxtaparanodes diffuse towards the node but the juxtaparanodal molecules are present (lower left panel). Nodal disruption by means of removal of key tethering proteins Dystroglycan and Spectrin βIV results in reduced Nav clustering but does not affect either paranodes or juxtaparanodes (lower right panel). From (Poliak and Peles 2003).

Proper formation and maintenance of each of these domains described above is essential for normal neuronal excitability and signal transduction, as well as for neuronal homeostasis. Especially disorganization of nodal and juxtaparanodal ion channel complexes leads to alterations in nerve conduction. Computational models have shown that even subtle paranodal injury or a small change in the degree of nodal constriction significantly reduces the conduction velocity along the fibers (Halter and Clark 1993, Babbs and Shi 2013). Additionally, the diffusion of VGKCs reported in *Tag-1*$^{-/-}$ and *Caspr2*$^{-/-}$ mice in combination with paranodal loosening could cause repetitive discharges after a single stimulus (Poliak and Peles 2003).

A.7. TAG-1 structure and functional importance in myelinated fibers

TAG-1, as already mentioned, is a GPI-anchored protein of the IgSF. The protein bears 6 Ig-like and 4 fibronectin (FNIII)-like domains. TAG-1 is found at juxtaparanodal domains of myelinated fibers in the adult CNS and PNS and is expressed by both the glial and neuronal membrane (Furley, Morton et al. 1990, Karagogeos, Morton et al. 1991, Pavlou, Theodorakis et al. 2002, Traka, Dupree et al. 2002).

Tag-1$^{-/-}$ mice show hypomyelination in the optic nerve and selective loss of small caliber axons, loss of Caspr2 and VGKC diffusion towards the internode (Traka, Goutebroze et al. 2003, Chatzopoulou, Miguez et al. 2008, Savvaki, Panagiotaropoulos et al. 2008). Additionally, Tag-1 null mice exhibit hypersensitivity to convulsive stimuli and reduced performance in behavioral tests for learning and memory (Fukamauchi, Aihara et al. 2001, Savvaki, Panagiotaropoulos et al. 2008). Furthermore, the glial isoform alone is sufficient for rescuing the mutant phenotype of the JXP and the behavioral deficits, pointing clearly to the importance of this molecule for the juxtaparanodal molecular architecture (Savvaki, Theodorakis et al. 2010).

A.8. Disruption of perinodal domains in demyelination and MS

Disorganization of nodal, paranodal and juxtaparanodal components has been reported in MS lesions. Specifically, in early active demyelinating MS lesions, the paranodal molecules Nfasc155 and Caspr are found in elongated clusters, while VGKCs overlap with the PNs due to their diffusion towards nodal areas (Coman, Aigrot et al. 2006, Howell, Palser et al. 2006) (Figure 9ii). As demyelination proceeds, paranodal clusters are even more increased in length and VGKCs diffuse further. In chronic inactive lesions (CILs), paranodal Caspr is completely absent in the lesions and diffuse in the perilesions, where juxtaparanodal Caspr2 and VGKC appear diffused, as well (Figure 9iii). Na_v clusters are also increased in length in the plaques, meaning that they are the last component to get disorganized (Coman, Aigrot et al. 2006) (Figure 9iv).

However, in partially remyelinated plaques, intermediate-sized Na_v+ aggregates, Nfasc155+ and Caspr+ PNs as well as Caspr2+ and VGKC+ JXPs appear, while their length is restored to normal levels in fully remyelinated tissue (or shadow plaques) (Coman, Aigrot et al. 2006, Howell, Palser et al. 2006) (Figure 9v-vi). We have recently shown in two

different rodent models that during demyelination, initially the PNs elongate with subsequent JXP diffusion and down-regulation at the protein level. During remyelination, however, the PNs were found to form again followed by JXPs at later stages (Zoupi, Markoullis et al. 2013). Additionally, an activated microglia-mediated effect of paranodal disruption has been described not only in MS NAWM, but also in presymptomatic experimental autoimmune encephalomyelitis (EAE) and CFA (Complete Freund's Adjuvant) injected mice (Howell, Rundle et al. 2010, Zoupi, Markoullis et al. 2013).

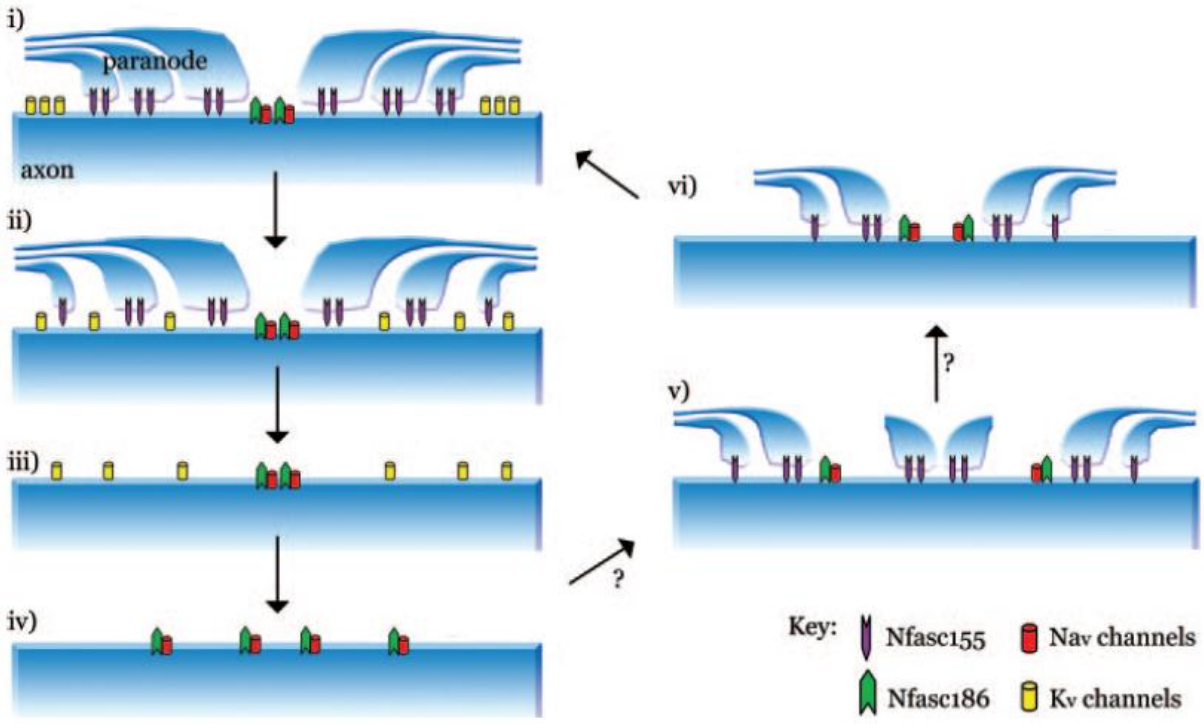

Figure 9. Schematic representation of reported perinodal changes during de- and remyelination in Multiple Sclerosis. (i) A normally myelinated fiber with unaffected organization. (ii) In the borders of demyelinating lesions, during initial stages, axo-glial junctions loosen and a relatively mild diffusion of paranodes leads to diffusion of VGKCs towards the node. (iii) Loss of paranodes and the associated molecules and demyelination precedes nodal disruption (iv). (v) Remyelinating fibers often exhibit atypical triple paranodal complexes flanking clustered nodal areas, which eventually result in normal reclustering, while juxtaparanodal regions are the last component that gets re-established (vi). From (Howell, Palser et al. 2006).

Among juxtaparanodal molecules TAG-1 is of particular interest in the context of demyelinating pathology, since it has been identified in a screening for possible autoantigens in MS and is one of the two molecules that are known to mediate axonal pathology under autoinflammatory conditions, with the second one being Nfasc186, as shown in a rodent EAE model (Derfuss, Parikh et al. 2009, Lindner, Ng et al. 2013). Moreover, it is the only perinodal molecule that is expressed by both the neuronal and glial membrane. Importantly,

the components of the juxtaparanodal complex have also been implicated in other autoimmune pathologies which we will not refer to, since it is not the focus of this study.

A.9. Experimental models of MS in mice

The complexity of MS and the need of unraveling the disease mechanisms and testing potential therapies have urged researchers to develop several animal models of demyelination. Unfortunately, each one of them shows only particular similarities to the pathophysiology of the human disease (Ransohoff 2012). Among these are models applying toxic, immune-mediated, viral or genetic demyelinating protocols, either systemically or focally. The most commonly used model is that of the Experimental Autoimmune Encephalomyelitis (EAE), while an emerging as widely used among the toxin-mediated protocols is that of the lysophospatidylcholine (LPC)-induced demyelination. Here we will briefly discuss both models.

The EAE model is an artificially-driven autoimmune model, usually induced in the C57BL/6 mouse strain, although it is possible to be applied on a range of experimental model organisms. It has been shown that the histopathology of EAE mimics that of MS in several aspects, such as that it is a T-cell-driven disease and that these cells are autoreactive against myelin components (i.e. MBP, MOG and PLP) (Waksman and Adams 1962, Yasuda, Tsumita et al. 1975, Bernard, Leydon et al. 1976, Steinman and Zamvil 2006, Croxford, Kurschus et al. 2011). A basic difference between EAE and MS is that in the C57BL/6 mouse strain the disease is induced by a harsh induction and is monophasic, while MS is spontaneous and dynamic. Nevertheless, researchers were able to induce a relapsing-remitting form, most prominently in the SJL/J strain (Dal Canto, Melvold et al. 1995). Additionally, in EAE lesions are found only in the spinal cord WM and are mostly dominated by CD4+ T-cells, while MS plaques are found also in the brain, both in WM and GM and the disease is mostly CD8+ T-cell-driven (Paterson and Day 1979, Babbe, Roers et al. 2000, Huseby, Liggitt et al. 2001). Recently it has also been proposed that the age-related iron accumulation seen in humans is simulated neither in mice nor in EAE, although it is not certain yet whether this phenomenon is really correlating with MS pathology (Lassmann and van Horssen 2011).

On the other hand, EAE studies have greatly contributed to the understanding of basic MS pathology and they have the advantage of being able to time precisely enough the onset

and phases of immune response and clinical symptomatology and correlate it with any histopathological finding. For example, one drug currently widely used in MS was developed thanks to observations derived from EAE research. This drug is, in fact, a humanized monoclonal blocking antibody against the surface molecule α4β1integrin, found on the surface of mononuclear cells and inhibits them from passing through the BBB (Yednock, Cannon et al. 1992).

Another limitation of EAE is that it is not permissive for remyelination studies, since even at chronic stages the inflammatory environment is such that remyelination is only partial. In this case, toxic models are useful, since the focal and precise administration of the toxin followed by its removal causes reversible demyelination (Blakemore and Franklin 2008). Among these, that of the focal injection of LPC in white matter causes precisely located lesions, which are able to fully remyelinate in a matter of weeks and has been widely used to elucidate the cellular and molecular determinants of the process (Blakemore, Eames et al. 1977, Foote and Blakemore 2005, Miller and Fyffe-Maricich 2010).

In conclusion, demyelinating mouse models certainly do not resemble MS either in the complexity or in all mechanisms, but they are certainly useful in order to answer specific questions about the pathogenesis of the disease, to examine the mode of action of potential therapies and to address the mechanisms and the role of specific proteins in remyelination. In our study we used both fore mentioned models to assess the role of TAG-1 in de- and remyelination.

A.10. Goal of the study

Our study focused on the role of TAG-1 in demyelination and remyelination in rodent models of MS and the effects of the MS pathology in all three molecules comprising the juxtaparanodal complex (TAG-1, Caspr2 and VGKCs).

In the first part of this study we attempted to elucidate the importance of the glial and neuronal isoform of TAG-1 altogether in de- and remyelination using two mouse models, one of systemic/immune system-mediated and one of focal demyelination. The questions we aimed to answer were:

- Does the absence of TAG-1 render the white matter more vulnerable to demyelination?
- If so, is there a subsequent correlation with increased axonal loss?
- Is remyelination affected in TAG-1 null animals?

In the second part of the study we analyzed the expression and localization of TAG-1 in relation to its juxtaparanodal partners, Caspr2 and VGKCs in chronic MS tissue. Our goal was to assess the following questions:

- How does the chronic pathology of MS affect the juxtaparanodes in the lesions, perilesions and the NAWM?
- Is the expression and localization of the three molecules of the juxtaparanodal complex similarly affected?

B. MATERIALS AND METHODS I

B.1. Laboratory Animals

In this study, the following animal lines were used:

1. C57B110/CBA background

- *Tag-1*+/+ mice
- *Tag-1-/-* mice (Fukamauchi, Aihara et al. 2001)

The *Tag-1-/-* mice are lacking TAG-1 due to the removal of the sequence between the 2nd and 5th exon of the gene coding for the protein. Previous studies in our lab showed that the TAG-1 absence results in Caspr2 loss, the diffusion of VGKCs from the JXPs and the decrease of internodal distance (Savvaki, Panagiotaropoulos et al. 2008). Furthermore, *Tag-1-/-* mice exhibit behavioral defects concerning learning and memory tasks, as well as hyperexcitability to convulsive stimuli (Fukamauchi, Aihara et al. 2001, Savvaki, Panagiotaropoulos et al. 2008).

2. C57BL/6 background

One of our main goals was to study the possible vulnerability of mice lacking TAG-1 (or expressing only rTAG-1 by oligodendrocytes) to demyelinating protocols and to study the remyelination extend. In order to successfully induce the EAE (see section below) all animals had to belong to the C57BL/6 background. For this purpose, we back-crossed *Tag-1-/-* and *Tag-1-/-;plpTg*$^{(rTag\text{-}1)38}$ mice in the C57BL/6 background and obtained again the aforementioned genotypes.

B.2 Genotyping

Animals from breedings are handled at an early age (postnatal days 5-10) and a small piece of tail is collected after they are marked according to their fingers.

B.2.1 Genomic DNA extraction from tail pieces

1. Lysis of the tail by addition of 400 μL Tail Lysis Buffer, 5 μL of protease K (stock: 20 mg/mL) and incubation at 55°C for several hrs or overnight.
2. Addition of 1 μL RNase (stock: 10 mg/mL) and incubation at 37°C for 10 min.
3. Addition of 1 volume (V) of phenol and moderate mixing for 10 min at RT.
4. Addition of 1 volume (V) of chloroform and moderate mixing for 10 min at RT.
5. Centrifuge at 13000 g, 5 min, RT and transfer supernatant to a new eppendorf tube.
6. Addition of 1 volume (V) of chloroform and moderate mixing for 10 min at RT.
7. Centrifuge at 13000 g, 5 min, RT and transfer supernatant to a new eppendorf tube.
8. DNA precipitation: addition of ½ V ammonium acetate 10M and 2 V ice cold 100% EtOH and mixing by vigorous shaking or vortex.
9. Centrifuge at 13000 g, 15-20 min, 4°C.
10. Discard the supernatant and air-dry the pellet.
11. Resuspend in 100-150 μL sterile dH_2O.

Tail Lysis Buffer
100 mM NaCl
10 mM Tris HCl, pH 8.0
25 mM EDTA, pH 8.0
0.5% w/v SDS

B.2.2. Genotyping PCR

In order to identify the genotype of the animals used in this study one PCR was used to detect the wild type or knock-out band for *Tag-1* as mentioned in Fukamauchi et al. 2001

(primers “Tag-1 5’”, “Tag-1 3’”, “Neo 3’”) and one to detect the presence or absence of *rTag-1* as follows:

- Primer “PLP internal 7846 Forward” (PLP int for):

5’-AAGGAGACTGGAGAGACCAGG-3’

- Primer “rTAG-1 143 Reverse” (rTAG-1 rev):

5’-GAATCAACTGGAGACTCAGGC-3’

The setup of each reaction and the PCR programs used are shown below:

Gene	**PCR reaction (V_{total}=20 µL)**	**PCR program**		
Tag-1	1 µL genomic DNA (gDNA)	**Step**	**Temperature**	**Duration**
	2 µL 10xTaq Buffer (Minotech)	1.	94°C	4 min
	2 µL 2 mM dNTPs	2.	94°C	30 sec
	1.3 µL of primers Tag-1 5’ and 3’ (stock:50 ng/µL)	3.	61°C	45 sec
	1 µL of primer Neo 3’ (stock: 50 ng/µL)	4.	72°C	1 min
	1 µL 10% DMSO	5.	Repeat steps 2-4 32 times	
	0.6 µL Taq polymerase (stock 2U/µL, Minotech)	6.	72°C	5 min
	9.8 µL sterile dH_2O	7.	4°C	
PLP::rTag-1	1 µL genomic DNA (gDNA)	1.	94°C	4 min
	2 µL 10xTaq Buffer (Minotech)	2.	94°C	30 sec
	2 µL 2 mM dNTPs	3.	61°C	45 sec
	1.5 µL of each primer (stock:20 ng/µL)	4.	72°C	1 min
	0.6 µL Taq polymerase (stock 2U/µL, Minotech)	5.	Repeat steps 2-4 32 times	
	11.4 µL sterile dH_2O	6.	72°C	5 min

		7.	4°C	

B.2.3. Agarose gel electrophoresis

Following PCR run, reactions are loaded on a 1 or 2% agarose gel containing 0.25 mg ethidium bromide per mL and separated by electrophoresis in a tank filled with 1xTAE Buffer to detect PCR products. DNA fragments are detected under UV irradiation.

50xTAE Buffer
40 mM Tris-acetate
500 mM EDTA pH 8.0
Adjust pH to 8.5

B.3. Demyelinating Protocols

In this study we chose two demyelinating protocols to which we subjected the animals and studied the demyelination and remyelination: that of the toxic substance lysophosphatidylcholine (or lysolecithin-LPC) and the Experimental Autoimmune Encephalomyelitis (EAE). Both protocols are explained in detail below.

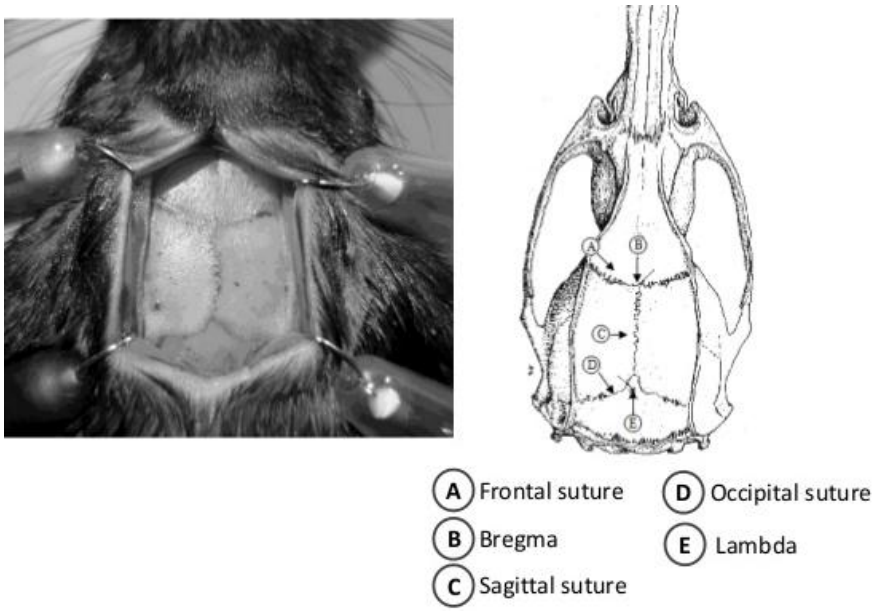

Figure 10. Schematic drawing of a mouse skull and important characteristic points. The bregma is defined as the point at which the frontal suture meets the sagittan suture (or midline). The lambda is defined as the point

at which the sagittal and occipital sutures meets and should be in a straight line from the bregma, usually 4±0.4 mm away.

B.3.1. Focal injection of lysophosphatidylcholine or lysolecithin (LPC)

To induce focal demyelination with LPC injection the protocol was standardized by adjustments on that published by Ferent et al. 2013 (Ferent, Ruat et al. 2013). Female mice of the C57B110/CBA background bred at the Animal Facility of IMBB were subjected to this protocol at 8-10 weeks of age.

Mice were weighted prior to the experimental procedure and received anesthesia by intra-peritoneal injection of ketamine/xylazine (per g of body weight: 100 μg of ketamine and 15 μg of xylazine diluted in sterile dH_2O in a final volume of 5 μL). Responsiveness to painful stimuli was checked by pinching of the tail or hind limb. Each mouse was fixed on a small animal stereotactic frame (Cat. No. 502610, World Precision Instruments) by means of a mouse nose clamp adaptor and ear bars which are incorporated on the frame. The head was positioned so as to assure that the height of the bregma and lambda (see Figure 10) was identical (by measuring the coordinates at the dorsoventral axis of the device), as well as that of the right and left hemisphere. The skull was exposed and a drill was used to create a small opening. 1 μL of either the vehicle solution (0.9% w/v NaCl in sterile dH_2O) or the LPC solution (1% w/v LPC in 0.9% w/v NaCl in sterile dH_2O) was injected at the following coordinates from the bregma at a flow of 0.1 μL/1.5 min:

- Anteroposterior axis (AP): +1 mm
- Mediolateral axis (ML): +1 mm
- Dorsoventral axis (DV): -2.3 mm

Next, animals were carefully removed from the frame, sutured and left to recover in a clean cage with excess of food and water.

Animals that received the vehicle were sacrificed at 5 days after the surgery (days post injection - dpi) while animals that received the toxin at 5, 10 and 15 dpi (see Figure 11). Following fixation the forebrain was collected and further processed.

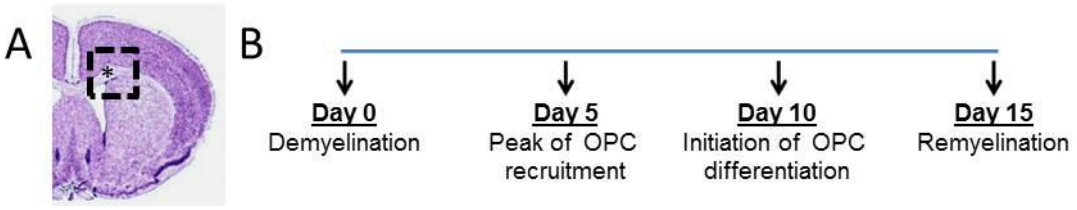

Figure 11. Overview of the experimental design and time points of the lysophosphatidylcholine-induced demyelination of the corpus callosum. (A) Following demyelination by means of a stereotactic injection of 1 μL 1% LPC in the corpus callosum (injection site indicated by an asterisk), animals were sacrificed at time points corresponding to discrete steps of OPC recruitment and differentiation **(B).**

B.3.2. Induction of Experimental Autoimmune Encephalomyelitis (EAE)

To assess the role of TAG-1 in demyelination and remyelination in a model of autoimmune demyelination we used the MOG_{35-55}-induced EAE model (adapted from (Ioannou, Alissafi et al. 2012)). Female mice of the C57BL/6 background bred at the Animal Facility of IMBB were subjected to this protocol at 8-10 weeks of age. A brief outline of the experimental protocol can be seen in Figure 12.

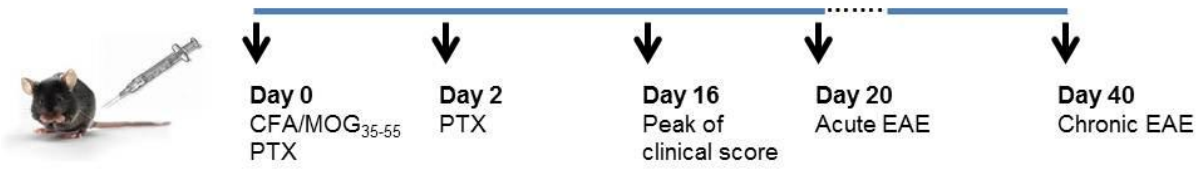

Figure 12. Schematic outline of the experimental design of EAE. 8-10-week-old female C57BL/6 mice were subjected to the protocol. Following induction, animals were sacrificed at 16, 20 and 40 dpi.

In the experimental group, referred from now on as "MOG_{35-55}", on day 0 mice received a subcutaneous injection of the adjuvant at the base of tail prepared as follows:

1. Mix in an eppendorf tube on ice:
    - 200 μg synthetic MOG_{35-55} peptide (CASLO) in 100 μL 1xPBS
    - 100 μL Complete Freund's Adjuvant (CFA, Cat. No. F5881, Sigma-Aldrich) with 4 mg/mL non-viable, desiccated Mycobacterium Tuberculosis H37 Ra (Cat. No. 231141, Difco Laboratories, BD Biosciences)
2. Sonication until mixture is white, stiff, viscous and of uniform consistency.

Additionally, on day 0 and day 2 mice received an intra-peritoneal injection of Pertussis Toxin (PTX, Cat. No. #181, List Biological Laboratories, Inc.) of 200 ng in 1xPBS in a final volume of 200 μL. This results in autoimmunity directed against myelin and CNS infiltration of autoreactive immune cells due to disruption of the blood-brain-barrier (BBB).

A second group of mice received the adjuvant lacking the peptide accompanied by the PTX and were used as the control group, from now on referred as "CFA". These mice present an unspecific, generalized immune reaction and BBB disruption. A third group of age-matched, naïve wild type female mice were included as a reference group.

Following injections mice were kept and monitored daily from day 7 and on until the time of sacrifice. The following clinical score scale was used to assess symptom severity:

Score	Description	Signs
0	No neurological signs	Normal behavior
1	Flaccid tail	Tail limp, lacking muscle tone
2	Hindlimb weakness or abnormal gait	Wobbly walk
3	Complete hind limb paralysis	Dragging hind limbs, abnormal righting reflex
4	Complete hind limb paralysis and fore limb weakness or paralysis	Movement in circles or only with one fore limb
5	Moribund or deceased	-

In addition to the clinical scoring, body weight was also recorded daily, since it is known that disease correlates with weight loss.

For characterizing the kinetics of the immune response wild type animals were sacrificed at 16, 20 and 41 days post-injection (dpi) and the spinal cord was collected and further processed. The comparative analysis of *Tag-1*+/+ and *Tag-1*-/- mice took place only at 20 dpi.

10xPBS (V_{final}=1 L)
70,1 g NaCl
12,8 g Na_2HPO_4
4,4 g NaH_2PO_4
2 g KCl
Fill up to a final volume of 1 L with dH_20

B.4. Histological Methods

B.4.1. CNS tissue collection and preparation

B.4.1.1. Tissue fixation, dissection and isolation

Adult mice received an intra-peritoneal injection of anesthesia (per g of body weight: 200 µg of ketamine and 30 µg of xylazine diluted in sterile dH_2O in a final volume of 10 µL). Responsiveness to painful stimuli was checked by pinching of the tail or hind limb. After lack of response was ensured, incisures were made to expose the sternum and internal organs, the diaphragm and ribcage was cut, finally exposing the heart. A peristaltic pump was used to circulate 20-25 mL 1xPBS through the vasculature by inserting a needle in the lower wall of the left ventricle and releasing extra pressure by an opening a small hole at the right atrium. Following clearance of the blood 50-60 mL of cold 4% PFA in 1xPBS were circulated to fix the tissues. CNS tissue (the forebrain in the case of the LPC protocol and the spinal cord in the case of the EAE) was carefully dissected and post-fixed in 4% PFA in 1xPBS on ice, for 20-30 min.

B.4.1.2. **Cry**oprotection

Following post-fixation, samples are washed 3 times in 1xPBS and submerged in 10 volumes of 30% sucrose, 0.1% NaN_3 in 1xPBS. Samples are kept at 4°C until the sucrose completely replaces the intracellular water, so that the samples sink at the bottom of the container.

B.4.1.3. Embedding, freezing and cryosectioning

After cryoprotection is complete, samples are embedded in a gel containing 15% w/v sucrose, 7.5% gelatin from porcine skin (Cat. No. G-2500, Sigma) in 1xPBS. To ensure uniform freezing, samples are submerged in methylbutane and are frozen at -35 to -40°C. Tissue blocks are then stored at -80°C before proceeding to cryosectioning (Leica). 10-14-μm-thick sections are collected on glass slides and stored in cryoboxes at -20°C until further processing.

B.4.2. Immunohistochemistry on cryosections derived from adult mice

Cryosections derived from CNS of adult mice were immunostained as described below:

1. Cryosections are removed from -20°C, encircled in Dako Pen (Cat. No. S200230, Dako, Agilent Technologies) and post-fixed in ice-cold acetone at -20°C for 10 min.
2. Washes (3x) in 1xPBS, 5 min each.
3. Incubation in Blocking Solution of 5% bovine serum albumin (fraction V, BSA) in 0.5% Triton X-100 in 1xPBS for 1 h, RT.
4. Incubation with the appropriate primary antibodies (see Table 1, Appendix) diluted in Blocking Solution at 4°C, overnight.
5. Washes (3x) in 1xPBS, 5 min each.
6. Incubation with the appropriate secondary fluorescently labeled antibodies (see Table 2, Appendix) in Blocking Solution for 1.5 h, RT.
7. Nuclear counterstaing with DAPI (0.1μg/mL in dH_2O, Sigma-Aldrich), for 5 min, RT or with TO-PRO®3 iodide (500 nM in 1xPBS, Molecular Probes, ThermoFisher Scientific) for 3 min, RT.
8. Washes (3x) in 1xPBS, 5 min each.
9. Mount using mounting medium containing MOWIOL® 4-88 Reagent (Cat. No. 475904, Calbiochem, EMD Chemicals, Merck KGaA).

10. Slide storage at 4°C until imaging take place and for long term storage after it is completed.

Mounting Medium for IHC
2.6 g MOWIOL® 4-88 Reagent
6 g glycerol
12 mL Tris 0.2 M pH 8.5
6 mL dH_2O

Imaging took place using two confocal microscopes (TCS SP2 and TCS SP8, Leica Microsystems GmbH).

B.5. Quantification of signal in immunohistochemical experiments

For the quantification of various cell types or structures in immunohistochemical experiments images were acquired using a confocal microscope (TCS SP2 and TCS SP8, Leica Microsystems GmbH) and under the same laser and detector settings for all samples.

B.5.1. Quantification of demyelination

Demyelinated white matter areas (WM lesions) were measured in the spinal cord of EAE-induced animals and the forebrain of LPC-injected mice.

- Coronal cryosections of the forebrain immunostained against PLP/GFAP were imaged with a 20x lens and further processed and analyzed in ImageJ software, version ImageJA 1.45b (Schneider, Rasband et al. 2012). Lesions were marked by hand and total demyelinated area was measured by the respective software tool. A minimum of 2 sections per animal was included in the quantification. Data were expressed as mean±standard error of the mean and statistical analysis was performed using the GraphPad Prism version 5.00 for Windows (GraphPad Software, San Diego, CA). Lesion area was compared across the time points within the same genotype using unpaired t test and differences were considered as significant when $P<0.05$.

- Coronal spinal cord cryosections immunostained against PLP/NF200 were imaged with a 20x lens and 0.75 digital zoom and further processed and analyzed in ImageJ software, version ImageJA 1.45b (Schneider, Rasband et al. 2012). Lesions were marked by hand and the area was measured by the respective software tool. Demyelination was expressed as a percentage of demyelinated area over the total area of the spinal cord white matter. A minimum of 2 sections per animal in each area of the spinal cord (cervical, thoracic, lumbar and sacral) was included in the quantification. Data were expressed as mean±standard error of the mean and statistical analysis was performed using the GraphPad Prism version 5.00 for Windows (GraphPad Software, San Diego, CA). Lesion area was compared between genotypes using non-parametric one-way ANOVA with Bonferroni's multiple comparison test and differences were considered as significant when $P<0.05$.

B.5.2. Quantification of autoimmune infiltrates

Infiltration of the spinal cord of CFA- or MOG-treated animals (see section below) by immune cells was quantified in a minimum of 2 sections per animal in each area of the spinal cord (cervical, thoracic, lumbar and sacral). Coronal spinal cord cryosections immunostained against MBP/IBA1 were imaged with a 20x lens and 0.75 digital zoom and further processed and analyzed in ImageJ software, version ImageJA 1.45b (Schneider, Rasband et al. 2012). Firstly, images were converted to RGB and channels were split in black-and-white. A Gaussian filter was applied to enhance signal-to-noise ratio and then a threshold was set to discriminate between postitively stained area and background. This resulted in a binary image (with single objects which were positively stained) which was analyzed using the particle analysis tool and the IBA1+ area was calculated as a percentage of the white matter, the gray matter and the total spinal cord area. Data were expressed as mean±standard error of the mean and statistical analysis was performed using the GraphPad Prism version 5.00 for Windows (GraphPad Software, San Diego, CA). Infiltration was compared between genotypes and between CFA-treated and induced mice in each area of the spinal cord using non-parametric one-way ANOVA with Bonferroni's multiple comparison test and differences were considered as significant when $P<0.05$.

B.5.3. Quantification of axonal density

Axonal density was quantified in the spinal cord of naïve adult animals (see section below) in 2 thoracic sections per animal. Coronal spinal cord cryosections immunostained against NF200 were imaged with a 20x lens and 0.75 digital zoom and further processed and analyzed in ImageJ software, version ImageJA 1.45b (Schneider, Rasband et al. 2012). Firstly, images were converted to RGB and then channels were split in black-and-white. A Gaussian filter was applied to enhance signal-to-noise ratio and then a threshold was set to discriminate between postitively stained area and background. This resulted in a binary image (with single objects which were positively stained for NF200) which was analyzed using the particle analysis tool. NF200+ single objects with an area ranging from 0.25 to 1600 μm^2 were automatically counted on one hemiside of the spinal cord white matter. Axonal distribution was expressed as number of axonal profiles per 1000 μm^2. Data were expressed as mean±standard error of the mean and statistical analysis was performed using the GraphPad Prism version 5.00 for Windows (GraphPad Software, San Diego, CA). Axonal density in the two genotypes was compared using unpaired t test and differences were considered as significant when $P<0.05$.

B.5.4. Quantification of axonal loss

Axonal loss was quantified in the spinal cord of CFA- or MOG-treated animals (see section below) in a minimum of 2 sections per animal in each area of the spinal cord (cervical, thoracic, lumbar and sacral). Coronal spinal cord cryosections immunostained against PLP/NF200 were imaged with a 20x lens and 0.75 digital zoom and further processed and analyzed in ImageJ software, version ImageJA 1.45b (Schneider, Rasband et al. 2012). Firstly, images were converted to RGB and then channels were split in black-and-white. A Gaussian filter was applied to enhance signal-to-noise ratio and then a threshold was set to discriminate between postitively stained area and background. This resulted in a binary image (with single objects which were positively stained for NF200) which was analyzed using the particle analysis tool. NF200+ single objects with an area ranging from 0.25 to 1600 μm^2 were automatically counted on one hemiside of the spinal cord white matter. Axonal loss was calculated as a percentage in comparison to the axonal density of naïve or CFA-treated mice. Data were expressed as mean±standard error of the mean and statistical analysis was performed using the the GraphPad Prism version 5.00 for Windows (GraphPad Software, San

Diego, CA). Axonal loss was compared between genotypes in each area of the spinal cord using non-parametric one-way ANOVA with Bonferroni's multiple comparison test and differences were considered as significant when $P<0.05$.

B.5.5. Quantification of clustering

For the quantification of clustering in naïve animals, analysis was performed on sagittal cerebellum cryosections labeled for Caspr/Kv1.1. The percentage of PNs with or without JXPs and JXPs without PNs were counted in a blinded fashion in 3-5 frames of an area of 79x79 μm per animal imaged with a 63x lens and 3x digital zoom and were expressed as percentage over the total number of both types of perinodal phenotypes, in order to eliminate the factor of heterogeneity of axonal density in the samples. Data were expressed as mean±standard error of the mean and statistical analysis was performed using the GraphPad Prism version 5.00 for Windows (GraphPad Software, San Diego, CA). Juxtaparanodal length measurements were compared using unpaired t test and differences were considered as significant when $P<0.05$.

B.5.6. Quantification of oligodendrocyte precursor cells and mature oligodendrocytes

The density of oligodendrocyte precursor cells and mature oligodendrocytes was quantified in the corpus callosum of vehicle and LPC-treated animals (see section below) at the various time points analyzed in a minimum of 2 sections per animal. Coronal cryosections of the forebrain immunostained against the mature OL marker CC-1 and the OPC marker PDGFRa were imaged with a 40x lens and further processed and analyzed in ImageJ software, version ImageJA 1.45b (Schneider, Rasband et al. 2012). CC-1+ and PDGFRa+ cells were counted manually at the corpus callosum area and expressed as number of positive cells per 10000 μm^2. Data were expressed as mean±standard error of the mean and statistical analysis was performed using the GraphPad Prism version 5.00 for Windows (GraphPad Software, San Diego, CA). Lesion area was compared across the time points within the same genotype using unpaired t test and differences were considered as significant when $P<0.05$.

B.6. Fluorescence Activated Cell Sorting (FACS)

For assessing the infiltrating cells of the spinal cord in EAE-induced mice, we performed FACS after isolation of total mononuclear cells and immunostaining against markers of specific types of immune cells. The procedure is explained in detail below.

B.6.1. Isolation of mononuclear cells from total spinal cords

Induced mice received an intra-peritoneal injection of anesthesia (per g of body weight: 400 µg of ketamine and 60 µg of xylazine diluted in sterile dH_2O in a final volume of 20 µL). Responsiveness to painful stimuli was checked by pinching of the tail or hind limb and we then proceeded to mononuclear cell isolation as follows:

1. Animals were perfused with ice-cold 1xPBS as described above (see section A.I.) in order to remove circulating blood and immune cells.

2. Spinal cords were dissected, cut using a clean razor blade and kept in 1xPBS. Spinal cords from 2-3 animals of the same genotype were pooled together.

3. Mechanical homogenization of spinal cords in 7 mL 1xPBS and cell isolation from the rest of the tissue by means of a 70 µm cell strainer (#352350, Falcon®).

4. Addition of 3mL of 30% isotonic Percoll® pH 8.5-9.5 (Mg^{2+} and Ca^{2+} free, Sigma-Aldrich) in the cell suspension and gentle mixing in RT.

5. Mononuclear cells were isolated using a Percoll® gradient as follows:

    - Slow stacking of the cell-containing Percoll mixture on top of 2 mL 70% Percoll® pH 8.5-9.5 (RT).

    - Centrifugation at 500 G, 18°C, 30 min, without brakes.

    - Careful transfer of 3-5 mL of the intermediate phase in a new tube.

    - Washing with a minimum of 8 mL 1xPBS and centrifugation at 500 G, 18°C, 7 min.

- Resuspension of pellet in 500-1000 μL Staining Buffer (5% fetal bovine serum-FBS in 1xPBS), counting of cells and proceeding to fluorescent staining.

B.6.2. Fluorescent staining of isolated cells and sample analysis

Cells were stained with fluorescence-conjugated antibodies against extracellular markers for 20-30 min, 4°C in Staining Buffer (see Table 3, Appendix) while for intracellular markers (i.e. FoxP3) staining was performed according to manufacturer's instructions (eBioscience) after the extracellular staining. Acquisition was performed using a cell-sorting unit consisting of the DakoCytomation MoFloT High-Performance Cell Sorter (Beckman Coulter, Inc.) and the SummitT software.

B.7. Morphological stainings

B.7.1. Hematoxylin & Eosin (H&E) morphological stain

This stain combines a basic (hematoxylin) and an acidic (eosin) dye, staining structures in the nucleus and the cytoplasm respectively. The final result is the staining of the nucleus in blue and the cytoplasm in pink.

1. Cryosections are removed from -20°C and left to dry shortly on the bench top.
2. Sections are dipped in 100% EtOH for 2 min.
3. Wash in dH_2O.
4. Submerge in hematoxylin for 45 sec-2 min.
5. Wash in dH_2O.
6. Submerge in eosin for 45 sec-2 min.
7. Wash in 70% EtOH.
8. Wash in 80% EtOH.
9. Wash in 95% EtOH.

10. Wash in 100% EtOH.

11. Fixation in xylene for 10 min.

12. Mounting using Entellan® new (Merck).

13. Observation at the brightfield.

Hematoxylin solution	**Eosin solution**
10% hematoxylin in 95% EtOH	0.25% w/v eosin
	0.5% v/v acetic acid in 80% EtOH

C. MATERIALS AND METHODS II

C.1. Human brain tissue samples

Post-mortem human brain samples used in this study were obtained from the UK MS Society Tissue Bank (http://www.ukmstissuebank.imperial.ac.uk/). All tissues have been collected following fully informed consent by the donors via a prospective donor scheme according to Ethics Committee approval. Details about all patients included in the study can be found in Table 4 (Appendix).

C.2. Characterization and classification of MS lesions

C.2.1. Neuropathological analysis of MS lesions

Following post-mortem tissue collection, brain tissue blocks of 1 cm^3 were incubated in 4% paraformaldehyde (PFA, Sigma-Aldrich), cryoprotected in 30% sucrose in 1xPhosphate Buffered Saline (1xPBS) and kept at -80°C. Next, 10 µm-thick cryosections were obtained using a cryostat (Leica) and processed using immunohistochemistry against ionized calcium-binding adapter molecule 1 (IBA1) and myelin oligodendrocyte glycoprotein (MOG) to assess inflammation and demyelination.

C.2.2. Classification of lesions

MS lesions were classified according to published criteria (Lucchinetti, Bruck et al. 1996, Lassmann, Raine et al. 1998, Frohman, Racke et al. 2006) and most recently published criteria from the UK MS Society Tissue Bank (Reynolds, Roncaroli et al. 2011) as outlined below:

- Chronic active slowly expanding lesions (referred to as chronic active lesions-CALs) were characterized by mild to moderate microglia activation and macrophage infiltration at the lesion margins, and early myelin degradation products restricted to single macrophages (Prineas, Kwon et al. 2001).

- Chronic inactive lesions (CILs) were those that had a sharp lesion edge lacking macrophage or microglia infiltration.

- Areas of NAWM were considered at least at 1 cm away from demyelinated plaques and excluding fiber tracts emerging from white matter lesions.

Extensive information on neuropathology of all cases and related details are included in Table 4 (Appendix).

C.3. Analysis of mRNA

All aqueous solutions used in RNA extraction and analysis were made using DEPC-treated dH_20 (cleared of RNases).

DEPC-treated dH_20
Add 0.1% v/v diethyl pyrocarbonate (Sigma)
Incubate O/N at RT overnight or at 37°C for at least 2 h
Autoclave

C.3.1. RNA extraction

Extraction of total RNA (tRNA) was performed on samples from control WM (n=6 cases) and MS NAWM (n=5 cases, 1 primary progressive (PPMS) and 4 secondary progressive MS (SPMS) cases), chronic active (n=5 lesions from 4 cases, 1 from a PPMS case and 4 from SPMS cases) and chronic inactive (n=4 lesions from 3 cases, 2 lesions from a PPMS case and 2 lesions from two SPMS cases) lesions (see Table 4, Appendix) in immunohistochemically characterized snap-frozen human brain tissue blocks (Markoullis, Sargiannidou et al. 2012). Total RNA was extracted using the RNeasy Lipid Tissue Mini Kit (Cat. No. 74804, QIAGEN) according to the manufacturer's instructions.

Alternatively, tRNA was extracted using Trizol® (Invitrogen) as follows:

- 1 mL of Trizol® is added per 50-100 mg of starting tissue and tissue is homogenized using a dounce. At this point the homogenate can be stored at -80°C for a minimum of one year.
- Incubate the homogenized sample at the bench top for 5 min (room temperature, RT) and transfer to an eppendorf tube.
- Centrifuge at 12000 g, 10 min, 4°C.
- Add 0.2 mL chloroform per mL of Trizol® and shake vigorously for 15 sec.
- Incubate at the bench top for 2-3 min (RT).
- Centrifuge at 12000 g, 15 min, 4°C.
- Transfer supernatant (aqueous phase, RNA-containing) to a new eppendorf and add 0.5 mL isopropanol per mL of Trizol® initially used.
- Incubate at the bench top for 10 min (RT).
- Centrifuge at 12000 g, 10 min, 4°C (tRNA precipitation).
- Remove supernatant and wash pellet with 1 mL 75% EtOH. At this point the sample can be stored at -20°C for up to a year.

- Vortex and centrifuge at 7500 g, 5 min, 4°C.
- Discard the supernatant and dry the pellet, for 5-10 min (RT).
- Resuspend tRNA in DEPC-treated dH20 and dissolve by incubating for 10 min, at 55-60°C. Store at -80°C.

C.3.2. Reverse transcription

After resuspension tRNA is subjected to DNase treatment using the RNase-Free DNase set (Cat. No. 79254, QIAGEN) as follows:

1. Mix in an eppendorf tube:
    - ≤ 87.5 µL tRNA-containing solution
    - 10 µL Buffer RDD
    - 2.5 µL DNase I stock solution (2.7 Kunitz units/µL)
    - Add RNase-free water up to a final volume of 100 µL.
2. Incubate at the bench top (20-25°C) for 10 min.

Following DNase treatment, proceed to RNA cleanup to remove the enzyme and any added salts from the buffer:

1. Add 1 volume (V) of chloroform and vortex for 3-5 min.
2. Centrifuge at 12000 g, 5 min, 4°C and transfer supernatant to a new eppendorf tube.
3. Add 1/10 V NaCH3COOH 3M, pH 5.2 and 3 V ice cold 70% EtOH.
4. Vortex and keep at -80°C for at least 1 h or at -20°C overnight. At this point the sample can be stored for a longer period.
5. Centrifuge at 12000 g, 10 min, 4°C.
6. Wash the pellet with 1 V 70% EtOH and air-dry for 5-10 min, RT.

7. Redissolve in DEPC-treated dH_2O.

Next, tRNA concentration was measured with Nanodrop ND100 and its integrity was checked roughly by running 1 μg of tRNA in a 1.5% agarose gel to detect, if any, DNA contamination and the ribosomal bands (in human material the two bands that can be detected are that of the 28s and 18s, corresponding to a band of 5 and 1.9 kb respectively).

A total of 100 ng tRNA per reaction in a volume of 20 μL was subjected to reverse transcription using the TaqMan RT-PCR reagents (Applied Biosystems, Cat. No. N808-0234) and a GeneAmp PCR System (Applied Biosystems, Life Technologies, Thermo Fisher Scientific Inc.).

Alternatively, reverse transcription was performed using the AffinityScript Multi Temperature cDNA Synthesis Kit (Cat. No. #200436, Agilent Technologies) according to the manufacturer's instructions as follows:

1. Set up the reaction (add in the following order):
   - 3-5 μg of tRNA
   - RNase-free dH_2O to a total volume of 15.7 μL
   - 1 μL of oligo(dT) primer (stock: 0.5 μg/μL) or 3 μL of random primers (stock: 0.1 μg/μL)
2. Incubate for 5 min, at 65°C (primer melting).
3. Cool for 10 min, RT (primer annealing).
4. Add the following in order:
   - 2 μL 10xAffinityScript RT Buffer
   - 0.8 μL of dNTP mix (25 mM of each dNTP)
   - 0.5 μL of RNase Block Ribonuclease Inhibitor (stock: 40 U/μL)
   - 1 μL AffinityScript Multiple Temperature RT

5. Incubate for 10 min, at 25°C.

6. Incubate for 60 min, at 55°C.

7. Incubate for 15 min, at 70°C.

8. Store at 4°C or -20°C or use right away.

C.3.3. Real-time PCR and analysis

Expression levels of genes encoding TAG-1 (*Cntn2*), CASPR2 (*Cntnap2*), CASPR (*Cntnap1*) and GAPDH as the 'housekeeping' control gene (for primer sequences see Table 5, Appendix) were examined by quantitative real-time PCR analysis using the iTaq™ Universal SYBR® Green Supermix (Cat. No. #172-5121, Bio-Rad Laboratories, Inc.) and a StepOnePlus Real-Time PCR system (Applied Biosystems, Life Technologies, Thermo Fisher Scientific Inc.).

For each gene, the standard curve was generated using as template cDNA acquired from post-mortem human cerebellum and the following quantities (corresponding to the tRNA input): 100, 10, 1, 0.1, 0.01 and 0.001 ng.

Each reaction was setup as below:

- cDNA solution (corresponding to the quantities above)
- 10 μL 2xiTaq™ SYBR Green Supermix with ROX (Bio-Rad)
- 2 μL forward primer (stock: 2 μM)
- 2 μL reverse primer (stock: 2 μM)
- dH_2O to a final volume of 20 μL

PCR runs were setup as below:

Step	Temperature	Time	
1.	95°C	2 min	
2.	95°C	15 sec	Repeat steps 2-4 40 times
3.	58°C	45 sec	
4.	72°C	30 sec	
5.	72°C	10 min	
6.	Melting curve according to the instrument's settings		

Following PCR runs, reactions were visualized on a 2% agarose gel to check for unspecific products or contamination.

PCR runs were performed for each sample in duplicates using cDNA corresponding to 10 ng of total RNA. Expression levels for each gene in MS samples (NAWM and chronic lesions) were calculated as the fold induction value (2^{DDCt}) relative to control cases and to MS NAWM (only chronic lesions).

Data are expressed as mean±standard error of the mean and statistical analysis was performed using GraphPad Prism version 5.00 for Windows (GraphPad Software). mRNA levels were compared using unpaired t test and differences were considered as significant when $P<0.05$. Expression levels in CALs and CILs were also calculated (2^{DDCt}) relative to the NAWM (mean ± SD).

C.4. Immunoblot analysis

Samples obtained from WM of non-MS control patients (n=3 cases), MS NAWM (n=3 cases, one PPMS case and two SPMS cases) and chronic lesions (n=2 active lesions and 1 inactive from 3 cases, all being SPMS cases) (see Table 4, Appendix) were collected from characterized snap-frozen tissue blocks as explained above.

C.4.1. Tissue lysis and sample preparation

Dissected areas from snap-frozen tissue blocks were lysed in ice-cold NP40 buffer

followed by a brief sonication on ice with a dismembrator (Fisher Scientific). Protein concentration was measured with Nanodrop ND100. Lysates were either stored at -20°C (or -80°C for longer term storage) or immediately used for sample preparation.

Each sample was prepared with 60 µg of total protein with the addition of the appropriate amount of 2x or 4xLaemmli Sample Buffer. After mixing, samples are incubated for 5 min at 100°C and subsequently cooled on ice. Prepared samples were stored at -20°C or ran right after preparation.

NP-40 Buffer	**2xLaemmli Sample Buffer**
0.5% w/v NP-40	125 mM Tris-base
10 mM Tris–HCl, pH 7.4	4% sodium dodecyl sulfate (SDS)
2 mM EDTA	20% glycerol
100 mM NaCl	100 mM dithiothreitol (DTT)
0.017 mg/ml phenylmethylsulfonyl fluoride (Sigma-Aldrich)	Bromophenol blue
	Adjust pH to 6.8

C.4.2. Protein separation with SDS-polyacrylamide gel electrophoresis (SDS-PAGE)

Protein samples prepared as described above were fractionated by 8 or 12% SDS-polyacrylamide gel electrophoresis (SDS-PAGE, Bio-Rad). Gels were prepared as outlined below:

Stacking gel (1 minigel 1.5 mm-thick)	**Separating gel (For 1 minigel 1.5 mm-thick)**		
	8% acrylamide	**12% acrylamide**	
1 mL 30% acrylamide	2.67 mL	4 mL	30% acrylamide
0.75 mL Tris-HCl 1M, pH 6.8 + 0.4% SDS	2.5 mL	2.5 mL	Tris-HCl 1.5M, pH 8.8 + 0.4% SDS
60 µL 10% ammonium persulfate (APS)	100 µL	100 µL	10% APS
6 µL N,N,N',N'-tetramethylethylenediamine (TEMED, Merck)	8 µL	8 µL	TEMED
4.1 mL dH_2O	4.63 mL	3.3 mL	dH_2O

The gel was placed in the wet electrophoresis tank (Bio-Rad) according to manufacturer's instructions and covered with 1 L 1xSDS-PAGE Running Buffer (see section below). Prepared samples were loaded in the buffer-submerged wells, next to a commercial protein ladder. The electrophoresis device was set to 80 V during the packing of the samples in the stacking gel and then to 100-120 V until the bromophenol blue exits the gel.

C.4.3. Western Blotting

The gel with the fractionated proteins was removed from the device and proteins were transferred to a Hybond-C extra membrane (Amersham, GE Healthcare Bio-Sciences) with the following wet-transfer method:

1. The stacking gel is removed and the rest of the gel is placed on top of a presoaked (in 1xTransfer Buffer) Hybond-C extra membrane of equal size between two pieces of presoaked Whatman paper (Whatman, GE Healthcare) on each side, flanked by two sponges, inside the plastic tray. The gel should be at the side of the tray which is coloured black and the membrane at the red or white side.

2. The whole plastic tray is closed carefully to avoid bubbles and placed in the transfer tank, with the black side towards the black side of the tank.

3. The tank is then filled with freshly made cold 1xTransfer Buffer until the plastic tray is completely submerged in the buffer and the accompanying ice container is also placed in the tank (this helps maintain the temperature as low as possible).

4. The whole tank is placed in a container filled with ice and then the device is set to 310 mA for 1h to ensure the transfer of the proteins from the gel to the membrane.

10xRunning/Transfer Buffer (RTB) (V_{final}=5 L)	**1xSDS-PAGE Running Buffer**	**1xTransfer Buffer**
50 g sodium dodecyl sulfate (SDS)	10% v/v 10xRTB in dH_20	10% v/v 10xRTB
720 g glycine		20% v/v methanol in dH_20
150 g Tris-base		
Fill up to a final volume of 5 L with dH_20		

C.4.4. Immunoblotting

1. The membrane is carefully removed from the apparatus and briefly washed in 1xPBS-T.
2. Blocking with 5% BSA in 1xPBS-T for 1 h at RT.
3. Incubation with the appropriate antibodies follows (see Table 1, Appendix) in 5% BSA in 1xPBS-T at 4°C overnight.
4. Washes (3x) with 1xPBS-T, 15 min each.
5. Incubation of the membrane with the appropriate horseradish-conjugated secondary antibodies (see Table 2, Appendix).
6. Washes (3x) with 1xPBS-T, 15 min each.
7. Visualization of signal with enhanced chemiluminescence (ECL Plus, Amersham, GE Healthcare Bio-Sciences).

10xRunning/Transfer Buffer (RTB) (V_{final}=5 L)	**1xSDS-PAGE Running Buffer**	**1xPBS-T**
50 g sodium dodecyl sulfate (SDS)	10% v/v 10xRTB in dH_20	0.1% v/v Tween-20 in 1xPBS
720 g glycine	**1xTransfer Buffer**	
150 g Tris-base	10% v/v 10xRTB	
Fill up to a final volume of 5 L with dH_20	20% v/v methanol in dH_20	

C.4.5. Quantification of results obtained by Western Blot

Band intensity was quantified using the ImageJ software, version ImageJA 1.45b (Schneider, Rasband et al. 2012) and normalized for loading against GAPDH. Expression levels are normalized against the mean of the values acquired from the control white matter samples and expressed as % percentage. Data are expressed as mean±standard error of the mean and statistical analysis was performed GraphPad Prism version 5.00 for Windows (GraphPad Software). Normalized protein levels were compared using unpaired t test and differences were considered as significant when $P<0.05$.

C.5. Immunohistochemistry on cryosections

Immunohistochemistry on cryosections (10 μm-thick) of PFA-fixed material from patients with non-neurological pathology (n=3 cases) and MS (n=5 cases) was performed as below:

11. Cryosections are removed from -20°C, encircled in Dako Pen (Cat. No. S200230, Dako, Agilent Technologies) and post-fixed in ice-cold methanol at -20°C for 8 min.

12. Washes (3x) in 1xPBS, 5 min each.

13. Incubation in Blocking Solution of 2% normal horse or goat serum (NHS or NGS respectively) in 0.5% Triton X-100 in 1xPBS for 20 min at RT.

14. Incubation with the appropriate primary antibodies (see Table 1, Appendix) diluted in

Blocking Solution at 4°C, overnight.

15. Washes (3x) in 1xPBS, 5 min each.
16. Incubation with the appropriate biotinylated secondary antibodies (see Table 2, Appendix) in Blocking Solution for 1h at RT.
17. Incubation with fluorescently marked streptavidin in combination with the appropriate secondary antibodies directly fluorescently labeled (see Table 2, Appendix) in Blocking Solution for 1 h, RT.
18. Nuclear counterstaing with DAPI (0.1μg/mL, Sigma-Aldrich), for 15 sec, RT.
19. Washes (2x) in dH_2O, 5 min each.
20. Wash in 1xPBS for 5 min.
21. Incubation in 70% EtOH for 5 min.
22. Incubation in Autofluorescence Eliminator Reagent (Cat. No. 2160, Chemicon, Merck Millipore, Merck KGaA) for 8-10 min.
23. Wash (3x) in 70% EtOH for 1 min.
24. Mount using Fluorescent Mounting Medium (Cat. No. S3023, Dako, Agilent Technologies).
25. Slide storage at 4°C until imaging take place and for long term storage after it is completed.

Imaging took place using two confocal microscopes (TCS SP2 and TCS SP8, Leica Microsystems GmbH).

C.5.1. Quantification of juxtaparanodal length and perinodal clustering

For the quantification of perinodal clustering, analysis was performed on control WM and MS tissue cryosections labeled for TAG-1 and Caspr. In this study we included control WM (n=3 cases), MS NAWM (n=4 cases), CAL (n=4 cases) and CIL (n=2 cases). Images

were acquired using the same laser and detector settings for all samples. The percentage of paranodes (PNs) with or without juxtaparanodes (JXPs) and juxtaparanodes without paranodes were counted in at least 5 frames of an area of 67x67 μm per case and were expressed as percentage over the total number of all three types of perinodal phenotypes, in order to eliminate the factor of heterogeneity of axonal density in the samples. The diameter and length of TAG-1+ JXPs was measured in the normally clustered cases (that is, when flanking PNs) in the same frames using the ImageJ software, version ImageJA 1.45b (Schneider, Rasband et al. 2012). Juxtaparanodal profiles were also measured in frames acquired from cryosections labeled for Caspr2 and Caspr, in the same way as for TAG-1. Data are expressed as mean±standard error of the mean and statistical analysis was performed GraphPad Prism version 5.00 for Windows (GraphPad Software, San Diego, CA). Juxtaparanodal length measurements were compared using unpaired t test and differences were considered as significant when $P<0.05$.

D. RESULTS I

D.1. Introduction of the *Tag-1-/-* genotype in the C57BL/6 background

In order to successfully induce EAE, we ought to use it on mice of the C57BL/6 strain. This strain shows the appropriate responsiveness due to the fact that it bears the major histocompatibility locus H-2 (MHC_{H-2}) shown to be indispensable for disease onset (Montgomery and Rauch 1982). This required the crossing of *Tag-1-/-* mice (belonging to the C57B110/CBA genetic background) with wild type mice of the C57BL/6, followed by crossing of the resulting *Tag-1+/-* again with wild type mice of the C57BL/6 for 4 consecutive generations (see Figure 13). Eventually, the mice that arose were of approximately 98% purity concerning the genetic background and *Tag-1+/-* mice were then crossed between them to generate both wild type and knock out animals.

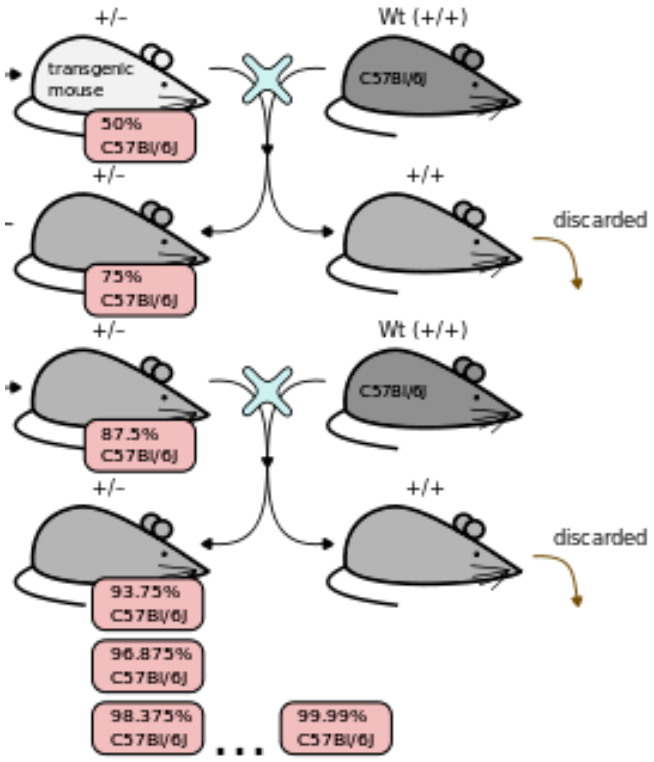

Figure 13. Schematic showing the procedure of back-cross of any transgenic or mutant mouse in the C57BL/6 background. Successive crosses resulted in a continuously purer, closer to the C57BL/6, genetic background.

D.1.1. Analysis of the *Tag-1-/-* juxtaparanodal phenotype in the C57BL/6 background

Following the backcross and the generation of *Tag-1+/+* and *Tag-1-/-* mice in the C57BL/6 background, we analyzed comparatively the cerebellum of these animals. We have previously reported that in the absence of TAG-1 JXPs suffer from Caspr2 loss and VGKC diffusion, both in the CNS and PNS (Traka et al 2003). The mutant juxtaparanodal phenotype was further examined in the optic nerve, hippocampus and cerebellum, yielding similar results (Savvaki et al 2008; Savvaki et al 2010).

Before proceeding to further experiments on the backcrossed mice, we asked whether the genetic background would have an effect on the mutant phenotype. We performed immunohistochemical experiments on cryosections derived from adult cerebellum against the paranodal marker Caspr (Figure 14, in red) and the juxtaparanodal markers Caspr2 (Figure 14, panels A-D) and the isoform Kv1.1 of the VGKCs (Figure 14, panels E-H). *Tag-1+/+* and *Tag-1-/-* animals from both fore mentioned genetic backgrounds were examined comparatively.

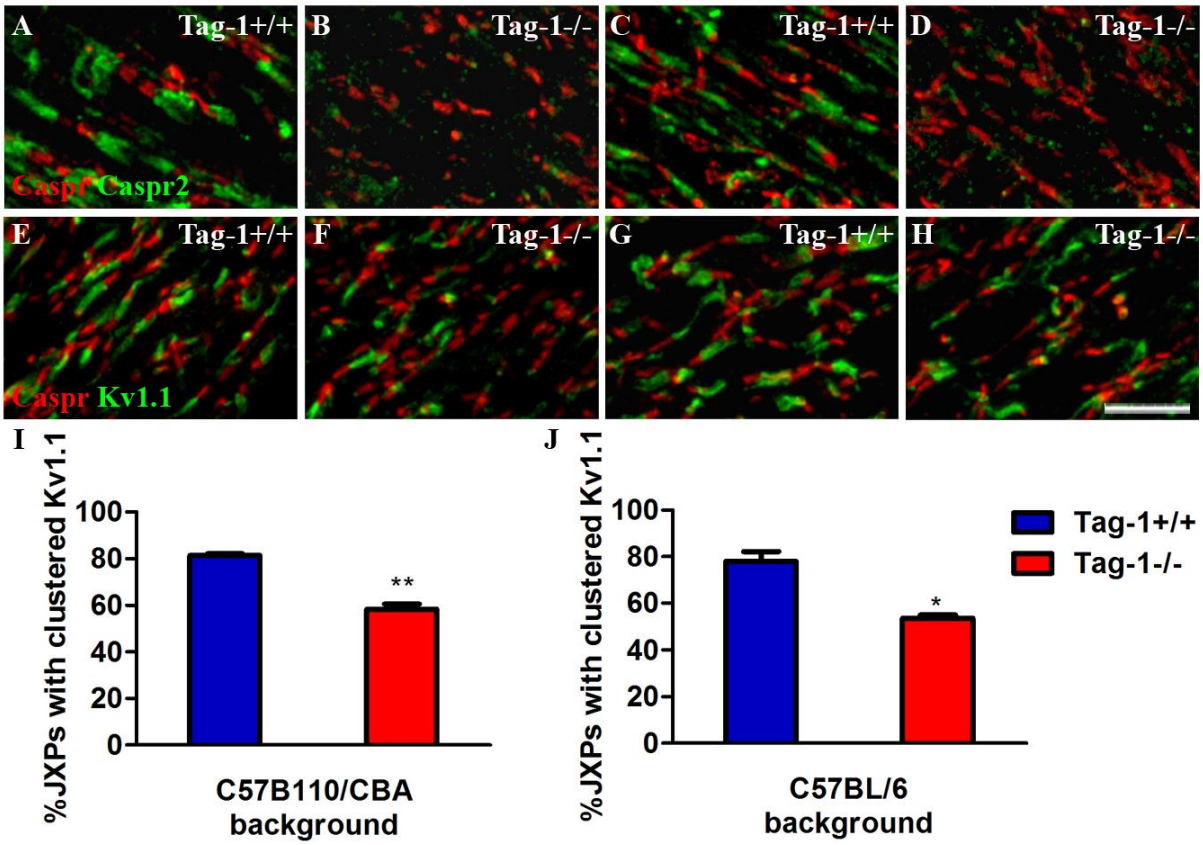

Figure 14. Comparison of the juxtaparanodal phenotype of *Tag-1*$^{-/-}$ mice in the C57B11/CBA and C57BL/6 genetic background in the cerebellum. Immunohistochemistry on cryosections from adult cerebellum against Caspr (in red) and either Caspr2 or the Kv1.1 isoform of VGKCs (both in green), in the C57B110/CBA (A, B, E, F) and the C57BL/6 (C, D, G, H) background depicts loss of Caspr2 in the absence of TAG-1 and the reduction of VGKC clustering. (I, J) Quantification of VGKC clustering in the C57B11/CBA and C57BL/6 genetic background respectively resulted in 81.4% and 77.9% in *Tag-1*$^{+/+}$ and 58.4% and 53.5% in *Tag-1*$^{-/-}$(n=2 in all cases). Scale bar in (A-H) =10 μm. JXPs: juxtaparanodes (P<0.05 : *; P<0.01 : **)

Caspr2 clustering was not quantified but the loss of the protein was obvious in both backgrounds (Figure 14, panels A-D). VGKC clustering was found, as expected, significantly reduced in both backgrounds when TAG-1 was absent, exhibiting a slightly more statistical significance in the C57B110/CBA background compared to that in the C57BL/6 background (28.3% versus 31.3% respectively, see Figure 14, graphs at panels I, J). Similar observations were made on cryosections from optic nerve and spinal cord of adult mice (data not shown).

Conclusion: *JXP clustering does not depend on the genetic background. The described diffusion of Caspr2 and VGKCs in Tag-1-/- in the C57B110/CBA strain remained also in the C57BL/6 background, although with a slight difference in statistical significance.*

D.2. Characterization of the stages and clinical picture of MOG_{35-55}-induced Experimental Autoimmune Encephalomyelitis (EAE)

Following the assessment of the juxtaparanodal phenotype in the C57BL/6 background, we proceeded to EAE-induction experiments on these wild type mice in order to characterize the clinical course, symptom severity and the most well established histopathological findings in EAE (i.e. infiltration, demyelination and axonal loss). In this protocol, researchers artificially activate the immune system in the periphery in the presence of a small myelin antigen (in this case the peptide MOG_{35-55}) to induce autoimmunity directed against myelin. In addition, they introduce a BBB-disrupting factor (pertussis toxin) to allow the infiltration of the autoreactive immune cells in the CNS (for full protocol description, see section "Materials and Methods"). This approach, depending on the mouse strain and occasionally the laboratory conditions and mouse handling, will result either in an acute neurological disease of the spinal cord with ascending symptoms or a relapsing-remitting form, which is less frequent and usually occurs in another mouse strain (Ransohoff 2012).

The induced disease was characterized by discrete stages of symptom severity, while the control group that received only the CFA did not exhibit any of the symptoms (Figure 15).

Initially, the first days post-induction (dpi) are symptom-free, and an initial onset is seen around 10-11 dpi. In a matter of 3-5 days the clinical score reaches a maximum, which lasts for 2-4 days, followed by partial recovery. Almost a week later, animals show the first relapsing-remitting episode and relapses from then on are characterized by reduced symptom gravity overtime (Figure 15).

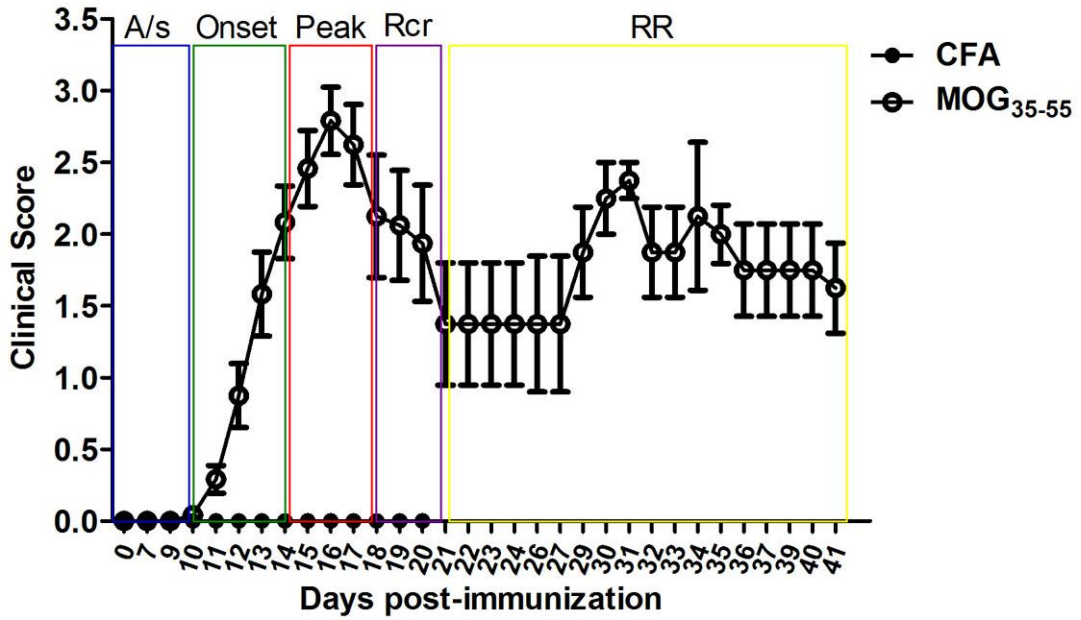

Figure 15. Clinical course of EAE in the C57BL/6 background. The diagram depicts the discrete stages of the acute disease followed by a relapsing-remitting stage assessed by daily scoring (MOG_{35-55}) versus the control CFA group, in which no symptoms were observed. N=12 (MOG_{35-55} group), 3 (CFA). Scale of clinical symptoms: 0: no neurological signs; 1: flaccid tail; 2: hindlimb (HL) weakness or abnormal wait; 3: complete HL paralysis; 4: complete HL paralysis and weakness of the forelimbs. CFA: CFA:Complete Freund's Adjuvant; A/s: asymptomatic; Rcr: recovery; RR: relapsing-remitting.

Based on the clinical course outlined above, we analyzed the degree of spinal cord infiltration, WM demyelination and axonal loss at the following time points: 16 dpi, corresponding to the peak of disease, 20 dpi where recovery has already initiated and 40 dpi, a point at which the pathology is regarded as chronic.

The infiltration of the WM of the spinal cord by macrophages and microglia was examined through inspection of the ionized calcium-binding adapter molecule 1 (IBA1) in the whole of the spinal cord, from cervical to sacral areas (Figure 16, panels A-D). Compared to CFA-treated animals, the induced group showed an increase in IBA1+ cells in the spinal cord WM already at 16 dpi, which increased further by 20 dpi (Figure 16, panels A-C and graph E). At 40 dpi, however, infiltration had cleared and was comparable with that of the CFA

group (Figure 16, panel D). All of these observations were also confirmed through H&E morphological staining (Figure 17, panels B and H-K).

Comparison of the degree of IBA1+ cell infiltration between the discrete areas of the spinal cord from rostral to caudal shows that this correlates with the relative WM versus GM area and not with the entry point of autoreactive cells to the CNS, which is thought to be the sacral area. For instance, cervical and thoracic levels have a higher WM/GM ratio versus lumbar areas that is also reflected at the WM infiltration. At the sacral level of the spinal cord, however, our results show inconsistency compared to the other areas (Figure 16, graphs E and F).

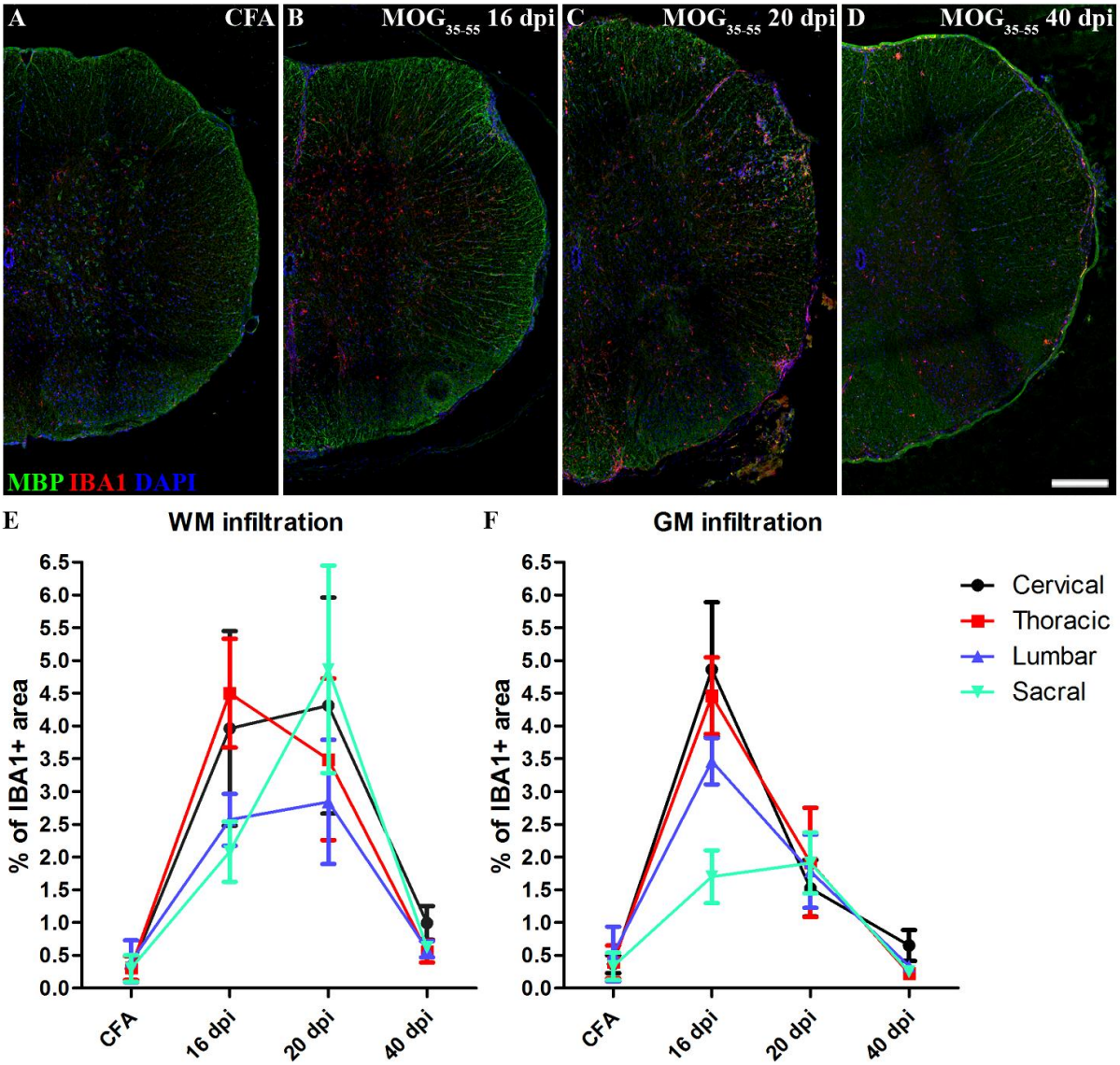

Figure 16. Evaluation of spinal cord infiltration in EAE in wild type mice. (A-D) Representative images from the thoracic spinal cord in CFA-treated and EAE-induced wild type mice. Immunohistochemistry against the macrophage/microglia marker IBA1 (red) and the myelin protein MBP (green) shows the increased infiltration of the spinal cord at 16 and 20 dpi. Note that lesions are not obvious with staining against MBP. (E) Graph of the quantified spinal cord infiltration of the white matter and (F) gray matter, at cervical, thoracic, lumbar and sacral levels. Nuclei are shown in blue (DAPI nuclear staining). (A-D) Scale bar=200 μm. WM: white matter; GM: gray matter.

Interestingly, the infiltration of the GM of the spinal cord shows a somehow different pattern. It is found increased greatly at 16 dpi and almost matches the degree of IBA1 coverage of the WM, but it subsides already 4 days later since it is found reduced compared to the IBA1 infiltration of the WM. At 40 dpi it is reaching the levels of CFA-treated animals (Figure 16, graph F). Notably, total spinal cord infiltration is almost identical to the pattern of GM infiltration while H&E morphological staining shows the coincidence of infiltrates with the IBA1+ staining (Figure 17).

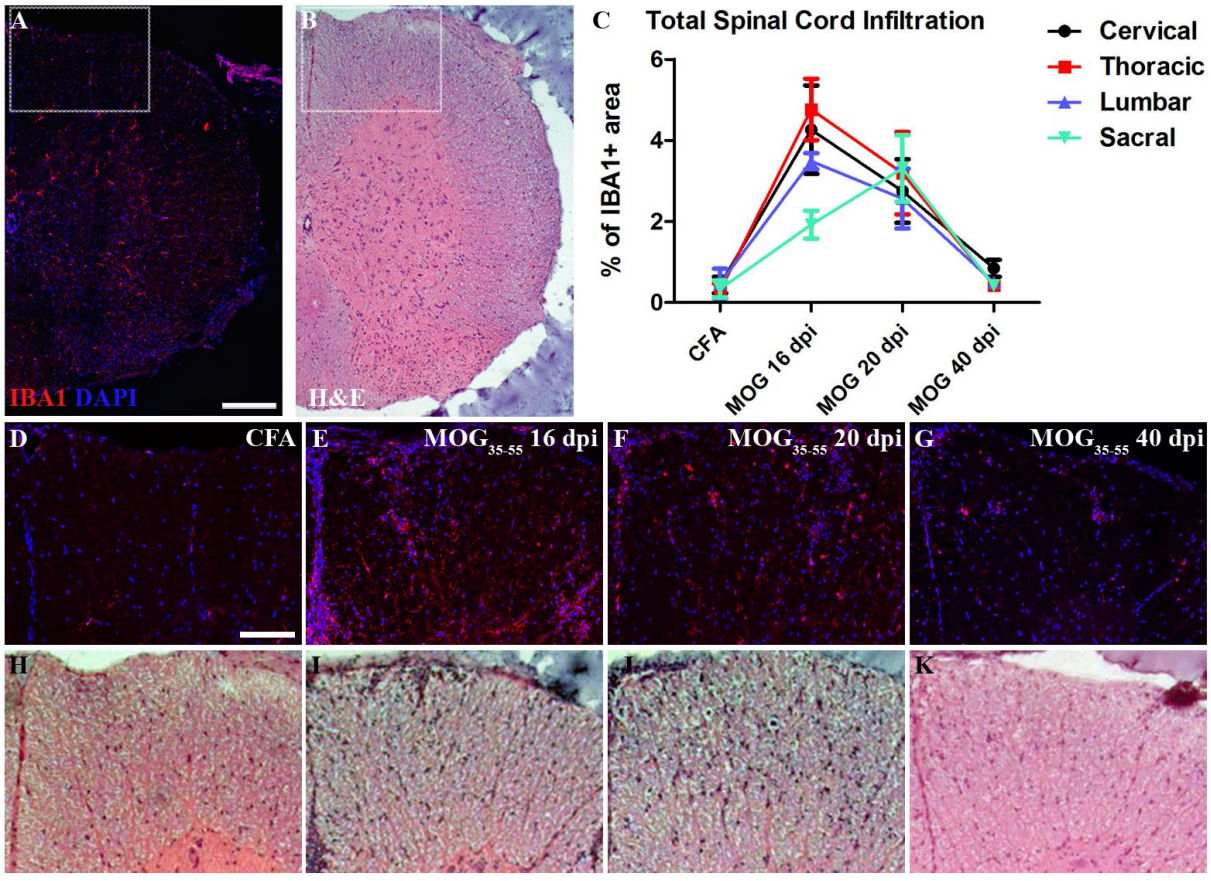

Figure 17. Total spinal cord infiltration in EAE in wild type mice. (A, B) A thoracic spinal cord section of a CFA-treated mouse analysed by immohistochemistry against IBA1 and H&E morphological staining, respectively. (C) Infiltration was quantified through IBA1 immunoreactivity in total spinal cord sections, peaking at 16 dpi and then gradually returning to similar levels as in the CFA group. (D-E) IBA1 signal in the

WM of the thoracic spinal cord in CFA and induced animals correlated with the H&E staining (H-K). In (A, D-G) nuclei are visualized with DAPI staining (in blue). Scale bar in (A, B) = 200 μm and in (D-K) 100 μm.

Next, we analyzed the degree of demyelination through immunostaining against the myelin protein PLP and axonal loss through immunostaining against the 200kDa neurofilament protein (NF200) in all spinal cord areas (Figure 18). As a result of EAE, lesions that were always associated with increased cellularity (as seen by DAPI nuclear staining) are observed at all examined time points without great variability. On the other hand, axonal loss is established even at 16 dpi and is gradually reduced but not reversed, since it is still at high levels at 40 dpi at most areas.

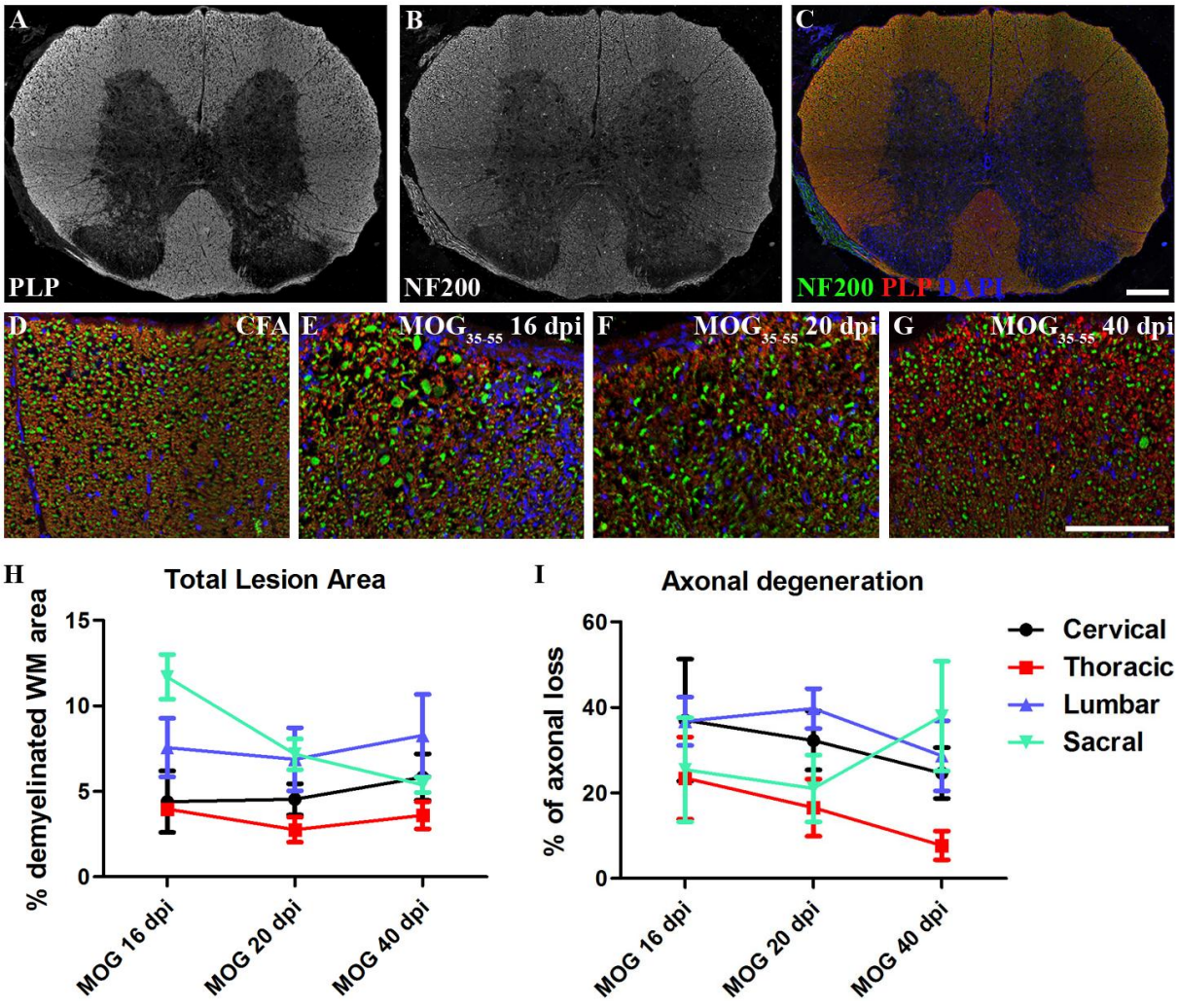

Figure 18. Analysis of demyelination and axonal loss in EAE in wild type mice. (A-C) Image from the thoracic spinal cord in a CFA-treated mouse showing immunohistochemistry against the myelin protein PLP (red) and the neurofilament marker NF200 (green). (D-G) Representative images from the thoracic spinal cord in CFA-treated and EAE-induced wild type mice with evident axonal loss which is partially reversed at 40 dpi. (H) Graph of the quantified demyelinated areas of the WM in EAE-induced mice and (I) the axonal loss at cervical,

thoracic, lumbar and sacral levels compared to CFA-treated mice. Nuclei are shown in blue (DAPI nuclear staining). Scale bar (A-C) =200 μm, **(D-G)** 100 μm.

Overall, at 16 dpi microglial/macrophage infiltration is uniform in the WM and GM, demyelination is more profound compared to later stages and axonal degeneration has already initiated. At 20 dpi, we observed infiltrates mostly found at WM areas and a significant degree of demyelination in all areas accompanied by axonal loss ranging from 20-40%, which is reduced compared to 16 dpi in areas that are further from the infiltrate entry point (i.e. cervical and thoracic areas). While at 40 dpi IBA1+ infiltration is greatly reduced, cells of immune or other identity are populating areas of former lesions while there is a significant degree of axonal recovery, but not is sacral areas.

The above observations point to the fact that a meaningful time point to study is 20 dpi, where demyelination and axonal loss are prominent. Additionally, while at 16 dpi infiltrates cover in the same degree the spinal cord WM and GM, at 20 dpi the inflammation is mostly focused at the WM. Another important observation is that the sacral portion of the spinal cord does not yield results that are consistent with other areas, probably due to its small cross-section area, which increases variations, even though it is the portion of the spinal cord with the highest degree of inflammation and relative demyelination.

Conclusion: *Following EAE induction, the peak of the neurological symptoms or the acute phase of the disease coincides with detectable demyelination, microglia/macrophages infiltrating the spinal cord and significant axonopathy. A few days after, clinical symptoms have decreased only mildly, infiltration is mildly reduced, especially in the GM, while axonal loss and demyelination persist. During the chronic stage of EAE, infiltration levels are similar to those in animals that do not present autoimmunity, while demyelination persists and axonal loss has partially been reversed.*

D.3. EAE induction on *Tag-1*+/+ versus *Tag-1*-/- mice

D.3.1. Analysis of susceptibility and disease course and duration in the absence of TAG-1

Apart from the JXP phenotype that we have already described, *Tag-1* null mice show hypomyelination of the optic nerve and loss of small caliber axons (Chatzopoulou et al 2008). Taking in account the implication of the protein in MS pathology as a potential autoantigen

(Derfuss et al 2009), we were led to test the potential hypothesis that in its absence demyelination or remyelination might be affected.

As mentioned, following EAE induction, at 20 dpi there is substantial inflammation, demyelination and axonal loss, followed by the occurrence of clear clinical symptoms. Thus, we chose to induce EAE to wild type and *Tag-1-/-* mice and analyze comparatively their clinical picture and pathology at the tissue level.

Initially, following induction, both genotypes began to show symptoms on the same days (see Figure 19, graph B and Table 1 - onset), but mutant animals showed significantly reduced symptom severity. Eventually, both genotypes reached the same maximum score (Figure 16, graph A), but in animals lacking TAG-1 this happened 2-3 days later compared to wild type, followed by similar levels of partial recovery in both cases (Figure 19, graph B).

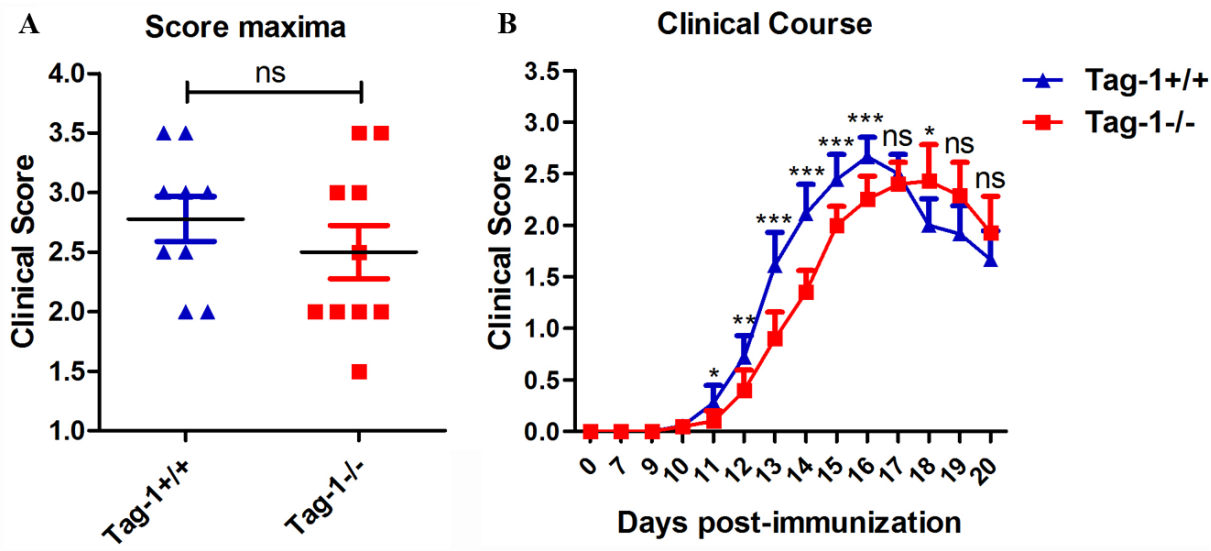

Figure 19. Clinical course and severity of EAE in *Tag-1*+/+ and *Tag-1-/-* mice. (A) Graph representing the maximum score that was reached in every induced animal over the course of the days of scoring. (B) Graph showing the course of symptoms after daily scoring. N=9 (*Tag-1*+/+) and 10 (*Tag-1-/-*). Scale of clinical symptoms: 0: No neurological signs; 1: Flaccid tail; 2: Hindlimb (HL) weakness or abnormal wait; 3: Complete HL paralysis; 4: Complete HL paralysis and weakness of the forelimbs; 5: Moribund or deceased. (ns: non-significant; P<0.05: *; P<0.01 : **; P<0.0001 : ***)

Furthermore, the responsiveness of *Tag-1*+/+ and *Tag-1-/-* animals to the induction was found comparable, indicating similar onset of inflammation and/or response of the tissue to pathology, as well as the efficacy of the used protocol (see Table 1 - % of prevalence).

Table 1. Clinical characteristics of EAE on *Tag-1*+/+ versus *Tag-1*-/- mice.

Genotype	Onset (dpi)	Peak (dpi)	Recovery (dpi)	Prevalence (%)	N
***Tag-1*+/+**	10-14	14-17	18 and on	78.6	14
***Tag-1*-/-**	10-13	16-19	20 and on	77.8	18

*Dpi: Days post-induction

Next, we went on to analyze the degree of demyelination and axonal degeneration at the acute stage (i.e. at 20 dpi), in the two genotypes as previously described. At least in wild type mice, the most prominent demyelination and axonal loss were observed at cervical and lumbar levels, while this holds true only for the lumbar area in the case of mutant animals, since we observed that the cervical spinal cord of *Tag-1*-/- mice was spared from demyelination (Figure 20). However, even in the absence of demyelination, axonal loss in cervical areas is pronounced in both genotypes. Overall, in wild type mice, the degree of axonal loss correlates with the degree of demyelination. Additionally, the thoracic spinal cord, even though is similarly demyelinated in *Tag-1*+/+ and *Tag-1*-/- mice, the extent of axonal loss in the latter case is smaller.

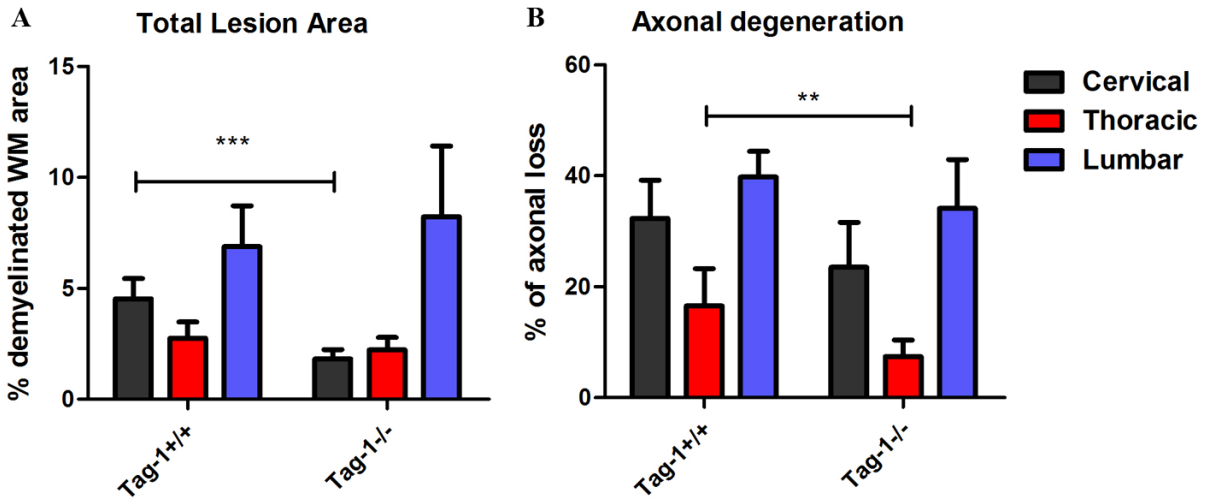

Figure 20. Analysis of demyelination and axonal loss in EAE in *Tag-1*+/+ versus *Tag-1*-/- mice. (A) Graph of the quantified total demyelinated areas of the WM in EAE-induced mice and (B) the axonal loss at cervical, thoracic and lumbar levels compared to CFA-treated mice. N=6 (*Tag-1*+/+) and 7 (*Tag-1*-/-). WM: white matter. (P<0.01 : **; P<0.0001 : ***)

We also asked whether the axonal density at the spinal cord differs in *Tag-1*+/+ versus *Tag-1*-/- naïve animals. To address this question, we performed analysis of axonal

counts through NF200 staining in the spinal cord in the areas of the ventral and lateral funiculus, two well-defined axonal tracts. Our analysis showed that there is no substantial difference in axonal density in either area in the presence or absence of TAG-1 (Figure 21).

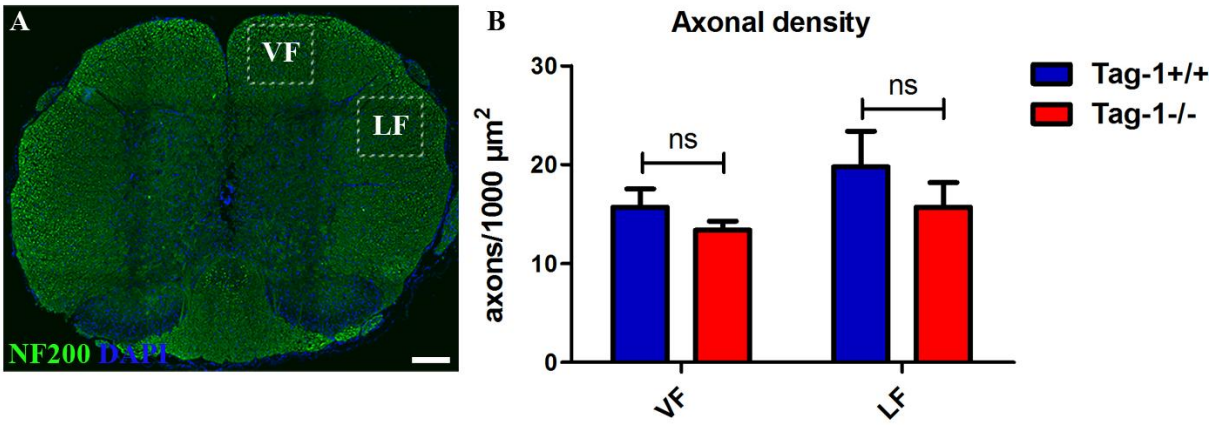

Figure 21. Analysis of axonal density in the spinal cord of naive *Tag-1*+/+ versus *Tag-1*-/- mice. (A) Representative section of the spinal cord at the thoracic level stained for the neurofilament marker NF200. Insets show the areas that were analyzed by counting axonal profiles and normalizing against the area in which they were distributed. (B) Quantification of the axons at thoracic spinal cord segments revealed no significant difference between *Tag-1*+/+ (N=2) and *Tag-1*-/- mice (N=2). Scale bar in (A) = 200 µm. P=0.30 in the VF and 0.39 in the LF. VF: ventral funiculus; LF: ventral funiculus; ns: non-significant.

Conclusion: *Following EAE induction, Tag-1-/- mice show a delay in neurological decline compared to Tag-1+/+, while both genotypes are comparably susceptible to the induction. Neuropathological findings at the acute stage are spread at the whole of the spinal cord in wild type mice, while in Tag-1-/- they seem to affect mostly caudal areas. Additionally, Tag-1-/- mice exhibit axonal loss at cervical levels in the absence of demyelination, a phenotype that cannot be explained by reduced axonal density in naïve animals.*

D.3.2. Analysis of the profile of inflammatory infiltrates in the absence of TAG-1

From the analysis of the EAE-induced wild type animals, we had noticed that IBA1 infiltration levels at 20 dpi correlate with total lesion area and axonal loss. Additionally, at 20 dpi there was a preference of IBA1+ for the WM versus to the GM of the spinal cord. Based on these observations, we asked whether the same happens in the absence of TAG-1. To address this, we performed quantification of IBA1+ area in total spinal cord sections and at WM or GM areas.

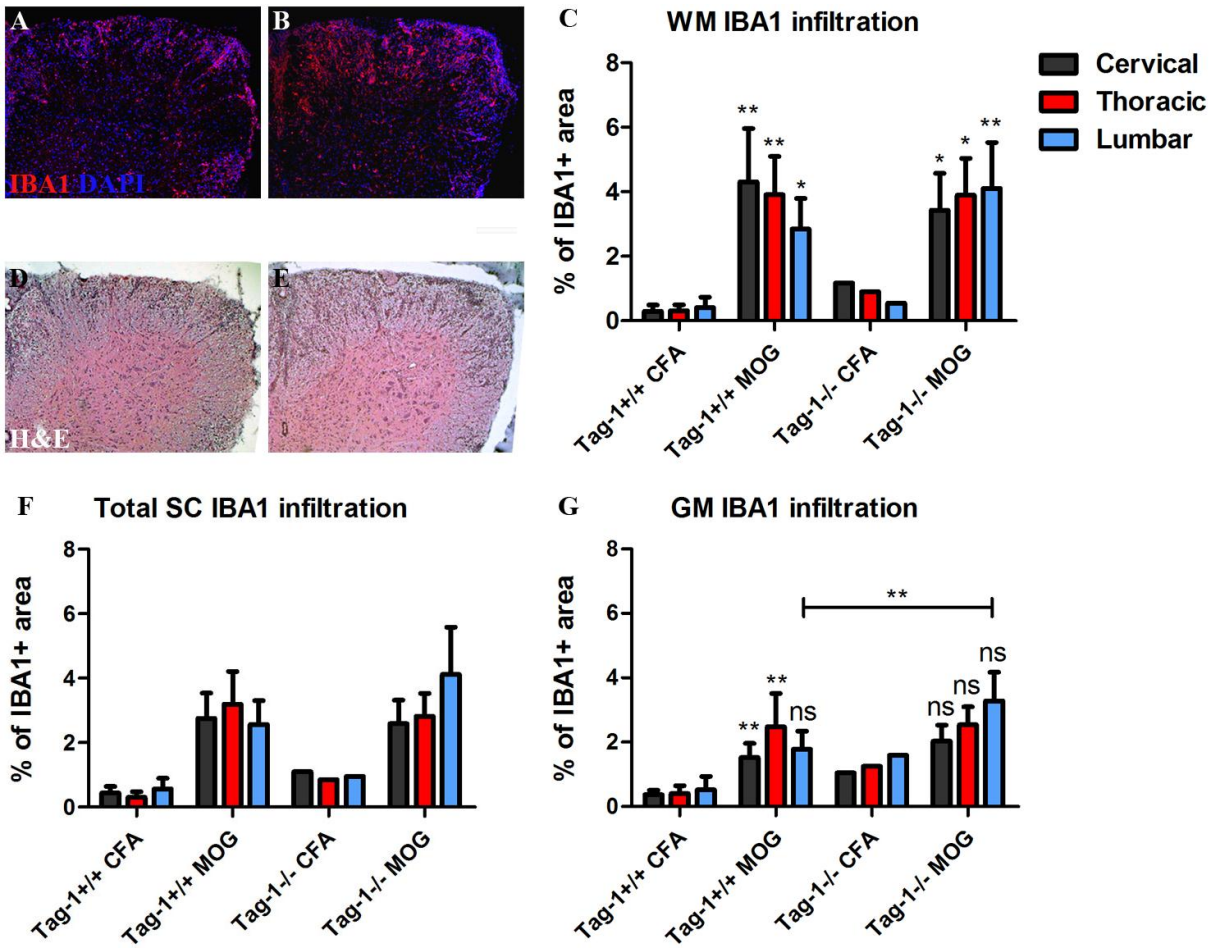

Figure 22. Analysis of IBA1+ infiltrates in the spinal cord of induced *Tag-1*+/+ versus *Tag-1*-/- mice. (A-B) Representative images of the spinal cord at the lumbar level stained for IBA1 of an induced Tag-1+/+ and Tag-1-/- mouse respectively. (C) Quantification of infiltrates at the white matter of the spinal cord. (D-E) Representative images of H&E staining of the spinal cord at the lumbar level of an induced Tag-1+/+ and Tag-1-/- mouse respectively. (F, G) Quantification of total spinal cord infiltrates and only of the gray matter respectively. N=6 (*Tag-1*+/+) and 7 (*Tag-1*-/-). Scale bar in (A-B, D-E) = 200 μm. WM: white matter; GM: gray matter; SC: spinal cord. (ns: non- significant; P<0.05: *; P<0.01 : **)

Inspection of the spinal cord from cervical to lumbar levels revealed that *Tag-1*-/- induced animals show increased IBA1+ signal at the lumbar spinal cord, while in the rest of the spinal cord infiltration seems comparable (Figure 22, panels A-B and D-E and graph F). This increase seems to correspond mainly to increased levels of WM infiltrates (Figure 22, graphs C and G). Interestingly, the majority of microglial cells that occupy the spinal cord of wild type mice are found at the rostral part of the spinal cord (i.e. cervical and thoracic), while in knock-out mice the seem to be mostly located at lumbar levels, indicating a possible delay in the progression of the cells from the posterior towards the anterior spinal cord.

Nevertheless, IBA1+ cells (i.e. microglia and macrophages) do not account alone for disease onset or progression in EAE, since other cells of the adaptive and innate immune system take part in this procces. In order to address directly the activation of the immune system, we chose to isolate the total mononuclear cells from the spinal cords of induced animals at the peak of disease for both genotypes (i.e. at 17 dpi) and perform an analysis for markers of T cells and B cells using Fluorescence Activated Cytometry Sorting (FACS).

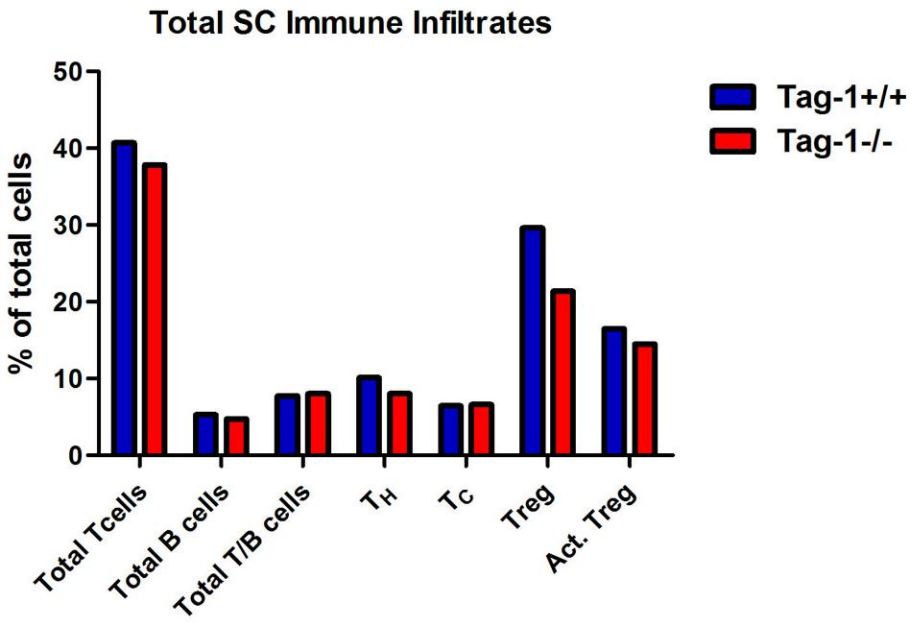

Figure 23. Analysis of spinal cord-infiltrating T- and B-cells in induced *Tag-1*+/+ and *Tag-1*-/- mice. Analysis of immune infiltrates was performed on total mononuclear cells of spinal cords using specific markers for each subpopulation. Each sample represents pooled cells from 3 animals per genotype. SC: spinal cord; T_H: helper T cells; T_C: cytotoxic T cells; Treg: regulatory T cells; Act. Treg: activated regulatory T cells.

This analysis showed that the percentages of total T cells, B cells, as well as the subpopulations of helper and cytotoxic T cells (T_H and T_C respectively) are comparable in *Tag-1*+/+ versus *Tag-1*-/- (Figure 23). Interestingly though, a significant difference was observed in the fraction of the regulatory T cells (Tregs), which was found approximately 28% reduced in *Tag-1*-/- compared to wild type animals. However, the portion of activated Treg was similar between the two genotypes.

In summary, we were not able to detect gross differences between induced animals of the two genotypes concerning either the vulnerability to demyelination or the neuropathological findings associated with the disease. Nevertheless, we encountered a significant difference involving the autoimmune infiltrates residing in the affected spinal cord.

The finding that Treg cells, responsible for the development of self-tolerance, are significantly reduced in *Tag-1-/-* mice around the peak of the symptoms points to an abnormality in mechanisms governing autoimmunity (Sakaguchi et al 2008).

Conclusion: *During acute EAE, microglial/macrophagal WM infiltrates in wild type animals are found in increasing levels from caudal to rostral levels of the spinal cord, while in knock-out animals the levels increase in the opposite direction, pointing to a possible delay in spreading of the cells. Furthermore, at the peak of the symptoms, Tregs were found significantly reduced in Tag-1-/- mice, suggesting failure in self-tolerance.*

D.4. Study of the role of TAG-1 in the demyelination and remyelination following LPC insult

Another way of inducing demyelination is through the use of toxin-mediated methods. Among these, the protocol using focal LPC injections in a selected white matter area induces timely and spatially restricted demyelination, which is considered reversible. As shown previously, following the induction of EAE, remyelination does not occur even at 40 dpi, despite the fact that axonal loss is partially reversed. In order to study de- and remyelination in a model that allows efficient remyelination without the effect of the systemic immune activation, we subjected adult mice to stereotactic LPC-injection at the corpus callosum (cc) (Figure 24, panel I). In this experimental setup, demyelination is induced at the day of injection or day 0 and after myelin clearance, lesions are obvious at 4-5 days post-injection (dpi) (Figure 24, panel B). At 5 dpi, OPC recruitment peaks and differentiation towards OLs starts at 10 dpi.

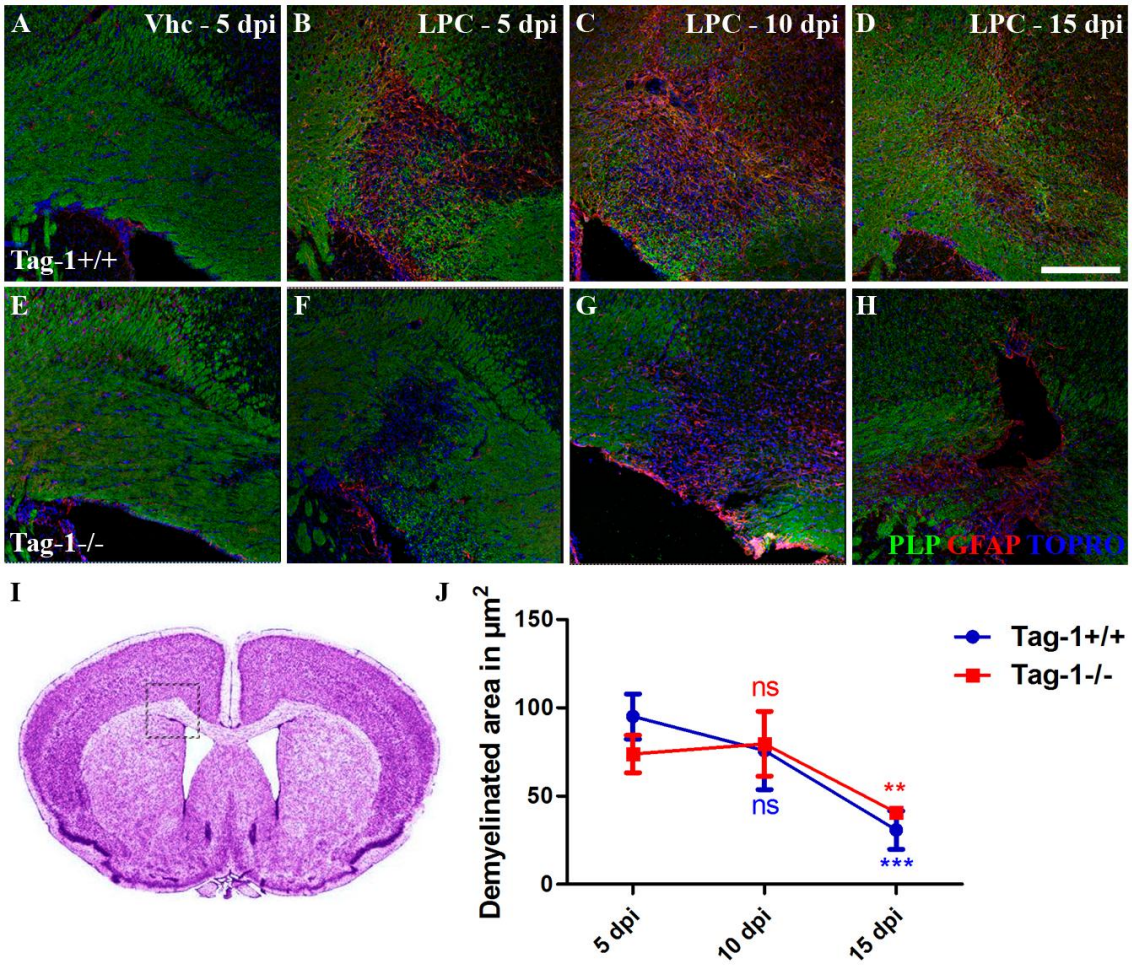

Figure 24. LPC-induced demyelination and remyelination in the corpus callosum of *Tag-1*+/+ and *Tag-1*-/- mice. (A-D and E-H) Representative images from the injection site in *Tag-1*+/+ and T*ag-1*-/- mice respectively at 5, 10 and 15 dpi. Immunohistochemistry against the astroglial marker GFAP (red) and the myelin protein PLP (green) shows the lesion and local astrogliosis and the gradual remyelination. (I) Cresyl staining of a coronal section of the mouse forebrain, with an inset showing the examined area of the corpus callosum. (J) Graph of the quantified lesion area at 5 (N=2 for each genotype), 10 (N=3 for each genotype) and 15 dpi (N=4 for *Tag-1*+/+ and 2 for *Tag-1*-/-). Statistics were performed by comparing each time point within the same genotype with 5 dpi. Nuclei are shown in blue (TO-PRO-3 nuclear staining). Scale bar in (A-H) =200 µm. Vhc: vehicle. (ns: non-significant; P<0.01 : **; P<0.0001 : ***)

No effect was induced by vehicle injection (Figure 24, panels A and E), while substantial demyelination was observed at 5 dpi in both genotypes and increased focal cellularity (seen by TOPRO nuclear staining, Figure 24, panels B and F). Remyelination was of a significant degree in both genotypes only at 15 dpi, reaching 67.7% of the original lesion area in *Tag-1*+/+ and 46% in *Tag-1*-/- (Figure 24, panels C and G and graph J). Although not statistically significant due to limited sample size, *Tag-1*-/- mice showed a tendency of delay or partial failure in the remyelination process of the corpus callosum.

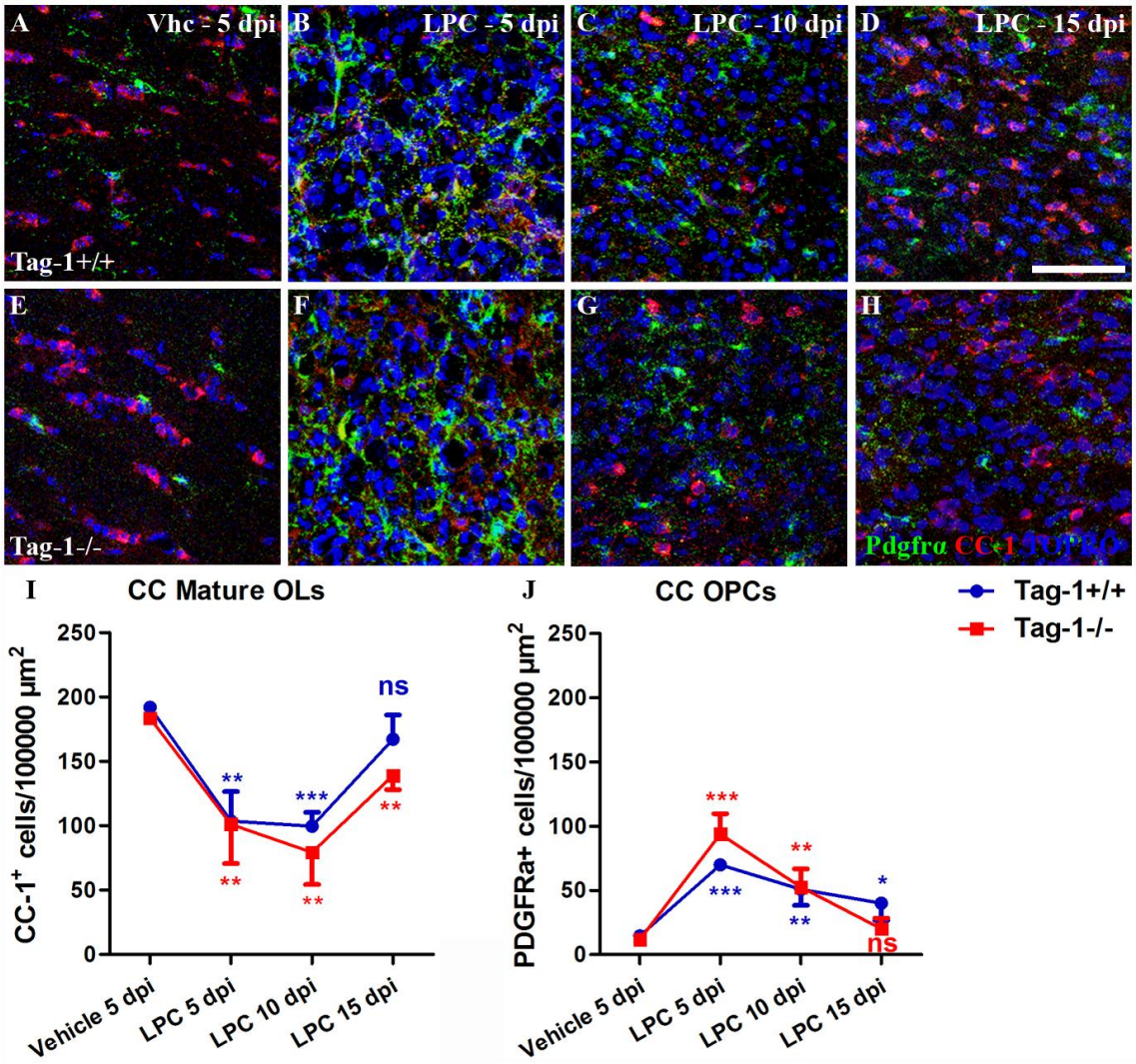

Figure 25. Changes in numbers of oligodendrocyte precursor cells and oligodendrocytes in LPC-induced demyelination and remyelination in the corpus callosum of *Tag-1*+/+ and *Tag-1*-/- mice. (A-G) Representative images from the injection site in the corpus callosum immunostained against the OL marker CC-1 (in red) and the OPC marker Pdgfrα (in green) at 5, 10 and 15 dpi. Note the increased density of cells in the site of injection at all time points following the procedure. (I) Quantification of the density of mature OLs and OPCs (J) in *Tag-1*+/+ and *Tag-1*-/- mice (N=2 for each genotype at 5 dpi either for vehicle or LPC injections), 10 (N=5 and 3 respectively) and 15 dpi (N=4 for *Tag-1*+/+ and 2 for *Tag-1*-/-). Statistics were performed by comparing each time point within the same genotype with 5 dpi. Nuclei are shown in blue (TO-PRO-3 nuclear staining). Scale bar in (A-H) = 50 µm. CC: corpus callosum; OLs: oligodendrocytes; OPCs: oligodendrocyte precursor cells; Vhc: vehicle. (ns: non-significant; P<0.05: *; P<0.01 : **; P<0.0001 : ***)

This observation lead us to examine the populations of OPCs and OLs at these time points, using immunohistochemistry against the OPC marker Pdgfrα and the OL marker CC-1 (Figure 25). Following vehicle injections, OPC and OL counts were identical in wild type and mutant animals (see Figure 25, panels A and E and graphs I and J). As expected, 5 dpi of LPC CC-1+ numbers were found reduced by almost 55% in both genotypes, followed by partial recovery in the case of wild type animals and in a smaller extent at mutant animals at 15 dpi

(counts of CC-1+ cells reached 87.4% of the vehicle-injected versus 75.9% in the case of mutant animals, see Figure 25, graph I). The levels of OPCs were found to be increased, as described in the literature, at 5 dpi and showed similar levels at the three analyzed time points, both in *Tag-1*+/+ and *Tag-1*-/-. Taking these results together, the small difference in remyelination at 15 dpi corresponds to a difference in CC-1 levels, which does not correspond to a difference in OPC numbers.

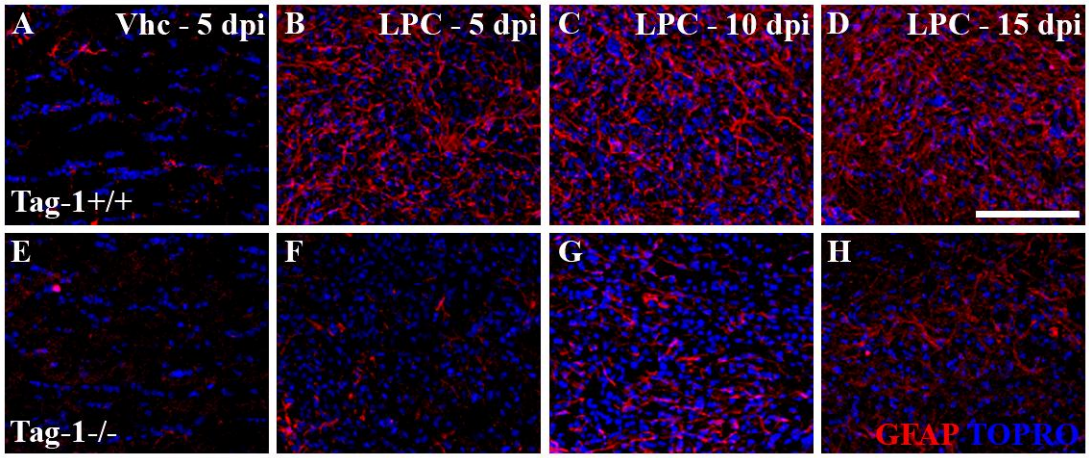

Figure 26. Astrogliosis following LPC-induced demyelination in the corpus callosum of *Tag-1*+/+ and *Tag-1*-/- mice. Representative images from cryosections immunostained against the astroglial marker GFAP (in red) in Tag-1+/+ (A-D) and Tag-1-/- mice (E-H). Nuclei are shown in blue (TO-PRO-3 nuclear staining). Scale bar in (A-H) = 100 μm. Vhc: vehicle.

Furthermore, nuclear staining revealed increased number of cells at the injection point at 5 dpi, partially corresponding to OPCs (see TOPRO nuclear staining in blue, Figure 25, panels B and F). Although a reduction can be noted at 10 and 15 dpi, the density of the cells does not go back to normal levels, indicating that other cell types are recruited to this area (Figure 25 panels C, D and G, H versus A, B). Among these, astrocytes certainly account, at least in a great part, for the encountered increase in cell numbers, although in knock-out animals astrogliosis is seen in smaller degree compared to wild type (Figure 26).

Studies of demyelination in mouse models have shown that complete disorganization of all perinodal domains occurs in discrete steps, initiating from the PNs and JXPs. During remyelination, nodal components recluster initially, followed by paranodal and, as a final event, juxtaparanodal reorganization (Howell et al 2006; Howell et al 2010; Zoupi et al 2013). Recently, unpublished data from our laboratory (Zoupi L., PhD thesis) arose from subjecting wild type and TAG-1 mutant animals to another model of toxic demyelination, the cuprizone

model (Groebe et al., 2009; Kipp et al., 2009; Matsushima and Morell 2001). In this model, 9 weeks following toxin removal, remyelination in the corpus callosum is quite progressed, allowing for the study of remyelination. During late stages of remyelination reclustering of VGKCs took place in the absence of TAG-1, proposing a TAG-1-independent clustering mechanism.

After assessing the degree of remyelination in the LPC model, we asked whether perinodal reclustering occurs in a significant degree or not and whether we could reproduce the results obtained from the cuprizone model. In this direction, we performed immunohistochemistry against the paranodal marker Caspr and the juxtaparanodal molecules Caspr2 and the Kv1.1 isoform of VGKCs on cryosections from animals sacrificed at 10 and 15 dpi. In all cases, as a control for normal clustering we considered the corpus callosum of the contralateral hemisphere of the injection site.

As described above, at 10 dpi remyelination is at preliminary stages, since the differentiation of OPCs to OLs just has begun. In wild type animals, however, this process is initiated faster and at 10 dpi there are already signs of remyelination attempts, while this was not the case in mutant animals. At this time, in the corpus callosum of *Tag-1*+/+ animals we were able to detect Caspr+ and Caspr2+ linear structures (Figure 27, panel B), indicating that the two proteins are reclustering along axons that have established contact with glial membranes. The same observation was obtained in the case of VGKCs, although in a more sparse pattern (Figure 28, panel B). No such reclustering was observed in knock-out animals for either juxtaparanodal molecule though (Figure 17, panel F and Figure 18, panel F).

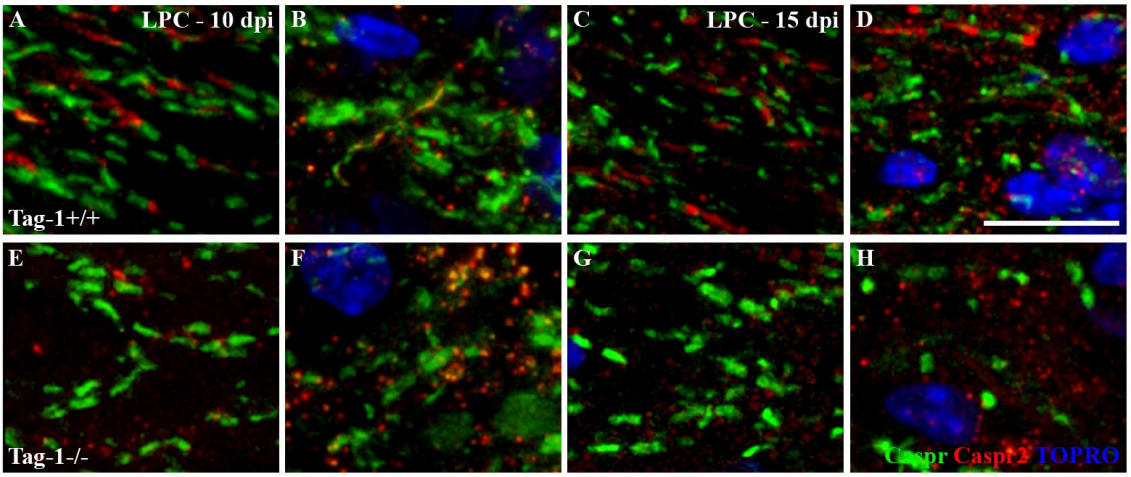

Figure 27. Reorganization of paranodes and Caspr2 clustering in remyelination following LPC-induced demyelination the corpus callosum of *Tag-1*+/+ and *Tag-1*-/- mice. Immunohistochemistry against the paranodal molecule Caspr (in green) and juxtaparanodal Caspr2 (in red) on cryosections from LPC-injected animals, comparing the unaffected, contralateral hemisphere (A, C, E, G) with the injected one at 10 (B, F) and 15 dpi (D, H). Nuclei are shown in blue (TO-PRO-3 nuclear staining). Scale bar in (A-H) = 10 μm.

At 15 dpi, the frequency of paranodal domains with similar morphology to those of the unaffected hemisphere is increased in both genotypes, indicating the progression of remyelination (in green, Figure 27, panels D and H). However, juxtaparanodal reclustering was fairly rare, but not absent, and any Caspr2+ or Kv1.1+ pattern was flanking Caspr+ PNs (Figures 27 and 28, panels D and H). While Caspr2 reclustering was absent in *Tag-1*-/- mice (Figure 27, panel H), we observed partial VGKC reclustering in levels similar to those of *Tag-1*+/+ mice (Figure 28, panel H). Thus, TAG-1-independent reclustering of VGKCs was possible in the LPC model of demyelination.

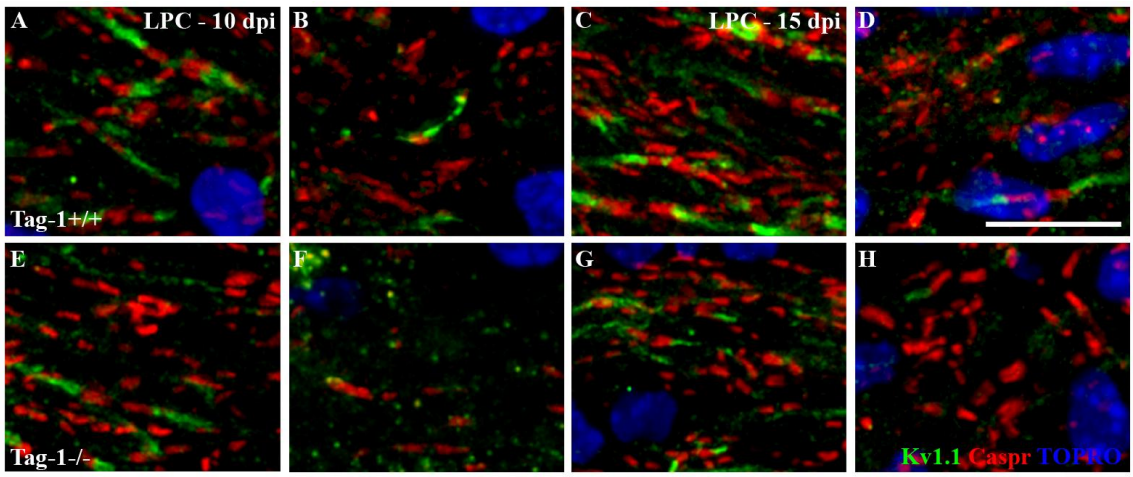

Figure 28. Reorganzation of paranodes and voltage gated potassium channel clustering in LPC-induced demyelination and remyelination in the corpus callosum of *Tag-1*+/+ and *Tag-1*-/- mice. Immunohistochemistry against the paranodal molecule Caspr (in red) and juxtaparanodal Kv1.1 (in green) on cryosections from LPC-injected animals, comparing the unaffected, contralateral hemisphere (A, C, E, G) with the injected one at 10 (B, F) and 15 dpi (D, H). Nuclei are shown in blue (TO-PRO-3 nuclear staining). Scale bar in (A-H) = 10 μm.

<u>Conclusion</u>: *Following recovery from LPC-induced demyelination in the corpus callosum, Tag-1-/- mice showed a delay in the restoration of OL numbers and remyelination, although OPC recruitment was unaffected. This proposes a defect in OPC differentiation, possibly associated with the decreased levels of astrogliosis in the affected area. During ongoing remyelination, VGKCs, but not Caspr2, recluster through a TAG-1-independent mechanism.*

E. RESULTS II

E.1. Analysis of the pattern of TAG-1+ juxtaparanodes

E.1.1.Analysis of the pattern of TAG-1+ juxtaparanodes in control white matter

As mentioned, in rodents, TAG-1 is localized at the juxtaparanodal regions of myelinated fibers and is expressed by both the glial cell and the axon (Traka, Dupree et al. 2002, Traka, Goutebroze et al. 2003, Savvaki, Panagiotaropoulos et al. 2008). However, the expression of TAG-1 in the normal human brain has not been studied. Thus, we first set on to perform immunohistochemical analysis of non-MS control WM, to reveal the localization of the protein in myelinated fibers. Using a monoclonal antibody that recognizes human TAG-1 (clone 1c12, see Table 3, Appendix) (Savvaki, Theodorakis et al. 2010) we observed a linear pattern that corresponds to that of JXPs and is adjacent to the paranodal marker Caspr (Figure 29, panels A, D and G). Additionally, we found, as expected, that TAG-1 immunoreactivity shows overlap with two known axonal components of the JXPs, Caspr2 and the isoform Kv1.2 of VGKCs (Figure 29, panels B, E, H and C, F, I respectively).

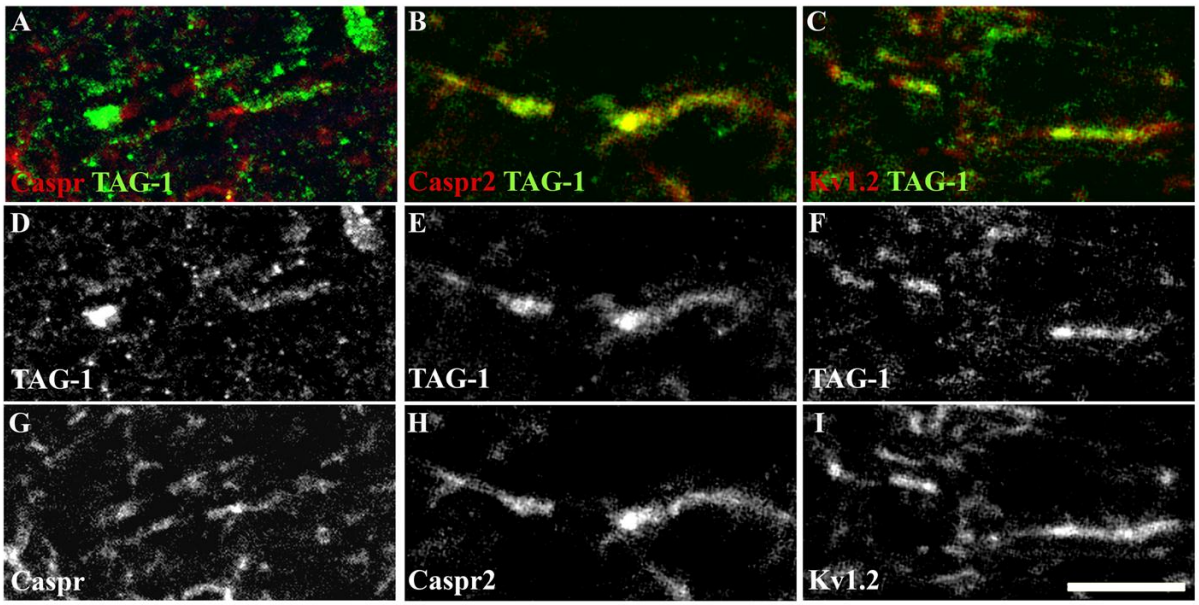

Figure 29. TAG-1 expression pattern in normal human white matter. Double immunohistochemistry (IHC) against TAG-1 (green) and Caspr (red) (A and separate channels in D and G) on cryosections from normal human white matter shows the juxtaparanodal localization of TAG-1 flanking the Caspr+ paranodes, while IHC against Caspr2 (B and separate channels in E, H) and the Kv1.2 isoform of voltage-gated potassium channels (VGKCs) (C and separate channels in F, I) (both shown in red), two juxtaparanodal molecules found on the axonal membrane, shows clearly their colocalization with TAG-1 (shown in green). Nuclei are stained with DAPI (in blue). Scale bar=10 μm.

Conclusion: *We showed for the first time that the localization of TAG-1 in normal human white matter is comparable to that described in rodents.*

E.1.2. Analysis of the localization of juxtaparanodal molecules in chronic Multiple Sclerosis normal appearing white matter

After establishing the localization of TAG-1 in control WM, we decided to assess the effect of the diffuse axonal pathology of the NAWM on juxtaparanodal molecules by analyzing TAG-1, Caspr2 and Kv1.2 in this area. We used post-mortem human tissue from MS patients (see Materials and Methods section and Table 4-Appendix, for disease course/duration) and performed immunohistochemistry (IHC) against TAG-1, Caspr2 and Kv1.2 and the myelin markers MBP or MOG (Figure 30).

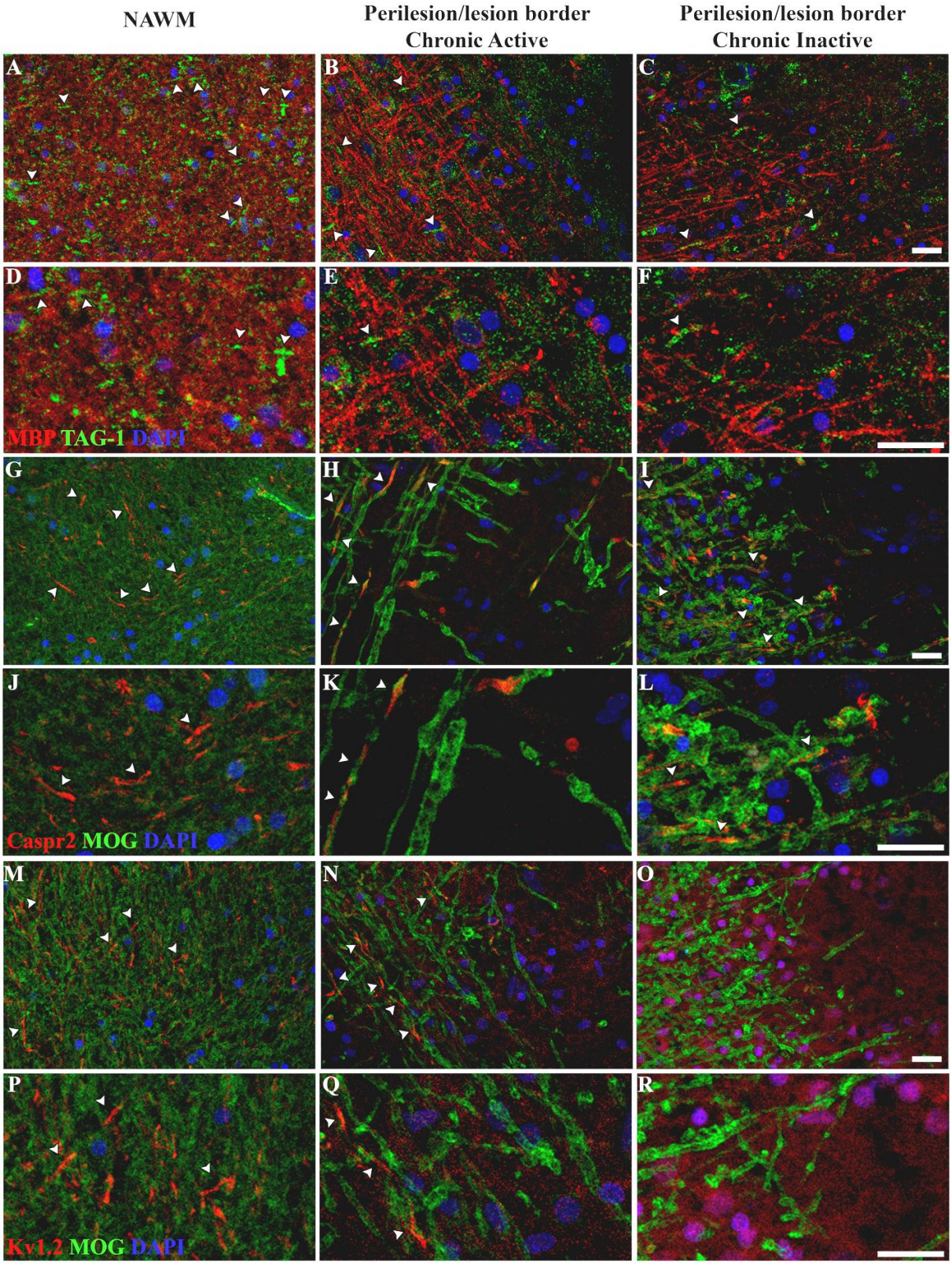

Figure 30. Juxtaparanodal diffusion in lesion areas in chronic demyelinated MS plaques. Double immunohistochemistry against TAG-1 (green) and the myelin marker MBP (red) on cryosections from post-mortem MS brain tissue shows the diffusion of TAG-1 in the demyelinated area of a chronic active (B and higher magnification in E) and a chronic inactive lesion (C, F) while the molecule is normally clustered in the normal-appearing white matter (NAWM) (A, D). Juxtaparanodes in the perilesion appear elongated (shown by

arrowheads). Double immunohistochemistry against Caspr2 (G-L) or Kv1.2 (M-R) (both shown in red) and the myelin marker MOG (green) on cryosections from MS brain shows the diffusion of the two juxtaparanodal molecules in the demyelinated area of a chronic active lesion and of a chronic inactive lesion. Caspr2 is normally clustered in the normal appearing white matter (NAWM) (G and higher magnification shown in J) but is diffuse in the perilesion and absent in the lesion in both active and inactive cases (panels H, I and K, L). Kv1.2 are shown diffuse in the demyelinated area of a chronic active lesion (N and higher magnification in Q) and of a chronic inactive lesion (O, P) while the molecule is normally clustered some cases in the NAWM (M, P) (in 50% of MS cases) and diffuse in others (data not shown). There is some immunoreactivity around chronic active lesions, while in the case of inactive lesions there is a loss of Kv1.2. Arrowheads point to TAG-1+, Caspr2+ or Kv1.2+ structures. Nuclei are stained with DAPI (in blue). Scale bar=20 μm.

TAG-1+, Caspr2+ and Kv1.2+ juxtaparanodal structures flanking Caspr+ PNs were evident in the NAWM of chronic MS cases (Figure 30, panels A, G, M and Figure 31, panels D, G and J respectively). Kv1.2 was found diffused in 50% of the MS cases examined, seen as diffuse signal and complete lack of clustered structures (data not shown).

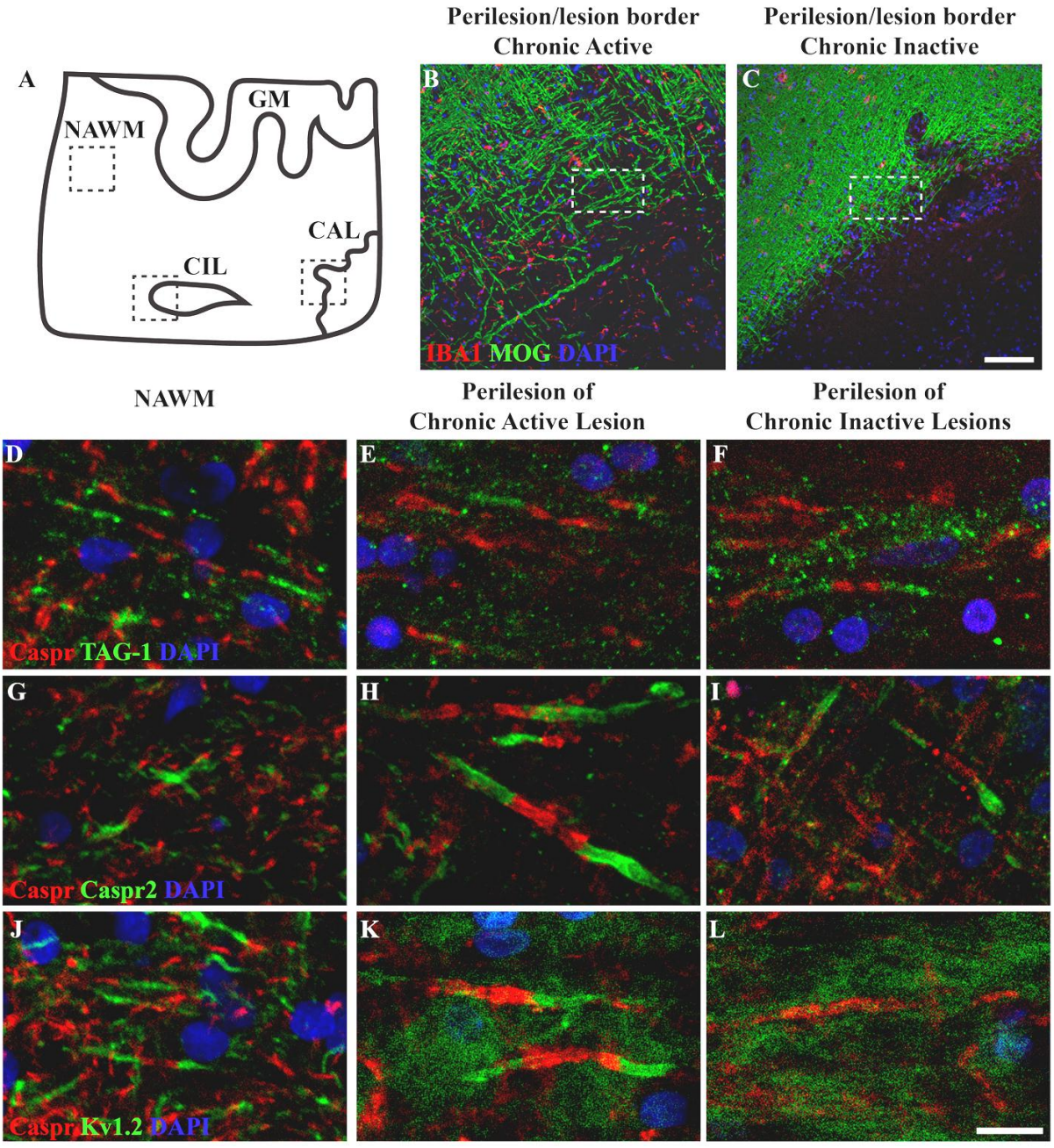

Figure 31. Juxtaparanodal persistance in the normal appearing white matter and perilesion areas of chronic demyelinated MS plaques. (A) Overview of the investigated areas in MS-obtained tissue and immunohistochemistry (IHC) against MOG (green) and IBA1 (red) of typical cases of chronic active lesions (CALs) (B) and chronic inactive lesions (CILs) (C). Dashed lines demarcate the areas shown in D-L. (D-L) Double IHC against the juxtaparanodal proteins (TAG-1, Caspr2 and Kv1.2, shown in green) and Caspr (red) on cryosections from MS brain. The presence of TAG-1+ and Caspr2+ clusters flanking Caspr+ paranodes (PNs) is observed in the area surrounding a CAL (E and H) and of a CIL (F and I) while the molecule is normally clustered in the normal appearing white matter (NAWM) (D and G). PNs lacking juxtaparanodes (JXPs) are obvious in the NAWM and perilesions. Kv1.2 is normally clustered in the NAWM of some cases (J), while around CALs there is still some immunoreactivity in some of MS cases (K), while in the case of CILs there is loss of VGKCs (L). Cell nuclei are visualized using DAPI (in blue). Scale bar=100 μm in B-C and 10 μm in D-L.

<u>Conclusion</u>: *VGKCs are found diffused half of the cases of chronic MS NAWM, indicating the susceptibility of the protein clustering even in the absence of demyelination, in areas of diffused pathology.*

E.2. Analysis of the localization of juxtaparanodal molecules in perilesions and chronic Multiple Sclerosis plaques

Next, we moved on to analyze all three juxtaparanodal molecules in the perilesions and lesion areas, discriminating between the chronic active and chronic inactive lesions (Figure 31, panels A, B, C). In early active lesions it has been shown that Kv1.2 channels translocate towards the PNs, which are found to be elongated (Howell, Palser et al. 2006). IHC showed TAG-1+ juxtaparanodal structures were present, although at lower density, at the borders of both chronic active and inactive lesions (Figure 30, panels B, C and higher magnification in E, F and Figure 31 and panels E, F) but were completely absent in the demyelinated area.

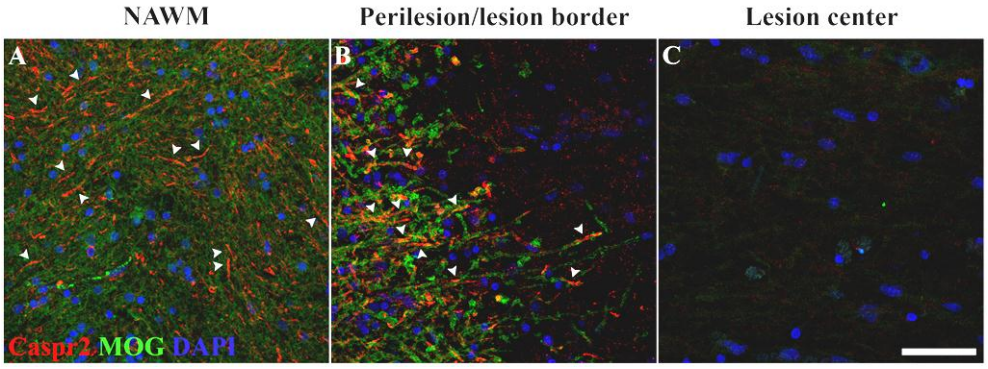

Figure 32. Absence of Caspr2 clustering in chronic lesion areas. Double immunohistochemistry against Caspr2 (red) and the myelin marker MOG (green) in chronic MS white matter. Caspr2+ juxtaparanodes were present in the NAWM (A) and preserved in the perilesion areas of chronic lesions (B). Demyelinated areas showed complete lack of Caspr2 (C). Arrowheads point to Caspr2+ structures. Cell nuclei are visualized using DAPI (in blue). Scale bar=20 μm.

We also examined the localization and pattern of Caspr2 and the Kv1.2 isoform of VGKCs in the vicinity of chronic demyelinated plaques. As TAG-1, Caspr2 was also absent in the demyelinating plaques (Figure 30, panels H, I, higher magnification in K, L and Figure 32) but clustered JXPs (although elongated) were obvious in the periplaque of active and inactive lesions (Figure 31, panels H and I). No obvious difference was observed between active or inactive plaques.

Absence of specific Kv1.2 immunoreactivity was observed in the periplaques of chronic inactive lesions (Figure 30, panel O, higher magnification in R and Figure 31, panel L). By comparison, in some of the chronic active lesions (Figure 31, panel K) there was evidence of Kv1.2+ structures (two out of four lesions examined) while in others none were detectable (data not shown). Finally, Kv1.2 immunoreactivity was completely diffused within the lesions in all of the cases examined (Figure 30, panels N, O and higher magnification in Q, R).

Conclusion: *TAG-1, Caspr2 and VGKCs are found diffused in demyelinating plaques, meaning either a cease in expression in demyelinated and stressed axons or a diffusion along the axonal membrane.*

E.3. Quantification of juxtaparanodal clustering in perilesions and MS NAWM

Previous studies have reported that in MS during the initial stages of demyelination, that is, in active demyelinating lesions, paranodal and juxtaparanodal molecules diffuse (Howell, Palser et al. 2006). On the other hand, during remyelination, PNs are the first perinodal structures that appear normally re-recruited while JXPs follow at later stages (Wolswijk and Balesar 2003, Coman, Aigrot et al. 2006, Howell, Palser et al. 2006, Zoupi, Markoullis et al. 2013). We therefore asked whether the percentage of normally clustered perinodal areas, as assessed through Caspr and TAG-1 immunoreactivity, differs in control WM in comparison with MS NAWM and perilesion areas of chronic MS cases.

We noticed that there is a significant reduction of normally clustered TAG-1+ JXPs in NAWM (Figure 33, panel B) as well as in the perilesions of chronic plaques (Figure 5C, D) in comparison with control cases (Figure 33, panel A). Specifically, in the control WM, normally clustered PNs with JXPs represent the majority of events (ca 73% of clusters), while PNs lacking JXPs are seen only as 22% of the total observed clusters. In the NAWM, the incidence of PNs without JXPs reaches nearly 45% (almost double compared to the control WM, $p<0.05$) and in the case of the perilesion areas of active or inactive plaques 55% ($p<0.001$) and 58% ($p<0.001$), respectively (Figure 33, panel E). In all cases, JXPs without PNs were very rarely observed (ca. 4% in the control WM and NAWM and ca 1.5% in the periplaques, $p>0.05$).

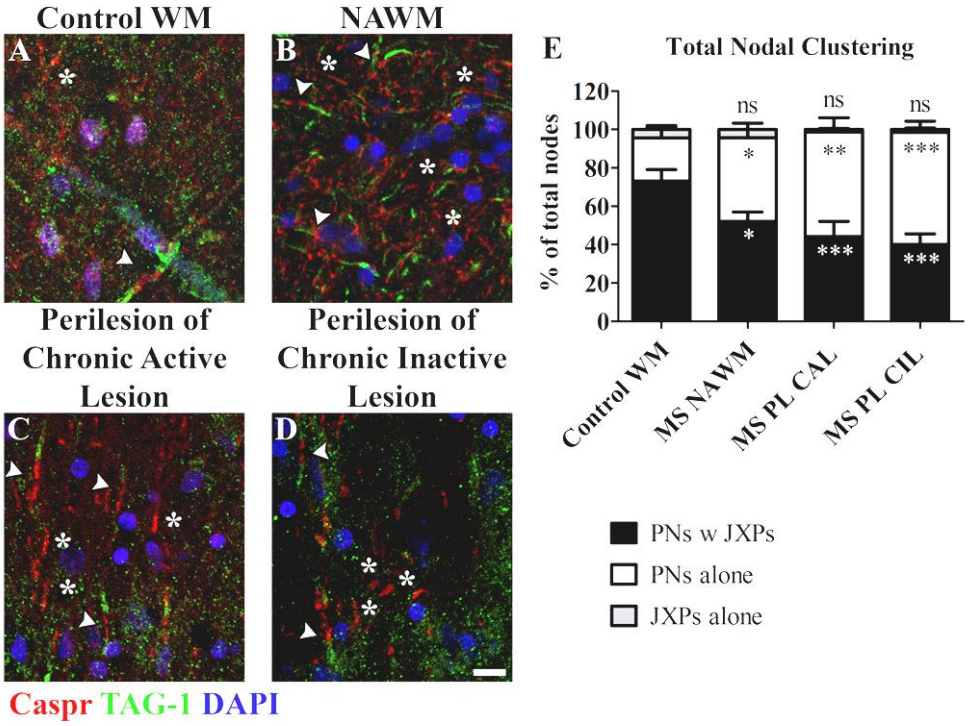

Figure 33. Normally clustered juxtaparanodes are reduced in normal appearing white matter and perilesion areas in chronic MS plaques. Double immunohistochemistry (IHC) against the paranodal Caspr (red) and TAG-1 (green) on cryosections from MS post-mortem brain tissue shows increased paranodes (PNs) without juxtaparanodes (JXPs) in the NAWM (B) compared to control white matter (A) and in greater extent in the perilesions of chronic active and inactive plaques (C, D). Arrowheads point to normally clustered JXPs flanking PNs, while asterisks show PNs without JXPs. JXPs lacking PNs were seen in the same extent in all areas. Nuclei were visualized with DAPI staining (blue). Scale bar=10 μm. Comparison of the percentages of each perinodal phenotype is shown in E in comparison with control white matter. (WM: white matter; NAWM: normal appearing white matter; PL CAL: perilesion of chronic active lesion; PL CIL: perilesion of chronic inactive lesion; ns: non-significant; P<0.05 : *; P<0.01 : **; P<0.001 : ***)

Immunostaining of control WM, NAWM and perilesion areas revealed the presence of some PNs lacking Caspr2 clustering in the NAWM and the perilesions (Figure 31, panels G-I, no quantification was performed). Caspr and VGKC immunostaining also showed a high degree of disruption of the VGKC clustering in the perilesions and even in the NAWM in the majority of the cases examined (see Figure 30, panels G-R, which shows the diffusion of Caspr2 and VGKC).

Conclusion: *TAG-1and Caspr2 normal clustering is found significantly reduced in the NAWM and perilesion areas.*

E.4. TAG-1 and Caspr2 diffusion in MS NAWM and chronic perilesions

The JXP length and diameter was assessed in control WM, MS NAWM and the perilesion areas of chronic active and inactive plaques (see Table 2). Double labeling for Caspr and either TAG-1 or Caspr2 was used to quantify the diameter and length of JXP that were normally clustered in the presence of PNs with length within the control range (4.1±1.4 μm) (shown in Figure 34, panels I and J). Juxtaparanodal length was comparable for both molecules in control WM (10.94±0.38 μm for TAG-1+ and 9.95±0.42 μm for Caspr2+ JXP) (Figure 34, panels A, E), which is indicative of the similar distribution of the two at the juxtaparanodal sites. In MS NAWM, both TAG-1+ and Caspr2+ JXP showed a tendency for reduced length (Figure 34, panels B, F): TAG-1+ JXP length was 10.94±0.38 μm in control WM and 10.04±0.36 μm in MS NAWM; Caspr2+ JXP length was 8.71±0.34 μm in MS NAWM and 9.95±0.42 μm in the control WM.

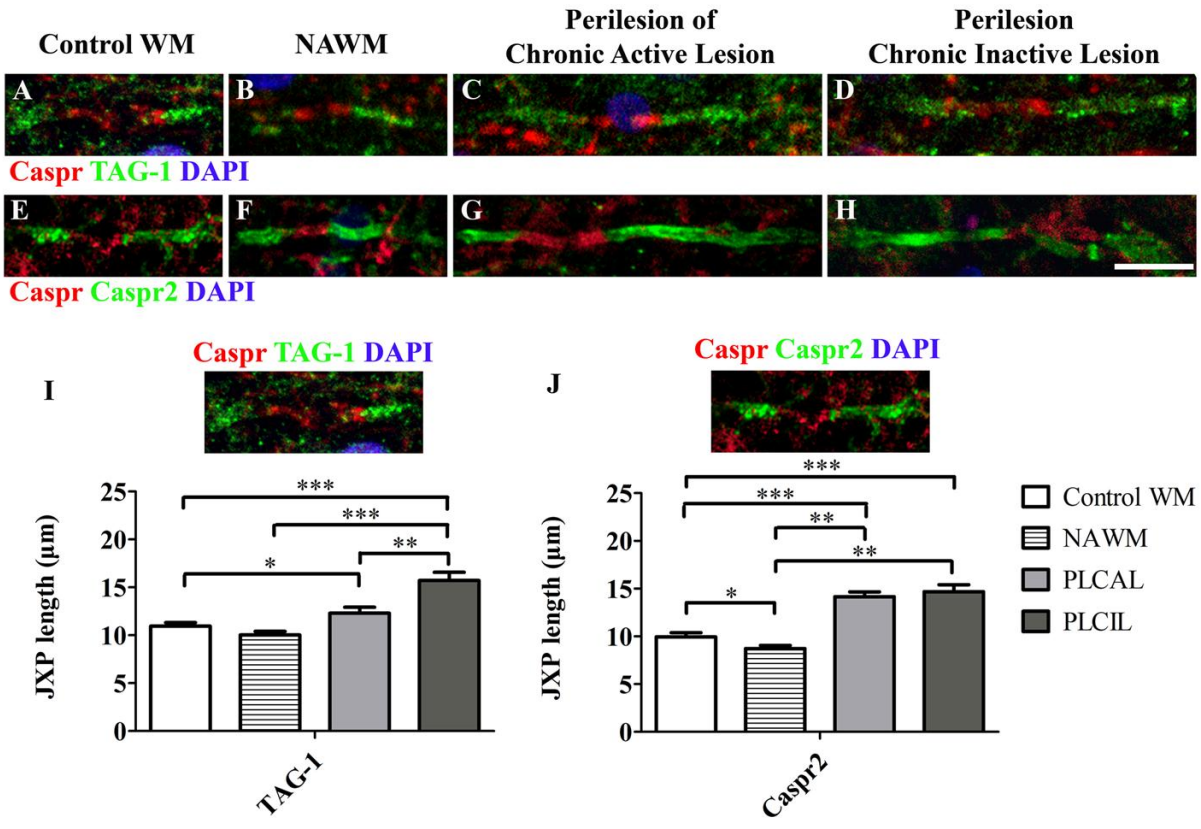

Figure 34. Juxtaparanodal diffusion in perilesion areas in samples from patients with chronic MS. Double immunohistochemistry against TAG-1 (green) with Caspr (red) (A-D) and Caspr2 with Caspr (green and red respectively) (E-H) shows the diffusion of the two molecules depicted as an increase in the juxtaparanodal length. Quantification of the juxtaparanodal length (graphs in I, J) shows comparable diffusion of the two in perilesions of chronic inactive lesions (PLCIL) while in areas surrounding active lesions Caspr2 (perilesions of

chronic active lesions-PLCAL) appears more diffuse than TAG-1. Scale bar=10 μm. (WM: white matter; NAWM: normal appearing white matter; JXP: juxtaparanodal; P<0.05 : *; P<0.01 : **; P<0.001 : ***)

In perilesion areas, TAG-1 was found mildly diffused around CALs (Figure 34, panel C) and more significantly diffused around inactive plaques (Figure 34, panel D), with respective mean JXP lengths at 12.31±0.6 μm and 15.71±0.86 μm (Figure 34, panel I). In comparison to the juxtaparanodal length observed in control myelinated fibers, these correspond to a 12.5% increase in the periplaques of CAL (P<0.05) and to a 43.6% increase in the perilesion areas of CIL (P<0.0001). Caspr2, on the other hand, was found diffused to the same extent both in the perilesions of chronic active and inactive plaques compared to the normal juxtaparanodal length (Figure 34, panels G and H), reflected approximately in a 45% increase (P<0.0001) (Figure 34, panel J).

Table 2. Quantification of JXP length in control WM, MS NAWM and perilesions

Juxtaparanodal length or diameter in μm	Control WM		MS NAWM		Perilesion of CALs		Perilesion of CILs	
	Mean±SEM	n	Mean±SEM	n	Mean±SEM	n	Mean±SEM	n
TAG-1+ JXP length	10.94±0.39	145	10.04±0.37	148	12.31±0.61	112	15.71±0.87	123
TAG-1+ JXP diameter	1.60±0.04	145	1.24±0.03	148	1.32±0.04	112	1.79±0.05	123
Caspr2+ JXP length	9.95±0.42	160	8.73±0.34	154	14.16±0.49	214	14.67±0.73	113
Caspr2+ JXP	1.29±0.03	160	1.04±0.03	154	1.16±0.03	214	1.37±0.05	113

WM: White Matter; MS NAWM: Multiple Sclerosis Normal Appearing White Matter; PLCAL: Perilesion of Chronic Active Lesions; PLCIL: Perilesion of Chronic Inactive Lesions; JXP: Juxtaparanode

Conclusion: *The remaining clustered TAG-1+ or Caspr2+ juxtaparanodes in the perilesions are found increased in length in the perilesions and unaffected in the NAWM of chronic MS, indicating the commencing of the protein diffusion prior to complete demyelination.*

E.5 Analysis of the protein levels of juxtaparanodal molecules in MS NAWM and chronic lesions

To clarify whether the diffusion of the JXP complex in demyelinating plaques is an outcome of complete absence of the molecules, diffusion or reduced expression, we performed analysis of the mRNA and protein levels of key perinodal molecules. All three juxtaparanodal proteins analyzed by immunoblot (TAG-1, VGKCs, using a Kv1.2-isoform

specific antibody, and Caspr2) showed a tendency for reduction in the lesions, even though not statistically significant (Figure 35, panels A, B).

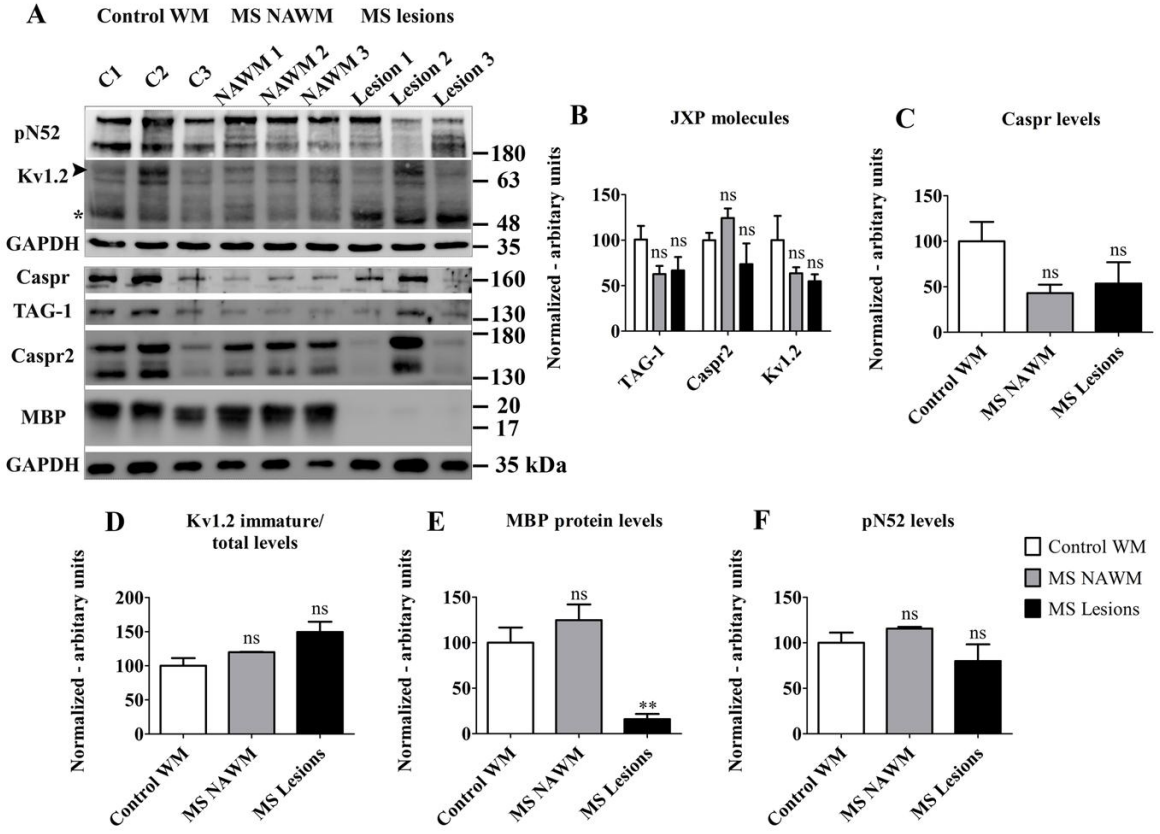

Figure 35. Immunoblot analysis of paranodal and juxtaparanodal molecules in chronic MS lesions. (A) Immunoblot was performed using three cases per group (control white matter-WM, normal appearing white matter-NAWM, 1-2 derived from secondary progressive MS cases and 3 from a primary progressive MS case and MS lesions, all from secondary progressive MS cases, 1,2: chronic active lesions, 3: inactive lesion) (B) TAG-1 shows a tendency for reduced expression in the almost completely demyelinated lesions, accompanied by a decrease in Caspr2 and VGKC levels. (C) The paranodal molecule Caspr is reduced but not significantly in the NAWM and lesion areas. Increased ratio of the immature, non-glycosylated isoform of VGKCs (Kv1.2 isoform, shown by an asterisk) to the total Kv1.2 levels (mature band is shown by an arrowhead) points towards axonal stress in the lesion (D). (E) MBP protein levels show that lesions are almost completely demyelinated and the phosphorylated N52 levels (pN52), a neurofilament marker, show a small non-significant decrease in axonal density (F). (C1-C3: control 1-3; NAWM1-3: normal appearing white matter 1-3; JXP: juxtaparanodal; ns: non-significant; $P<0.01$: **)

TAG-1 and Kv1.2 appeared reduced in the NAWM (Figure 35, panel B), while paranodal Caspr showed reduced levels of expression in NAWM and lesions (Figure 35, panel C). Assessment of the levels of the immature (non-glycosylated) isoform of Kv1.2 normalized to its total levels was non-significantly increased in the lesions (Figure 35, panel D). It should be noted that not all lesions showed the same profile of protein levels, even though they all had a similar extent of demyelination, as shown by MBP loss (Figure 35,

panel E). This is due to the fact that human pathology is extremely heterogeneous and variations in several proteins have been reported across different individuals suffering from MS (Maier, Baron et al. 2007). Additionally, the reduction of the protein levels is not due to axonal loss, since no significant change was observed in neurofilament levels, as shown by pN52 (Figure 35, panel F). Nevertheless, we were able to detect signs of axonal stress in lesion areas (Figure 36), as reported already in the literature, although axonal transections are more common in early, actively demyelinating lesions characterized by high inflammation levels (Trapp, Peterson et al. 1998, Bjartmar and Trapp 2003).

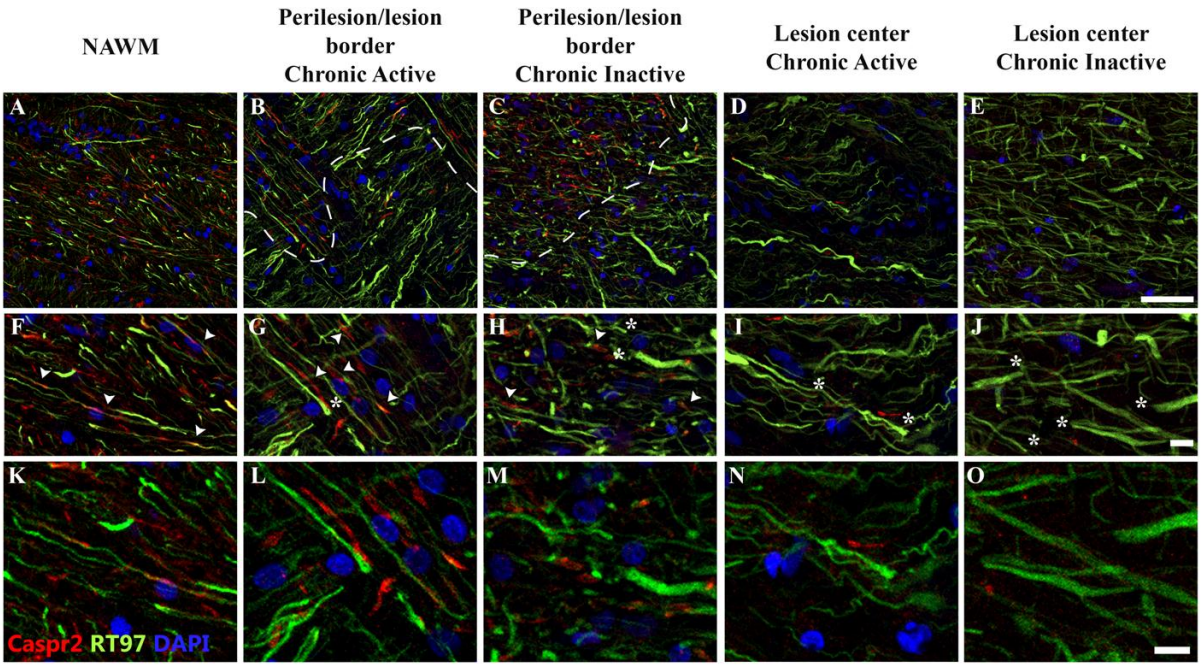

Figure 36. Correlation of axonal pathology and juxtaparanodal diffusion in chronic MS lesions. Immunohistochemical analysis was performed in MS-derived white matter against heavy neurofilament subunits (labelled with RT97, shown in green) and the juxtaparanodal molecule Caspr2 (in red). While in the NAWM there are normal Caspr2 clusters (A, F and K), in the periplaque several axonal segments are lacking Caspr2+ juxtaparanodes and the denuded axons in the lesion exhibit end bulbs or transections (shown by asterisks) (B, G, L for chronic active lesions, C, H, M for chronic inactive). Both in chronic active and inactive lesion centers there is a loss of Caspr2 and several axonal transections (D, E, I, J, N, O). Arrowheads point to Caspr2+ structures. Lesion areas are demarcated by dashed lines. Nuclei were stained with DAPI (blue). Scale bar=50 μm in A-E and 10 μm in F-O. (NAWM: normal appearing white matter)

To assess the transcript levels of some perinodal molecules, we analyzed the expression of TAG-1, Caspr2 and Caspr through Real-Time PCR. No significant difference was observed between control WM and MS NAWM (Figure 35, panel A). In the CALs, both Caspr and Caspr2 showed increased mRNA levels compared to the control WM but not to the MS NAWM (Figure 35, panels A and B), while TAG-1 was unaffected. Specifically, Caspr2

showed a 3.3-fold increase in CALs compared to control WM levels (P<0.05), while Caspr was 4-fold increased (P<0.05). In the CILs, Caspr2 was even more upregulated (almost 4.8-fold increase compared to control WM levels, P<0.005) in comparison to control WM and NAWM and Caspr showed an 5.5-fold increase in CILs compared to control WM levels (P<0.005). TAG-1 appeared again unaffected in the CILs. Overall, Caspr and Caspr2 showed similar changes in mRNA levels, with a clear increase in the lesions, while TAG-1 showed stable levels of expression.

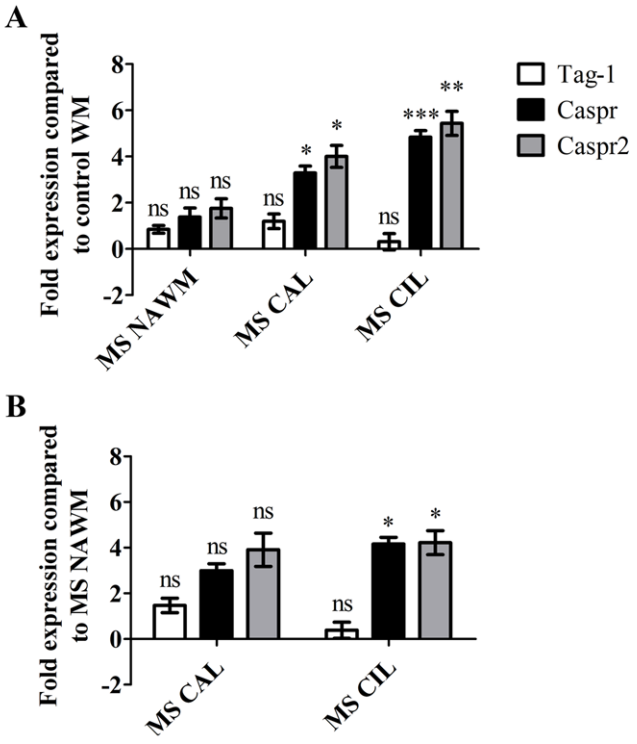

Figure 37. Analysis of expression levels of paranodal and juxtaparanodal molecules in post-mortem MS brain tissue compared to control white matter and normal appearing white matter. Real-Time PCR analysis of the levels of the mRNA coding for TAG-1, Caspr and Caspr2 in MS normal-appearing white matter (MS NAWM) (n=5 cases, all secondary progressive MS-SPMS), CAL (n=5 lesions from 4 cases, one being a primary progressive MS case-PPMS) and CIL (n=4 lesions from 3 cases, two from SPMS and two from PPMS) normalized to that of control white matter (n=6 cases) as shown in (A) and levels in CAL and CIL also expressed in relation with NAWM (B). The levels of the mRNA coding for TAG-1 did not show statistically significant changes across cases, whereas both Caspr2 and Caspr mRNA was increased in CALs and even more evidently in CILs compared to control WM. Only CIL showed increased levels of Caspr and Caspr2 mRNA in relation to NAWM. (WM: white matter; ns: non-significant; P<0.05 *, P<0.01 **, P<0.001 ***)

<u>Conclusion</u>: *TAG-1, VGKCs, Caspr2 and paranodal Caspr were detected both in mRNA and protein levels in the lesions. Protein levels between control WM, NAWM and demyelinated lesions did not show statistically significant differences, but a tendency for reduction was*

observed for all of the proteins in the lesions. Additionally, an axonal homeostatic mechanism is probably driving the upregulation of transcription in Caspr and Caspr2.

F. DISCUSSION I

The goal of the first part of this study was to explore the role of TAG-1 in demyelination and remyelination under distinct circumstances. Specifically, we chose to study these processes in wild type and knock-out mice that have been subjected either to systemically driven, autoimmune demyelination or to focal toxic demyelination, addressing the following questions: does the absence of TAG-1 render the CNS vulnerable to systemic autoimmune-driven demyelination? Are axons affected in a greater extent? Is remyelination following focal demyelination of the CNS affected in *Tag-1-/-* mice? We analyzed cellular and molecular factors that are directly or indirectly related to myelin destruction and formation. Since the two experimental approaches were carried out using two different mouse strains, we began our study by comparing characteristic and well-described phenotypes of *Tag-1-/-* mice in these strains.

F.1. Characterization of the juxtaparanodal *Tag-1-/-* phenotype in the C57BL/6 background

The organization and maintenance of the domains that are encountered along mammalian myelinated fibers (i.e. nodes of Ranvier, paranodes and juxtaparanodes) depends on several molecular complexes that are restricted at these sites, found either on the axonal or glial membrane (Susuki and Rasband 2008, Zoupi, Savvaki et al. 2011). The assembly of the complexes in the CNS depends on glia-derived signals and interactions between OLs and axons, initiating at paranodal areas, which stabilize also nodal domains (Rasband, Peles et al. 1999, Susuki, Chang et al. 2013). Juxtaparanodal formation depends on two events, the first being the establishment of paranodal junctions between glial and neuronal membranes and the second the formation of the complex between TAG-1/Caspr2/VGKCs (Traka, Dupree et al. 2002, Poliak, Salomon et al. 2003). The loss of either Caspr2 or TAG-1 causes juxtaparanodal disruption, while TAG-1 is considered to interact also homophilically with its counterpart found on the glial membrane (Pavlou, Theodorakis et al. 2002, Poliak, Salomon et al. 2003, Traka, Goutebroze et al. 2003, Tzimourakas, Giasemi et al. 2007, Savvaki, Panagiotaropoulos et al. 2008). Notably, the glial TAG-1 isoform alone is capable of rescuing juxtaparanodal assembly and maintenance in the CNS (Savvaki, Theodorakis et al. 2010).

Recently, researchers observed that genetic variability between distinct mouse strains affects several phenotypes (Keane, Goodstadt et al. 2011). One relevant example to our study is the variation in VGKC distribution between the 6C3 and 6C2 mouse strains in the PNS (Buchner, Geisinger et al. 2012).

As mentioned before, the CNS of *Tag-1-/-* mice is characterized by loss of Caspr2 and diffusion of VGKCs in the C57B110/CBA strain (Traka, Goutebroze et al. 2003, Savvaki, Panagiotaropoulos et al. 2008). The introduction of the *Tag-1-/-* in the C57BL/6 strain in our laboratory was necessary in order to apply successfully the EAE model and urged us to test whether the juxtaparanodal phenotype already reported occurred in the C57BL/6 strain.

Our analysis of the myelinated fibers of the cerebellar WM showed that juxtaparanodal VGKC disruption is somehow less pronounced in the C57BL/6 strain. Nevertheless, we should keep in mind that the small sample size might be accounting for this result, but it is not surprising when taking in consideration that VGKCs are indeed dependent on the genetic variations between strains. In the case of Caspr2, absence of TAG-1 results in loss of the protein from JXPs regardless of the genetic background. This discrepancy might be explained by a differential mechanism of recruiting the two molecules at juxtaparanodal domains during development and the proposed direct interaction of Caspr2 with TAG-1 (Traka, Dupree et al. 2002, Savvaki, Theodorakis et al. 2010).

F.2. The EAE model

F.2.1. Study of neuropathology and tissue damage during EAE in wild type mice

The induction of EAE has been one of most commonly used MS simulations in mice, even though scientists agree that there are certain aspects of MS pathology that cannot be recreated in this model, including the CD8+ T cell-driven population of the lesions versus the CD4+ T cells in mice, the very common MS GM lesions which are not observed in induced mice and brain pathology, which is typically seen in MS versus the spinal cord findings in mice (Lassmann and van Horssen 2011, Ransohoff 2012, Dendrou, Fugger et al. 2015).

Nevertheless, significant correlations have been established between EAE and MS studies using post-mortem tissue, such as the presence of microglial load, WM lesions that fail to remyelinate and axonal loss. In progressive MS NAWM, an abundance of IBA1+ cells

as well as activated (or ramified) microglia coincides with paranodal and juxtaparanodal disruption along with axonal stress, an observation confirmed both in the spinal cord WM of CFA treated and presymptomatic EAE induced mice (Howell, Rundle et al. 2010). Axonal damage has been reported mostly in early MS lesions with high inflammation levels and is thought to accumulate during disease progression (Trapp, Peterson et al. 1998, Bjartmar and Trapp 2003). In EAE, while axonal loss in the spinal cord is detectable in acute phases, it also persists in chronic stages, opposing to the fact that there is partial remyelination (Herrero-Herranz, Pardo et al. 2008, Markoullis, Sargiannidou et al. 2012).

Our results show that CFA treated animals have low levels of IBA1+ microglia at the peak of the disease in induced animals, in agreement with what was already reported (Markoullis, Sargiannidou et al. 2012). In the spinal cord of induced animals, IBA1+ cells are increased in the spinal cord WM at the peak of the disease and a few days later, while they reach the levels of CFA treated animals at the chronic stage (40 dpi). However, another study using a slightly different induction protocol reports that microglial cells persist at 50 dpi (Markoullis, Sargiannidou et al. 2012). This may be explained by the fact that in the fore mentioned study used a protocol which results in a chronic disease (by means of immunizing the mice against recombinant MOG), while the one that we used is considered a monophasic variation (using a synthetic peptide of MOG consisting of 20 aminoacids). Additionally, microglial activation has been found to precede onset of clinical symptoms and to persist in late CFA treated and induced mice (Howell, Rundle et al. 2010). However, since microglial activation was assessed through CD11b-IR and not IBA1, these results do not contradict ours. We also found that at the peak of clinical score the infiltration of the GM by IBA1+ cells is at its maximum, a fact that, to our knowledge, is not reported in the literature and should be investigated further. In as little time as 4 days, GM microglial levels drop significantly, indicating that after disease onset and peak of neurological symptoms, microglial cells now become more restricted to the WM. Considering the high occurrence of GM lesions in MS, a potential effect of the even transient infiltration of the GM in the neurological decline or complex behavioral traits in mice should be assessed by a variety of behavioral tests.

Demyelinated lesions always correlated with microglia/macrophages at the area and did not become remyelinated, even at later stages. We also observed significant axonal swellings and loss during acute disease, which were partially reversed at cervical and thoracic spinal cord levels, but not at lumbar areas during the chronic disease stage (i.e. at 40 dpi).

Axons of the lumbar spinal cord area are characterized by increased vulnerability to axonal stress, already evident at the onset of clinical symptoms (Soulika, Lee et al. 2009). During the chronic stage, cervical and thoracic axons seem to partially recuperate from damage but even in the absence of remyelination, proposing that in EAE axons have the potential of spontaneous recovery even if they are lacking the contact with the glial membrane all along their length. This reversal of pathology seems to favor proximal versus distal CNS axonal segments, considering that it occurs in axons residing in cervical and thoracic spinal cord areas, but not in the lumbar portion. It has been shown that a specific subtype of reversible axonal degeneration, or focal axonal degeneration (FAD), occurs in EAE just before, at the onset and 2 days post-onset of clinical symptoms (Nikic, Merkler et al. 2011). FAD occurs in discrete steps characterized by differences in abnormal axonal morphology, progressing from normal-appearing axons to appearance of axonal bulbs and subsequent fragmentation. Furthermore, it correlates with the presence of microglia and, surprisingly, takes place in axons that are still found ensheathed by myelin segments but reside inside acute lesions. Similarly, in actively demyelinating MS lesions, axons with abnormal morphologies (e.g. swellings, axonal bulbs) were still found associated with myelin (Trapp, Peterson et al. 1998, Bjartmar, Kidd et al. 2001, Nikic, Merkler et al. 2011).

F.2.2. Study of EAE in wild type versus *Tag-1-/-* mice

In the previous section we described the histopathological findings following EAE induction in wild type mice, in order to clarify the correlation of the onset and course of symptomatology with the histological observations. As mentioned, *Tag-1-/-* mice exhibit significant hypomyelination, apart from the juxtaparanodal alterations already discussed (Chatzopoulou, Miguez et al. 2008). Our goal was to subject wild type and knock-out mice to EAE and then compare the findings that we established and discussed above, during the acute phase of the induced disease.

Mice lacking TAG-1 are characterized by the same day of onset and mean scores as wild type animals, but show a delay of 2-3 days to reach the peak of symptoms. However, in both cases remission was observed 3-4 days after the peak. The onset of symptoms in EAE coincides with the appearance of infiltrate-associated axonopathy at the lumbar spinal cord and the peak of activated T cells in peripheral lymphoid tissues (Herrero-Herranz, Pardo et al. 2008, Soulika, Lee et al. 2009). The progression of neurological decline, however, is

associated with increase in mononuclear cell numbers in the spinal cord and a selective loss of small caliber axons of the corticospinal tract, since the observed axonal loss, synchronous with disease initiation, is not further increased with disease progression (Black, Liu et al. 2006, Liu, Li et al. 2008, Soulika, Lee et al. 2009, Recks, Stormanns et al. 2013).

In *Tag-1-/-* mice, ultrastructural (EM) analysis has shown a reduction in small caliber axons of the optic nerve (ON) and an increase in large caliber axons (Chatzopoulou, Miguez et al. 2008, Savvaki, Theodorakis et al. 2010). Although no such analysis has been performed on axons of the spinal cord but in the ON, we can hypothesize that the loss of small caliber axons could occur in the spinal cord as well, since the juxtaparanodal phenotype is similar between the two tissues. The decreased progression of symptoms in knock-out mice might be due to a decreased rate of axonal degeneration in the spinal cord, taking into account that small caliber axons are more susceptible to axonopathy and larger caliber axons would develop the pathology slower.

The degree of demyelination a few days after the peak of disease in cervical to lumbar areas of the spinal cord was similar between *Tag-1+/+* and *Tag-1-/-* mice. However, lesions seemed to affect the spinal cord along its length in the first case, while in knock-out mice lumbar areas where more vulnerable to demyelination. Additionally, in wild type mice the degree of demyelination always correlated with the axonal loss severity, while in the cervical spinal cord of knock-out mice axonal loss is detected in higher degree, when correlated with the demyelinated area. To our knowledge, such a phenotype has not been described in the literature so far. On one hand, one possible explanation might be that although the myelin has started to get destroyed, the clearance by macrophages has not progressed in order to have obvious lesions. On the other hand, it might indicate the increased vulnerability to degeneration of proximal axons arising from descending tracts, possibly correlating with increased infiltration by immune cells. However, levels of WM microglial/macrophage infiltrates are not in agreement with this hypothesis.

The assessment of axonal density in the dorsal and lateral funiculi of the spinal cord through immunohistochemistry did not result in a significant reduction in the absence of TAG-1, even though in the mean values in that case were 15-20% reduced compared to the control. Our results contradict those reported for the adult ON, where a significant reduction in axonal density was reported through EM analysis (Chatzopoulou, Miguez et al. 2008).

However, we should take in consideration that the resolution of confocal microscopy versus that of EM is far reduced. While the assessment of axonal loss in the EAE model through fluorescence microscopy yields similar results with that of the inspection of semi-thin, toluidine-stained spinal cord sections using EM (Markoullis, Sargiannidou et al. 2012), it is not the most appropriate technique of comparing axonal diameter or axonal density.

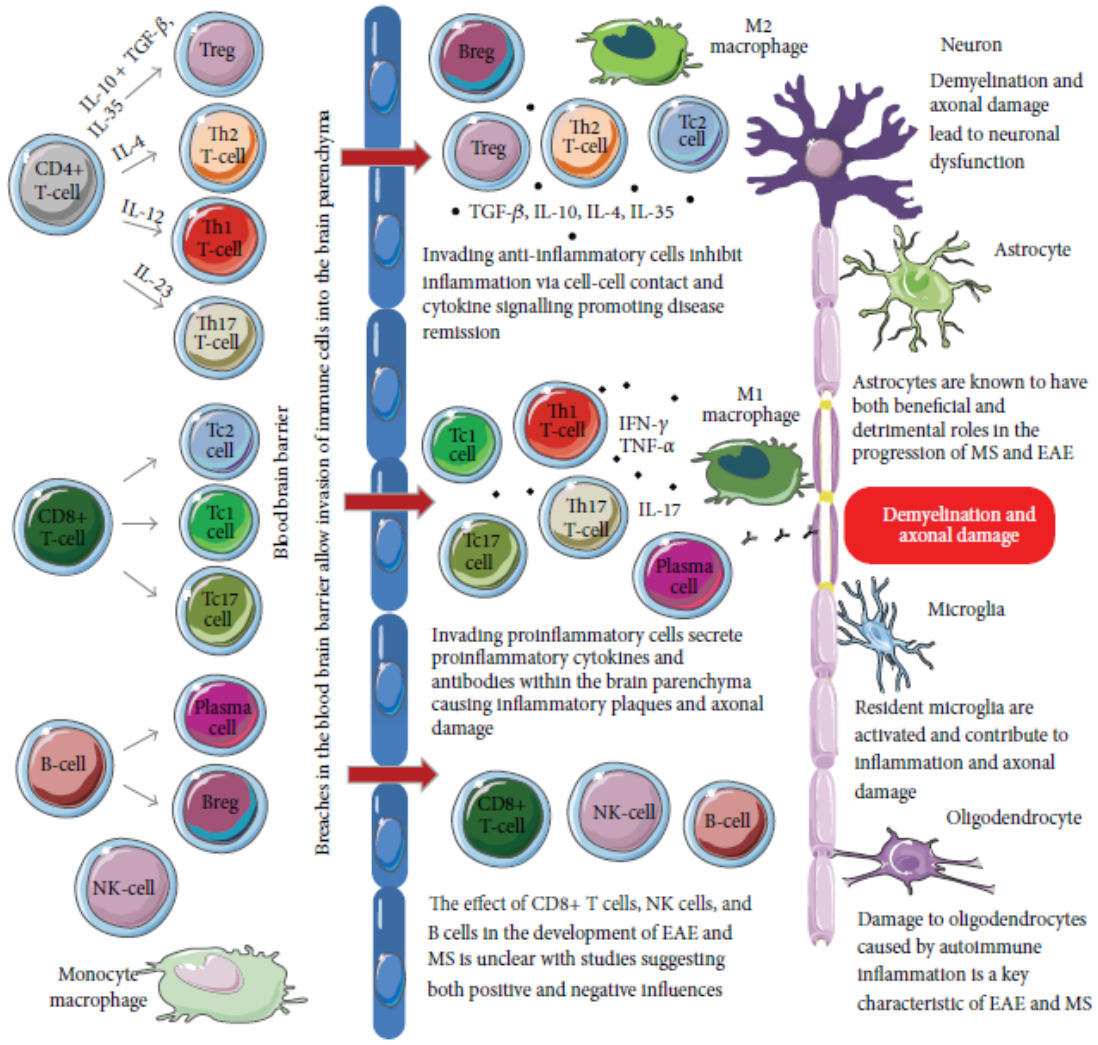

Figure 38. Schematic representation of infiltrating cells contributing to EAE and MS pathology. Disease mechanisms in both cases depend on the innate and adaptive component of the immune system. Autoreactive cells from the periphery cross the breached blood-brain-barrier (BBB) and invade the CNS. Tissue damage (demyelination and axonal loss) is caused directly by the autoimmune infiltrates, complement activation and autoantibody appositions, while anti-inflammatory cell populations govern the remissions. Other cell types found at the lesions, such as microglia and astrocytes, have an unclear role in disease pathogenesis. From (Duffy, Lees et al. 2014).

Since EAE was developed as a model recapitulating several hallmarks of MS-related pathology, a great deal of characterization of all immunological processes and involved cell

types has been made (see Figure 38). MS is considered a CD8+ T cell-driven disease, although lesions are also populated by smaller numbers of CD4+ T cells (Paterson and Day 1979, Babbe, Roers et al. 2000, Huseby, Liggitt et al. 2001). Additionally, MS and EAE tissues are characterized by the activation of resident microglia and infiltration by microglial cells and macrophages (Lucchinetti, Bruck et al. 2000, Ponomarev, Shriver et al. 2005, Ajami, Bennett et al. 2011). In EAE, however, microglial cells are implicated not only in the initiation of the disease, but also in the progression and are correlating with defects of paranodal and juxtaparanodal domains, as well as acute axonal stress (Bhasin, Wu et al. 2007, Howell, Rundle et al. 2010).

TAG-1 absence had no effect on total infiltrating numbers of T or B cells, either in the relative numbers of the first population over the latter. Even more specifically, the populations of CD4+ T cells (or helper T cells - T_H) and CD8+ T cells (or cytotoxic T cells – T_c) were comparable between wild type and knock-out mice. However, a significant difference is observed in the CD4+; CD25+; FoxP3+ T cell subpopulation, found notably decreased in knock-out mice at the peak of the symptoms. These cells, also known as regulatory T cells (Tregs), are thought to be a key component of autoimmunity. In fact, under normal circumstances, naturally arising Tregs in the thymus are responsible for the development of immune self-tolerance and homeostasis at the periphery (Sagakuchi 2004). Yet, the depletion of these cells or the mutation of the gene coding for the transcription factor FoxP3, which drives their differentiation, causes autoimmunity both in mice and humans (Fontenot and Rudensky 2005). Tregs are thought to exert the suppression of autoimmunity through interaction with antigen-presenting cells (APCs), and in particular the subpopulation of dendritic cells (DCs) in a variety of proposed mechanisms (Sakaguchi, Yamaguchi et al. 2008).

Apart from its localization at the JXPs, TAG-1 is expressed in various subtypes of neurons and is implicated in neurogenesis, neurite outgrowth, fasciculation and neuronal migration and maturation, among other processes (Furley, Morton et al. 1990, Stoeckli, Kuhn et al. 1991, Kunz, Spirig et al. 1998, Fitzli, Stoeckli et al. 2000, Denaxa, Chan et al. 2001, Kyriakopoulou, de Diego et al. 2002, Liu and Halloran 2005, Chatzopoulou, Miguez et al. 2008, Ma, Futagawa et al. 2008, Wolman, Sittaramane et al. 2008, Lieberoth, Splittstoesser et al. 2009, Wang, Karagogeos et al. 2011, Okamoto, Namba et al. 2013, Bastakis, Savvaki et al. 2015). Although the expression and role of the protein has been elaborately described in the

nervous system, its expression in the immune system was firstly documented only recently by Alvarez and colleagues. In the fore mentioned study, TAG-1 was found to be a tissue-restricted antigen (TRA), normally expressed by thymic epithelial cells (Alvarez, Collado et al. 2015). The expression of any TRA by these cells ensures the development of tolerance of the immune system against this protein. Our findings point to a potential direct implication of the protein in driving autoimmune responses, opposed to the notion that it was only an autoantigen, which was established when detected as a target of autoimmunity in a subset of MS patients (Derfuss, Parikh et al. 2009). TAG-1 could be expressed by a cell population of the immune system acting directly or inderectly on Tregs or it might even be present in the latter cell type.

Taking into account the proposed role of TAG-1 as key in the shaping of self-tolerance, we could hypothesize that the absence of the protein during thymic clonal selection might have an effect on the establishment of the population of Tregs. Further investigation of the cells of the immune system is in order, not only in induced animals, but also in naïve knock-out mice in order to uncover any potential involvement of the protein in either normal or pathology-driven responses of the immune system. Nevertheless, since the human immune system is in many ways different from that in mice, it would be of great interest to analyze the expression of TAG-1 in the human immune system as well. Such an analysis could yield significant results that would help us understand further the mechanisms of autoimmunity in human conditions such as MS, among others.

F.3. Study of LPC focal de- and remyelination in wild type versus *Tag-1-/-* mice

The LPC-induced demyelination is one of the preferred models for the study of remyelination, since it involves the induction of well-defined lesions in any WM area. Thus, the local tissue microenvironment is more permissive towards remyelination compared to protocols of either systemic toxin administration (e.g. cuprizone) or immune-mediated demyelination (e.g. EAE) (Ransohoff 2012). LPC is highly lipophilic and after focal injection in any WM area is incorporated in the membrane of glial cells. LPC stimulates the recruitment of macrophages, subsequently leading to myelin endocytosis (Lauber, Bohn et al. 2003).

Recent data generated in our laboratory showed that, when subjected to toxic, cuprizone-induced demyelination, the numbers of CC-1+ OLs and PDGFRα+ OPCs are not as greatly affected in *Tag-1-/-* mice as in *Tag-1+/+*, even though demyelination and remyelination levels were comparable (Zoupi L, PhD thesis, 2013). These observations meant either that these cell populations are recruited to affected areas earlier that the analyzed time points, but OLs are not able to generate mature myelin, or that mature OLs in *Tag-1-/-* mice were not as vulnerable to cuprizone-induced demyelination as the *Tag-1+/+*. Additionally, in the absence of TAG-1, juxtaparanodal VGKCs were reclustered after remyelination took place. We decided to further study the role of TAG-1 in remyelination by inducing focal lesions in the corpus callosum and to address the same questions.

Following LPC-injections (at 5 dpi), prior to remyelination, lesion formation was slightly smaller in knock-out mice compared to wild type, a phenotype that remained in all examined stages post-injection. However, the degree of OL degeneration and OPC recruitment was similar, suggesting, a delay in myelin clearance, even though OLs are ongoing death. Even though we need to take in consideration the small sample size, another possible explanation is that overall tissue density (e.g. due to significant differences in axonal density) differs in the absence of TAG-1, seen as reduced diffusion of LPC.

During the stage that OPCs initiate their differentiation, ratios of OPC numbers to OL numbers decrease, as expected, but without any substantial recovery of OL numbers or remyelination of the lesion. However, at the stage of ongoing remyelination, the corpus callosum of wild type mice shows significant remyelination accompanied by almost complete restoration in OL numbers, while OPCs remain just slightly increased compared to the vehicle-injected situation. In *Tag-1-/-* mice, during this stage, OLs are still reduced and remyelination is only partially complete, even though the recruited OPCs have been exhausted. This indicates that even though in the absence of TAG-1 OPCs are recruited successfully to the affected area, they possibly fail to differentiate and form mature myelin, while their decrease during remyelination might be due to apoptosis. Such an observation is reported for the first time and it points to the importance of further investigating whether this is a cell-autonomous or non-cell-autonomous effect. The subjection of mice which express only the glial isoform of TAG-1 (see (Savvaki, Theodorakis et al. 2010)) to LPC-induced demyelination and the analysis of subsequent OPC and OL numbers would answer whether the observed defect is due to the absence of the protein from the OLs or if the homophilic

interaction between the glial and neuronal membrane is indispensable for OPC differentiation. Another possible cause of the failure of OPC differentiation might be the hypothesized incomplete myelin clearance that we mentioned before, a mechanism that has been reported in focal lesions in rat brainstem (Kotter, Li et al. 2006).

Last but not least, while increased cell numbers are obvious during all stages following the toxin injection, they can be explained only in the case of the wild type animals as a reflection of recruitment of astroglia and OPCs, since knock-out mice have significantly less astroglial cells at the lesion area. We should point out that astroglial cells have been shown to have an altered morphology with more processes in the ON of *Tag-1-/-* mice during embryonic stages, although such a phenotype was not confirmed in the adult and the protein is not expressed by astroglial cells (Chatzopoulou, Miguez et al. 2008). However, since one also encounters microglia and macrophages in and around the injection site, we cannot exclude that this cell populations account for the increased cellularity observed in the knock-out mice (Pourabdolhossein, Mozafari et al. 2014, Sahel, Ortiz et al. 2015). Even so, increased numbers of microglia/macrophages at the lesion do not account for the defect in remyelination, since it has been shown that their recruitment is beneficial and indispensable for remyelination after LPC -induced demyelination of the corpus callosum (Kotter, Zhao et al. 2005, Miron, Boyd et al. 2013). Interestingly, failure of myelin clearance by microglia does impair remyelination following cuprizone-induced demyelination (Lampron et al. 2015). Since TAG-1 is not expressed by microglia, it is possible that a non-cell-autonomous mechanism in the absence of TAG-1 impairs the clearance of myelin debris following LPC-demyelination, eventually impairing the differentiation of the recruited OPCs.

Typically occurring LPC-induced demyelination at the PNS, or "segmental demyelination" causes the diffusion of nodal, paranodal and juxtaparanodal components, which reorganize during remyelination (Dugandzija-Novakovic, Koszowski et al. 1995, Novakovic, Deerinck et al. 1996, Rasband, Trimmer et al. 1998, Arroyo, Sirkowski et al. 2004). Another type of LPC-induced disruption, termed "paranodal demyelination", results not in the diffusion of nodal and perinodal components, but rather in their spatial displacement (Arroyo, Sirkowski et al. 2004). Although we cannot discriminate between the two types of disruption, we noticed paranodal reclustering but only sparse juxtaparanodal reclustering. Importantly, while in *Tag-1+/+* mice reclustering occurred both for juxtaparanodal Caspr2 and VGKCs, in *Tag-1-/-* we detected only VGKC+ clusters. Thus, the

TAG-1-independent VGKC clustering that was observed in the cuprizone model was also confirmed following focal demyelination of the CNS. Further analysis of the reclustering should be done to elucidate the potential mechanism governing this phenomenon. For instance, clustering of VGKCs should be investigated in several time points after complete remyelination takes place, to discriminate between their reclustering or maintenance at the JXPs in the absence of TAG-1. Additionally, the degree of VGKC reclustering should be analyzed comparatively in *Tag-1*+/+ and *Tag-1*-/- mice, in order to see whether there is a difference in the efficiency of the two mechanisms.

Outlook and Future Directions

This part of our study focused on elucidating the significance of TAG-1 in immune-driven demyelination and the remyelination following toxic demyelination. We analysed the role of the protein not only in tissue pathology, but also the potential recovery of the juxtaparanodal domains, where it is found enriched. Additionally, we discovered an unexpected role of the protein in immunity.

The main findings of our study are found below:

- Juxtaparanodal clustering of TAG-1 seems to be variable between different mouse strains, meaning that it is affected by genetic variability.
- Absence of TAG-1 causes a slight delay in neurological decline in a model of MS, potentially due to the reduced progression of axonal loss.
- TAG-1 mediates Treg accumulation at the spinal cord during the peak of neurological symptoms in a murine MS model.
- Astroglial and possibly also microglial cell responsiveness to tissue damage depends on TAG-1 through a non-cell-autonomous mechanism.
- OPC recruitment upon demyelination is independent of TAG-1, but the protein is directly or indirectly necessary for differentiation and production of mature myelin.
- VGKC clustering during remyelination is mediated through a TAG-1-independent mechanism, as shown before by our laboratory in the cuprizone model.

The conclusions of our work resulted in several clues regarding putative novel roles of TAG-1, pointing to the following questions:

- Is TAG-1 expressed by immune cells in naïve conditions? And if so, how does this change upon induction of a MS-like protocol?
- Does the absence of TAG-1 affect autoimmunity?
- Are DCs and APCs affected?
- How does chronic demyelination affect axons in the absence of TAG-1?
- How is the GM affected in the presence or absence of TAG-1 during EAE?
- Is remyelination complete in later stages after focal toxic demyelination in the absence of TAG-1?
- Which is the TAG-1-dependent mechanism by which astroglial cells become recruited upon damage?
- Are microglial cells recruited in lesion areas following demyelination and are capable of myelin clearance?
- Which is the mechanism responsible for recruiting VGKCs, but not Caspr2, in the absence of TAG-1?
- Which of the above phenotypes can be reversed by the glial or the neuronal isoform alone?

G. DISCUSSION II

The focus of this part of our study was the comparative analysis of all three juxtaparanodal components in post-mortem chronic MS brain, compared to control WM. The expression of TAG-1 in human control and pathological brain tissue is reported for the first time. To our knowledge, this work also constitutes the first attempt to focus on all three molecules of the juxtaparanodal complex, TAG-1, Caspr2 and VGKCs simultaneously in chronic MS NAWM, perilesions and lesion areas, addressing not only their localization, but also their levels. This is of particular interest since current MS treatments target mainly the relapsing-remitting manifestations of the acute, initial stages of MS, while the secondary progression leading to disability in the chronic stages is not addressed to the same extent (Weiner 2009). Since the alterations of the molecules comprising the juxtaparanodal complex, and even more specifically the VGKCs, have consequences on neuronal function, as shown in animal studies (Chiu, Zhou et al. 1999, Boyle, Berglund et al. 2001, Poliak, Salomon et al. 2003, Traka, Goutebroze et al. 2003, Glasscock, Qian et al. 2012, Colakoglu, Bergstrom-Tyrberg et al. 2014, Varea, Martin-de-Saavedra et al. 2015), our results might offer more insight into the molecular changes that occur during the chronic phase of the pathology and may be relevant for the development of novel therapeutic approaches.

G.1. Juxtaparanodal changes in the chronic MS NAWM

Previous studies have reported that the presence of activated microglia in the MS NAWM results in mild paranodal diffusion, the degree of which correlates with microglial numbers (Howell, Rundle et al. 2010). This paranodal phenotype, which has been observed also in early active demyelinating lesions, causes the translocation of VGKCs into the nodal area (Howell, Palser et al. 2006, Howell, Rundle et al. 2010) (see Figure 40, panel B). We can hypothesize that a subtle decrease in TAG-1 levels causes partial dissociation of the tripartite juxtaparanodal complex of TAG-1/Caspr2/VGKCs, which could explain the great degree of VGKC diffusion observed (Figure 40, panel C). TAG-1, which is found on axons and glia (Figure 39), may be mildly affected due to the loosening of the axon-glial contact at the paranodal loops, a phenotype known to characterize the MS NAWM, similarly to what has been described in $CGT^{-/-}$ mice that lack normal axoglial junctions at PNs (Traka, Dupree et al. 2002, Howell, Rundle et al. 2010).

Overall, the environment of diffuse pathology and axonal injury in the absence of demyelination in the NAWM affects TAG-1 and Caspr2 to a lesser extent than Kv1.2, since TAG-1+ and Caspr2+ JXPs are present and exhibit comparable length as those seen in control WM. Interestingly, the NAWM of either PPMS or SPMS does not differ in terms of axonal degeneration or the levels and clustering of paranodal and juxtaparanodal proteins analyzed. This is most likely explained by the fact that all cases were very chronic and pathological alterations at these late stages of the disease are similar and belong to the same spectrum (Antel et al 2012).

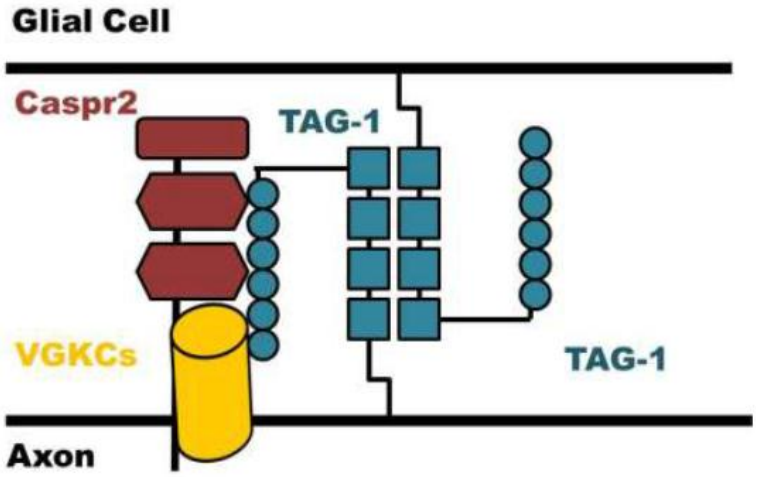

Figure 39. Model of the tripartite juxtaparanodal coplex. TAG-1 interacts directly with Caspr2 and the voltage gated potassium channels (VGKCs) through its Ig-like domains (round domains), while the FNIII-like domains (square domains) mediate homophilic interactions (Pavlou et al 2002; Tzimourakas et al 2008). Figure reprinted from Zoupi, PhD thesis, 2013.

G.2. Juxtaparanodal changes in the perilesions of chronic lesions

We observed that in the perilesions of chronic lesions, TAG-1 and Caspr2 clustering is reduced, while the preserved JXPs are elongated. While TAG-1 is less diffuse in the perilesions of CALs, this is not the case in those of CILs. Additionally, Caspr2 shows the same degree of diffusion at the margins of both types of chronic lesions.

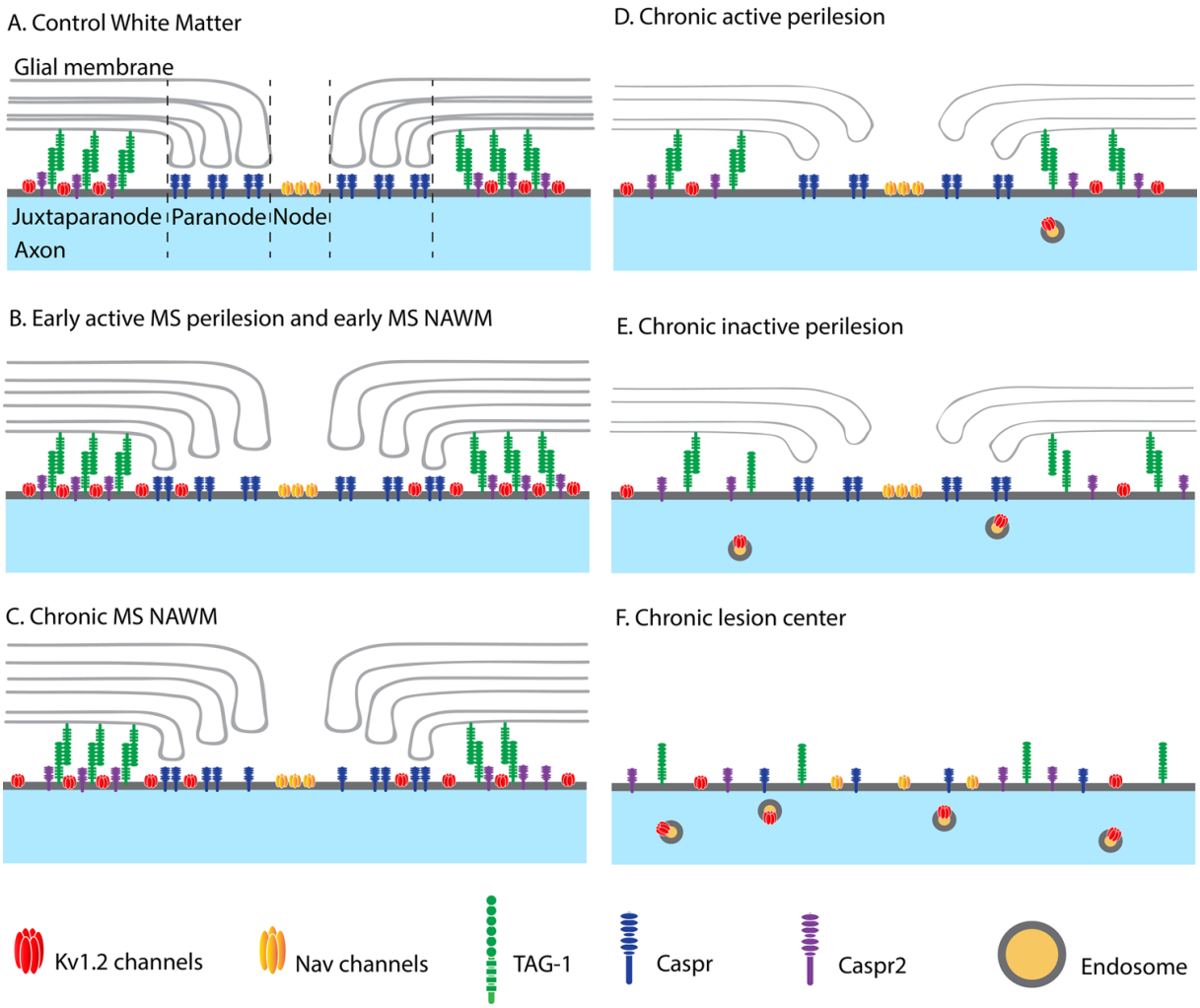

Figure 40. Model of perinodal changes in acute and chronic Multiple Sclerosis. (A) In a normal myelinated fiber nodal, paranodal and juxtaparanodal molecules are found inmutually exclusive domains due to the paranodal loops and intracellular tethering molecules, either in the axonal or glial cytoplasm. (B) Changes at the paranodes in early stages of demyelination in the normal appearing white matter and in the vicinity of the lesions loosen the contact between the glial and axonal membranes, causing some diffusion of the VGKCs towards the node (Howell et al., 2006, 2010). (C) In the NAWM of chronic cases the channels diffuse even more, presumably also to the internodes, and Caspr and TAG-1 are slightly down-regulated ((Howell et al., 2010) and this study). (D) Around chronic active lesions, paranodal junctions are defective (Wolswijk and Balesar, 2003) and juxtaparanodalmolecules diffuse,while possibly axonal stress results in the initiation of endocytosis of the VGKCs. (E) In the perilesion areas of chronic inactive lesions the paranodal disassembly persists (Wolswijk and Balesar, 2003) and there is probably an increased dissociation of the complexes and increasing endocytosis. (F) In the center of chronic lesions, all perinodal components are misplaced, as well as down-regulated, without domain-specific enrichment and the degree of axonal stress enhances further the endocytosis of the potassium channels (taking into account this study and Coman et al., 2006; Howell et al., 2006; Wolswijk and Balesar, 2003).

While the core of both chronic active and inactive lesions is similar, CALs have an active rim that expands slowly and is believed to contribute to disease progression, while CILs have sharp boundaries without ongoing demyelination but with significant

oligodendrocyte loss, astrogliosis and increased expression levels of apoptotic genes (Prineas, Kwon et al. 2001, Mycko, Papoian et al. 2004, Filippi, Rocca et al. 2012, Popescu and Lucchinetti 2012). Additionally, they differ in the extent of axonal injury at the borders of the plaques, which is greater in the case of the CALs and is correlated with the presence of activated microglia and macrophages (Kornek, Storch et al. 2000).

We hypothesize that TAG-1 is not affected as much as could be expected by the axonal injury that characterizes the perilesions of CALs, probably due to its expression by the glial cell as well as the axon. We could predict that in the case of CILs TAG-1 expression is reduced, leading to fewer homophilic interactions that would stabilize the molecule at the JXPs, eventually seen as further diffusion (see Figure 40, panel E). This hypothesis is further supported by the increased incidence of PNs without TAG-1+ JPXs around the lesions, which could be attributed to undetectable levels of the molecule. Caspr2+ JXPs, on the other hand, are similarly diffused in the vicinity of CALs and CILs, for which a dissociation of the molecule from the complex with TAG-1 would be a possible explanation. Taking this hypothesis a step further, we propose that the increased disruption of the complex causes the dissociation of VGKCs and in combination with the axonal stress in the periplaques, brings about the endocytosis of the molecule (Figure 40, panels D and E).

Our results suggest that juxtaparanodal integrity in the case of chronic disease is compromised even when paranodes persist, in contrast with the situation in the acute EAE and cuprizone models of demyelination (Zoupi, Markoullis et al. 2013). There, the PNs are the first domains to diffuse during the initial demyelinating stages and the first to be re-composed during remyelination (Zoupi, Markoullis et al. 2013). Thus, a possibility that we cannot exclude is that the presence of PNs without JXPs reflects remyelination attempts, especially around CILs, where the overall tissue environment might be permissive for myelin restoration, similarly to later stages of the EAE model and the recovery period after cuprizone-induced demyelination.

In summary, the perilesions of chronic active or inactive plaques are characterized by juxtaparanodal diffusion but not to the same degree concerning the three molecules. In parallel, PNs are preserved in numbers, but not in integrity, since they have been reported to be severely disrupted (Wolswijk and Balesar 2003). Our observations suggest that while Caspr2 and TAG-1 are preserved on the axonal membrane (and the glial membrane as far as

TAG-1 is concerned) for some time after the initial and possibly even later steps of demyelination, VGKCs are probably the first molecules to diffuse in the inflammatory environment and are more susceptible to the chronic demyelinating environment of MS brain.

G.3. Disruption of voltage-gated potassium channel clustering and clinical significance for MS

The observed defective localization of VGKCs is of significance in relation to a therapeutic approach used for symptomatic treatment of MS. 4-aminopyridine (4-AP) is a known selective inhibitor of the VGKCs and has been shown to improve conduction of action potentials along demyelinated axons and synaptic function, therefore ameliorating some of the motor symptoms of MS (Sherratt, Bostock et al. 1980, Smith, Felts et al. 2000). In mice lacking the Kv1.1 isoform of VGKCs a significant increase in the 4-AP-induced ectopic neuronal firing has been reported (Glasscock, Qian et al. 2012). One possible hypothesis is that the diffusion of VGKCs along the fibers in combination with the increased levels of the non-glycosylated isoform, leads to aberrant function of the channels, which eventually causes hypopolarization of the axons, thus making them less excitable. 4-AP efficacy could be explained in this case, since it blocks VGKCs and could restore the excitability of the axonal membrane.

G.4. Paranodal and juxtaparanodal molecules in the chronic lesion areas

Lastly, even though the juxtaparanodal components analyzed were never detected in clusters in demyelinated areas, we were able to assess their levels biochemically, which points to their presence on the axonal membrane or axolemma albeit in a diffuse manner (Figure 40, panel F). Furthermore, our results show that there is no significant difference between lesions in PPMS or SPMS cases when the disease reaches the chronic stages, which is in line with the general belief that the two do not differ in terms of pathophysiology, especially in later stages (Antel, Antel et al. 2012). It has been previously described that in the centers of chronic MS lesions there is paranodal Caspr disruption and juxtaparanodal disruption of VGKCs and Caspr2 (Wolswijk and Balesar 2003, Coman, Aigrot et al. 2006). The increase in Caspr and Caspr2 transcription levels in the lesions suggests a possible homeostatic mechanism of the demyelinated axon and correlates with the fact that the centers of chronic lesions are areas of increased transcriptional activity (Mycko, Papoian et al. 2004). Even though the two types of

chronic lesions have a similar center, characterized by complete demyelination, hypocellularity and lack of active microglia or macrophages, several genes are expressed at different levels between chronic active and inactive lesions, which explains the differential upregulation of the two genes between CALs and CILs (Mycko, Papoian et al. 2004, Popescu and Lucchinetti 2012). Moreover, significant variations are observed between lesions, even when they belong to the same type, as shown by our protein analysis. Specifically, there seems to be a correlation between increased axonal loss and an increase of JXP and paranodal molecules independently of the degree of demyelination. This might be the result of very recent demyelination or different inflammatory load, as mentioned in previous studies (Markoullis, Sargiannidou et al. 2012).

In the case of Kv1.2, we also noticed an increased immature-to-mature ratio of the molecule, which points to endocytosis, intracellular localization and retention in the endoplasmic reticulum and presence of axonal stress (Watanabe, Zhu et al. 2007) (see Figure 36, which shows typical morphological defects that point to axonal stress in the perilesion and lesion areas in our samples). While the effect of the loss of Caspr2 and TAG-1 on neuronal conduction has not been studied extensively, it has been shown that loss or diffusion of Kv1.1 results in altered neuronal excitability and transmission (Chiu, Zhou et al. 1999, Boyle, Berglund et al. 2001, Poliak, Salomon et al. 2003, Traka, Goutebroze et al. 2003, Glasscock, Qian et al. 2012, Varea, Martin-de-Saavedra et al. 2015).

In conclusion, this study shows significant juxtaparanodal perturbations occur either in the presence or absence of demyelination, an observation that correlates with the previously reported diffuse pathology of MS NAWM further supporting the concept of chronic MS as a "burned-out" stage of pathology. Moreover, the juxtaparanodal components TAG-1, Caspr2 and VGKCs are differentially altered in chronic MS WM and might explain some of the pathophysiological aspects of the chronic stage of the disease.

Outlook and Future Directions

In this part of our study, we demonstrate significant alterations of the three major juxtaparanodal proteins in chronic MS pathology, where the innate immune system plays a more important role than a disruption of the BBB from peripheral autoimmunity (Frischer, Bramow et al. 2009). Specifically, VGKCs are the most susceptible molecules since they

diffuse from the JXPs even prior to demyelination, followed by TAG-1 and Caspr2 (Figures 30, 31, 32 and 33). Also, juxtaparanodal integrity is compromised in the NAWM but not to the same degree as that described for PNs in another study, since we observed a very small percentage of JXPs lacking PNs (see Figure 32 of this study and (Howell, Rundle et al. 2010). The aforementioned observations could account in part for neuronal dysfunction reflected in neurological symptoms in chronic MS (Mahad, Trapp et al. 2015).

Our findings can be reviewed below:

- Diffuse NAWM pathology in chronic MS, which has been correlated with the presence of microglia, causes juxtaparanodal disruption.

- VGKC clustering is susceptible to chronic inflammation and is found greatly affected even in the absence of demyelination, which holds true also for TAG-1, although not in the same degree.

- Caspr2 is the least vulnerable molecule of the juxtaparanodal complex to disruption in chronic MS.

- TAG-1 and VGKC levels in the NAWM have a tendency of reduction, while Caspr2 a tendency for upregulation, potentially explaining the differences of the three molecules in vulnerability to diffusion.

- TAG-1 is found less disrupted upon acute axonopathy, a fact that could be explained by the homophilic interaction of the molecule between the axonal and glial membrane.

- The diffusion of VGKCs, even in the NAWM in chronic MS, might account for the efficacy of the potassium channel blocker 4-AP, which could not be explained so far.

- The core of chronic MS lesions shares the same molecular properties in the case of PPMS and SPMS.

- Paranodal and juxtaparanodal molecules are still expressed by denuded axons, indicating that contact with the glial cells is not necessary for the expression of these proteins.

- Axonal homeostatic mechanisms after chronic demyelination result in overexpression of paranodal Caspr and an enrichment of the ER in the immature form of VGKCs.

However, there are also questions that are driven by our conclusions, highlighted below:

- How are the components of the juxtaparanodal complex affected in cortical (gray matter) lesions?
- Is TAG-1 following the disruption pattern of VGKCs and Caspr2 in early, actively demyelinating MS lesions?
- How is mitochondrial damage associated with juxtaparanodal disruption?

BIBLIOGRAPHY

Ackerman, S. D., C. Garcia, X. Piao, D. H. Gutmann and K. R. Monk (2015). "The adhesion GPCR Gpr56 regulates oligodendrocyte development via interactions with Galpha12/13 and RhoA." Nat Commun **6**: 6122.

Ajami, B., J. L. Bennett, C. Krieger, K. M. McNagny and F. M. Rossi (2011). "Infiltrating monocytes trigger EAE progression, but do not contribute to the resident microglia pool." Nat Neurosci **14**(9): 1142-1149.

Albert, M., J. Antel, W. Bruck and C. Stadelmann (2007). "Extensive cortical remyelination in patients with chronic multiple sclerosis." Brain Pathol **17**(2): 129-138.

Alvarez, I., J. A. Collado, R. Colobran, M. Carrascal, M. T. Ciudad, F. Canals, E. A. James, W. W. Kwok, M. Gartner, B. Kyewski, R. Pujol-Borrell and D. Jaraquemada (2015). "Central T cell tolerance: Identification of tissue-restricted autoantigens in the thymus HLA-DR peptidome." J Autoimmun **60**: 12-19.

Antel, J., S. Antel, Z. Caramanos, D. L. Arnold and T. Kuhlmann (2012). "Primary progressive multiple sclerosis: part of the MS disease spectrum or separate disease entity?" Acta Neuropathol **123**(5): 627-638.

Arroyo, E. J., E. E. Sirkowski, R. Chitale and S. S. Scherer (2004). "Acute demyelination disrupts the molecular organization of peripheral nervous system nodes." J Comp Neurol **479**(4): 424-434.

Babbe, H., A. Roers, A. Waisman, H. Lassmann, N. Goebels, R. Hohlfeld, M. Friese, R. Schroder, M. Deckert, S. Schmidt, R. Ravid and K. Rajewsky (2000). "Clonal expansions of CD8(+) T cells dominate the T cell infiltrate in active multiple sclerosis lesions as shown by micromanipulation and single cell polymerase chain reaction." J Exp Med **192**(3): 393-404.

Babbs, C. F. and R. Shi (2013). "Subtle paranodal injury slows impulse conduction in a mathematical model of myelinated axons." PLoS One **8**(7): e67767.

Bacallao, K. and P. V. Monje (2015). "Requirement of cAMP signaling for Schwann cell differentiation restricts the onset of myelination." PLoS One **10**(2): e0116948.

Barres, B. A., I. K. Hart, H. S. Coles, J. F. Burne, J. T. Voyvodic, W. D. Richardson and M. C. Raff (1992). "Cell death and control of cell survival in the oligodendrocyte lineage." Cell **70**(1): 31-46.

Barres, B. A. and M. C. Raff (1993). "Proliferation of oligodendrocyte precursor cells depends on electrical activity in axons." Nature **361**(6409): 258-260.

Barres, B. A., R. Schmid, M. Sendnter and M. C. Raff (1993). "Multiple extracellular signals are required for long-term oligodendrocyte survival." Development **118**(1): 283-295.

Bastakis, G. G., M. Savvaki, A. Stamatakis, M. Vidaki and D. Karagogeos (2015). "Tag1 deficiency results in olfactory dysfunction through impaired migration of mitral cells." Development **142**(24): 4318-4328.

Bernard, C. C., J. Leydon and I. R. Mackay (1976). "T cell necessity in the pathogenesis of experimental autoimmune encephalomyelitis in mice." Eur J Immunol **6**(9): 655-660.

Bhasin, M., M. Wu and S. E. Tsirka (2007). "Modulation of microglial/macrophage activation by macrophage inhibitory factor (TKP) or tuftsin (TKPR) attenuates the disease course of experimental autoimmune encephalomyelitis." BMC Immunol **8**: 10.

Bjartmar, C., G. Kidd and R. M. Ransohoff (2001). "A real-time insight into disease progression and the role of axonal injury in multiple sclerosis." Arch Neurol **58**(1): 37-39.

Bjartmar, C. and B. D. Trapp (2003). "Axonal degeneration and progressive neurologic disability in multiple sclerosis." Neurotox Res **5**(1-2): 157-164.

Black, J. A., S. Liu, B. C. Hains, C. Y. Saab and S. G. Waxman (2006). "Long-term protection of central axons with phenytoin in monophasic and chronic-relapsing EAE." Brain **129**(Pt 12): 3196-3208.

Blakemore, W. F., R. A. Eames, K. J. Smith and W. I. McDonald (1977). "Remyelination in the spinal cord of the cat following intraspinal injections of lysolecithin." J Neurol Sci **33**(1-2): 31-43.

Blakemore, W. F. and R. J. Franklin (2008). "Remyelination in experimental models of toxin-induced demyelination." Curr Top Microbiol Immunol **318**: 193-212.

Boiko, T., M. N. Rasband, S. R. Levinson, J. H. Caldwell, G. Mandel, J. S. Trimmer and G. Matthews (2001). "Compact myelin dictates the differential targeting of two sodium channel isoforms in the same axon." Neuron **30**(1): 91-104.

Boyle, M. E., E. O. Berglund, K. K. Murai, L. Weber, E. Peles and B. Ranscht (2001). "Contactin orchestrates assembly of the septate-like junctions at the paranode in myelinated peripheral nerve." Neuron **30**(2): 385-397.

Buchner, D. A., J. M. Geisinger, P. A. Glazebrook, M. G. Morgan, S. H. Spiezio, K. J. Kaiyala, M. W. Schwartz, T. Sakurai, A. J. Furley, D. L. Kunze, C. M. Croniger and J. H. Nadeau (2012). "The juxtaparanodal proteins CNTNAP2 and TAG1 regulate diet-induced obesity." Mamm Genome **23**(7-8): 431-442.

Cahoy, J. D., B. Emery, A. Kaushal, L. C. Foo, J. L. Zamanian, K. S. Christopherson, Y. Xing, J. L. Lubischer, P. A. Krieg, S. A. Krupenko, W. J. Thompson and B. A. Barres (2008). "A transcriptome database for astrocytes, neurons, and oligodendrocytes: a new resource for understanding brain development and function." J Neurosci **28**(1): 264-278.

Cai, J., Y. Qi, X. Hu, M. Tan, Z. Liu, J. Zhang, Q. Li, M. Sander and M. Qiu (2005). "Generation of oligodendrocyte precursor cells from mouse dorsal spinal cord independent of Nkx6 regulation and Shh signaling." Neuron **45**(1): 41-53.

Charles, P., S. Tait, C. Faivre-Sarrailh, G. Barbin, F. Gunn-Moore, N. Denisenko-Nehrbass, A. M. Guennoc, J. A. Girault, P. J. Brophy and C. Lubetzki (2002). "Neurofascin is a glial receptor for the paranodin/Caspr-contactin axonal complex at the axoglial junction." Curr Biol **12**(3): 217-220.

Chatzopoulou, E., A. Miguez, M. Savvaki, G. Levasseur, A. Muzerelle, M. P. Muriel, O. Goureau, K. Watanabe, L. Goutebroze, P. Gaspar, B. Zalc, D. Karagogeos and J. L. Thomas (2008). "Structural requirement of TAG-1 for retinal ganglion cell axons and myelin in the mouse optic nerve." J Neurosci **28**(30): 7624-7636.

Chiu, S. Y., L. Zhou, C. L. Zhang and A. Messing (1999). "Analysis of potassium channel functions in mammalian axons by gene knockouts." J Neurocytol **28**(4-5): 349-364.

Ciccarelli, O., D. J. Werring, C. A. Wheeler-Kingshott, G. J. Barker, G. J. Parker, A. J. Thompson and D. H. Miller (2001). "Investigation of MS normal-appearing brain using diffusion tensor MRI with clinical correlations." Neurology **56**(7): 926-933.

Colakoglu, G., U. Bergstrom-Tyrberg, E. O. Berglund and B. Ranscht (2014). "Contactin-1 regulates myelination and nodal/paranodal domain organization in the central nervous system." Proc Natl Acad Sci U S A **111**(3): E394-403.

Colognato, H. and I. D. Tzvetanova (2011). "Glia unglued: how signals from the extracellular matrix regulate the development of myelinating glia." Dev Neurobiol **71**(11): 924-955.

Coman, I., M. S. Aigrot, D. Seilhean, R. Reynolds, J. A. Girault, B. Zalc and C. Lubetzki (2006). "Nodal, paranodal and juxtaparanodal axonal proteins during demyelination and remyelination in multiple sclerosis." Brain **129**(Pt 12): 3186-3195.

Compston, A. and A. Coles (2008). "Multiple sclerosis." Lancet **372**(9648): 1502-1517.

Craner, M. J., A. C. Lo, J. A. Black and S. G. Waxman (2003). "Abnormal sodium channel distribution in optic nerve axons in a model of inflammatory demyelination." Brain **126**(Pt 7): 1552-1561.

Croxford, A. L., F. C. Kurschus and A. Waisman (2011). "Mouse models for multiple sclerosis: historical facts and future implications." Biochim Biophys Acta **1812**(2): 177-183.

Dal Canto, M. C., R. W. Melvold and B. S. Kim (1995). "A hybrid between a resistant and a susceptible strain of mouse alters the pattern of Theiler's murine encephalomyelitis virus-induced white matter disease and favors oligodendrocyte-mediated remyelination." Mult Scler **1**(2): 95-103.

Davis, J. Q., S. Lambert and V. Bennett (1996). "Molecular composition of the node of Ranvier: identification of ankyrin-binding cell adhesion molecules neurofascin (mucin+/third FNIII domain-) and NrCAM at nodal axon segments." J Cell Biol **135**(5): 1355-1367.

de Castro, F. and A. Bribian (2005). "The molecular orchestra of the migration of oligodendrocyte precursors during development." Brain Res Brain Res Rev **49**(2): 227-241.

Denaxa, M., C. H. Chan, M. Schachner, J. G. Parnavelas and D. Karagogeos (2001). "The adhesion molecule TAG-1 mediates the migration of cortical interneurons from the ganglionic eminence along the corticofugal fiber system." Development **128**(22): 4635-4644.

Dendrou, C. A., L. Fugger and M. A. Friese (2015). "Immunopathology of multiple sclerosis." Nat Rev Immunol **15**(9): 545-558.

Denisenko-Nehrbass, N., K. Oguievetskaia, L. Goutebroze, T. Galvez, H. Yamakawa, O. Ohara, M. Carnaud and J. A. Girault (2003). "Protein 4.1B associates with both Caspr/paranodin and Caspr2 at paranodes and juxtaparanodes of myelinated fibres." Eur J Neurosci **17**(2): 411-416.

Derfuss, T., K. Parikh, S. Velhin, M. Braun, E. Mathey, M. Krumbholz, T. Kumpfel, A. Moldenhauer, C. Rader, P. Sonderegger, W. Pollmann, C. Tiefenthaller, J. Bauer, H. Lassmann, H. Wekerle, D. Karagogeos, R. Hohlfeld, C. Linington and E. Meinl (2009). "Contactin-2/TAG-1-directed autoimmunity is identified in multiple sclerosis patients and mediates gray matter pathology in animals." Proc Natl Acad Sci U S A **106**(20): 8302-8307.

Duffy, S. S., J. G. Lees and G. Moalem-Taylor (2014). "The contribution of immune and glial cell types in experimental autoimmune encephalomyelitis and multiple sclerosis." Mult Scler Int **2014**: 285245.

Dugandzija-Novakovic, S., A. G. Koszowski, S. R. Levinson and P. Shrager (1995). "Clustering of Na+ channels and node of Ranvier formation in remyelinating axons." J Neurosci **15**(1 Pt 2): 492-503.

Dugas, J. C., T. L. Cuellar, A. Scholze, B. Ason, A. Ibrahim, B. Emery, J. L. Zamanian, L. C. Foo, M. T. McManus and B. A. Barres (2010). "Dicer1 and miR-219 Are required for normal oligodendrocyte differentiation and myelination." Neuron **65**(5): 597-611.

Duncan, D. (1934). "The Importance of Diameter as a Factor in Myelination." Science **79**(2051): 363.

Emery, B., D. Agalliu, J. D. Cahoy, T. A. Watkins, J. C. Dugas, S. B. Mulinyawe, A. Ibrahim, K. L. Ligon, D. H. Rowitch and B. A. Barres (2009). "Myelin gene regulatory factor is a critical transcriptional regulator required for CNS myelination." Cell **138**(1): 172-185.

Esiri, M. M. (1980). "Multiple sclerosis: a quantitative and qualitative study of immunoglobulin-containing cells in the central nervous system." Neuropathol Appl Neurobiol **6**(1): 9-21.

Feinberg, K., Y. Eshed-Eisenbach, S. Frechter, V. Amor, D. Salomon, H. Sabanay, J. L. Dupree, M. Grumet, P. J. Brophy, P. Shrager and E. Peles (2010). "A glial signal consisting of gliomedin and NrCAM clusters axonal Na+ channels during the formation of nodes of Ranvier." Neuron **65**(4): 490-502.

Ferent, J., M. Ruat and E. Traiffort (2013). "Investigation of the proteolipid protein promoter activity during demyelination and repair." Differentiation **85**(4-5): 182-189.

Filippi, M., M. A. Rocca, F. Barkhof, W. Bruck, J. T. Chen, G. Comi, G. DeLuca, N. De Stefano, B. J. Erickson, N. Evangelou, F. Fazekas, J. J. Geurts, C. Lucchinetti, D. H. Miller, D. Pelletier, B. F. Popescu, H. Lassmann and M. R. I. f. i. M. S. w. Attendees of the Correlation between Pathological (2012). "Association between pathological and MRI findings in multiple sclerosis." Lancet Neurol **11**(4): 349-360.

Filippi, M., C. Tortorella and M. Bozzali (1999). "Normal-appearing white matter changes in multiple sclerosis: the contribution of magnetic resonance techniques." Mult Scler **5**(4): 273-282.

Fitzli, D., E. T. Stoeckli, S. Kunz, K. Siribour, C. Rader, B. Kunz, S. V. Kozlov, A. Buchstaller, R. P. Lane, D. M. Suter, W. J. Dreyer and P. Sonderegger (2000). "A direct interaction of axonin-1 with NgCAM-related cell adhesion molecule (NrCAM) results in guidance, but not growth of commissural axons." J Cell Biol **149**(4): 951-968.

Fogarty, M., W. D. Richardson and N. Kessaris (2005). "A subset of oligodendrocytes generated from radial glia in the dorsal spinal cord." Development **132**(8): 1951-1959.

Fontenot, J. D. and A. Y. Rudensky (2005). "A well adapted regulatory contrivance: regulatory T cell development and the forkhead family transcription factor Foxp3." Nat Immunol **6**(4): 331-337.

Foote, A. K. and W. F. Blakemore (2005). "Inflammation stimulates remyelination in areas of chronic demyelination." Brain **128**(Pt 3): 528-539.

Franklin, R. J. and C. Ffrench-Constant (2008). "Remyelination in the CNS: from biology to therapy." Nat Rev Neurosci **9**(11): 839-855.

Franklin, R. J. and S. A. Goldman (2015). "Glia Disease and Repair-Remyelination." Cold Spring Harb Perspect Biol **7**(7): a020594.

Friede, R. L. and T. Samorajski (1967). "Relation between the number of myelin lamellae and axon circumference in fibers of vagus and sciatic nerves of mice." J Comp Neurol **130**(3): 223-231.

Frischer, J. M., S. Bramow, A. Dal-Bianco, C. F. Lucchinetti, H. Rauschka, M. Schmidbauer, H. Laursen, P. S. Sorensen and H. Lassmann (2009). "The relation between inflammation and neurodegeneration in multiple sclerosis brains." Brain **132**(Pt 5): 1175-1189.

Frohman, E. M., M. K. Racke and C. S. Raine (2006). "Multiple sclerosis--the plaque and its pathogenesis." N Engl J Med **354**(9): 942-955.

Fukamauchi, F., O. Aihara, Y. J. Wang, K. Akasaka, Y. Takeda, M. Horie, H. Kawano, K. Sudo, M. Asano, K. Watanabe and Y. Iwakura (2001). "TAG-1-deficient mice have marked elevation of adenosine A1 receptors in the hippocampus." Biochem Biophys Res Commun **281**(1): 220-226.

Funfschilling, U., L. M. Supplie, D. Mahad, S. Boretius, A. S. Saab, J. Edgar, B. G. Brinkmann, C. M. Kassmann, I. D. Tzvetanova, W. Mobius, F. Diaz, D. Meijer, U. Suter, B. Hamprecht, M. W. Sereda, C. T. Moraes, J. Frahm, S. Goebbels and K. A. Nave (2012). "Glycolytic oligodendrocytes maintain myelin and long-term axonal integrity." Nature **485**(7399): 517-521.

Furley, A. J., S. B. Morton, D. Manalo, D. Karagogeos, J. Dodd and T. M. Jessell (1990). "The axonal glycoprotein TAG-1 is an immunoglobulin superfamily member with neurite outgrowth-promoting activity." Cell **61**(1): 157-170.

Gensert, J. M. and J. E. Goldman (1997). "Endogenous progenitors remyelinate demyelinated axons in the adult CNS." Neuron **19**(1): 197-203.

Giedd, J. N. (2004). "Structural magnetic resonance imaging of the adolescent brain." Ann N Y Acad Sci **1021**: 77-85.

Glasscock, E., J. Qian, M. J. Kole and J. L. Noebels (2012). "Transcompartmental reversal of single fibre hyperexcitability in juxtaparanodal Kv1.1-deficient vagus nerve axons by activation of nodal KCNQ channels." J Physiol **590**(Pt 16): 3913-3926.

Halter, J. A. and J. W. Clark, Jr. (1993). "The influence of nodal constriction on conduction velocity in myelinated nerve fibers." Neuroreport **4**(1): 89-92.

Hametner, S., I. Wimmer, L. Haider, S. Pfeifenbring, W. Bruck and H. Lassmann (2013). "Iron and neurodegeneration in the multiple sclerosis brain." Ann Neurol **74**(6): 848-861.

Herrero-Herranz, E., L. A. Pardo, R. Gold and R. A. Linker (2008). "Pattern of axonal injury in murine myelin oligodendrocyte glycoprotein induced experimental autoimmune encephalomyelitis: implications for multiple sclerosis." Neurobiol Dis **30**(2): 162-173.

Hildebrand, C., S. Remahl, H. Persson and C. Bjartmar (1993). "Myelinated nerve fibres in the CNS." Prog Neurobiol **40**(3): 319-384.

Hines, J. H., A. M. Ravanelli, R. Schwindt, E. K. Scott and B. Appel (2015). "Neuronal activity biases axon selection for myelination in vivo." Nat Neurosci **18**(5): 683-689.

Hornig, J., F. Frob, M. R. Vogl, I. Hermans-Borgmeyer, E. R. Tamm and M. Wegner (2013). "The transcription factors Sox10 and Myrf define an essential regulatory network module in differentiating oligodendrocytes." PLoS Genet **9**(10): e1003907.

Horresh, I., V. Bar, J. L. Kissil and E. Peles (2010). "Organization of myelinated axons by Caspr and Caspr2 requires the cytoskeletal adapter protein 4.1B." J Neurosci **30**(7): 2480-2489.

Horresh, I., S. Poliak, S. Grant, D. Bredt, M. N. Rasband and E. Peles (2008). "Multiple molecular interactions determine the clustering of Caspr2 and Kv1 channels in myelinated axons." J Neurosci **28**(52): 14213-14222.

Howell, O. W., A. Palser, A. Polito, S. Melrose, B. Zonta, C. Scheiermann, A. J. Vora, P. J. Brophy and R. Reynolds (2006). "Disruption of neurofascin localization reveals early changes preceding demyelination and remyelination in multiple sclerosis." Brain **129**(Pt 12): 3173-3185.

Howell, O. W., J. L. Rundle, A. Garg, M. Komada, P. J. Brophy and R. Reynolds (2010). "Activated microglia mediate axoglial disruption that contributes to axonal injury in multiple sclerosis." J Neuropathol Exp Neurol **69**(10): 1017-1033.

Huang, J. K., S. P. Fancy, C. Zhao, D. H. Rowitch, C. Ffrench-Constant and R. J. Franklin (2011). "Myelin regeneration in multiple sclerosis: targeting endogenous stem cells." Neurotherapeutics **8**(4): 650-658.

Huebner, E. A. and S. M. Strittmatter (2009). "Axon regeneration in the peripheral and central nervous systems." Results Probl Cell Differ **48**: 339-351.

Huseby, E. S., D. Liggitt, T. Brabb, B. Schnabel, C. Ohlen and J. Goverman (2001). "A pathogenic role for myelin-specific CD8(+) T cells in a model for multiple sclerosis." J Exp Med **194**(5): 669-676.

Ioannou, M., T. Alissafi, I. Lazaridis, G. Deraos, J. Matsoukas, A. Gravanis, V. Mastorodemos, A. Plaitakis, A. Sharpe, D. Boumpas and P. Verginis (2012). "Crucial role of granulocytic myeloid-derived suppressor cells in the regulation of central nervous system autoimmune disease." J Immunol **188**(3): 1136-1146.

Itoh, K., B. Stevens, M. Schachner and R. D. Fields (1995). "Regulated expression of the neural cell adhesion molecule L1 by specific patterns of neural impulses." Science **270**(5240): 1369-1372.

Kaplan, M. R., M. H. Cho, E. M. Ullian, L. L. Isom, S. R. Levinson and B. A. Barres (2001). "Differential control of clustering of the sodium channels Na(v)1.2 and Na(v)1.6 at developing CNS nodes of Ranvier." Neuron **30**(1): 105-119.

Karagogeos, D., S. B. Morton, F. Casano, J. Dodd and T. M. Jessell (1991). "Developmental expression of the axonal glycoprotein TAG-1: differential regulation by central and peripheral neurons in vitro." Development **112**(1): 51-67.

Keane, T. M., L. Goodstadt, P. Danecek, M. A. White, K. Wong, B. Yalcin, A. Heger, A. Agam, G. Slater, M. Goodson, N. A. Furlotte, E. Eskin, C. Nellaker, H. Whitley, J. Cleak, D. Janowitz, P. Hernandez-Pliego, A. Edwards, T. G. Belgard, P. L. Oliver, R. E. McIntyre, A. Bhomra, J. Nicod, X. Gan, W. Yuan, L. van der Weyden, C. A. Steward, S. Bala, J. Stalker, R. Mott, R. Durbin, I. J. Jackson, A. Czechanski, J. A. Guerra-Assuncao, L. R. Donahue, L. G. Reinholdt, B. A. Payseur, C. P. Ponting, E. Birney, J. Flint and D. J. Adams (2011). "Mouse genomic variation and its effect on phenotypes and gene regulation." Nature **477**(7364): 289-294.

Kessaris, N., M. Fogarty, P. Iannarelli, M. Grist, M. Wegner and W. D. Richardson (2006). "Competing waves of oligodendrocytes in the forebrain and postnatal elimination of an embryonic lineage." Nat Neurosci **9**(2): 173-179.

Kirby, B. B., N. Takada, A. J. Latimer, J. Shin, T. J. Carney, R. N. Kelsh and B. Appel (2006). "In vivo time-lapse imaging shows dynamic oligodendrocyte progenitor behavior during zebrafish development." Nat Neurosci **9**(12): 1506-1511.

Kornek, B., M. K. Storch, R. Weissert, E. Wallstroem, A. Stefferl, T. Olsson, C. Linington, M. Schmidbauer and H. Lassmann (2000). "Multiple sclerosis and chronic autoimmune encephalomyelitis: a comparative quantitative study of axonal injury in active, inactive, and remyelinated lesions." Am J Pathol **157**(1): 267-276.

Kotter, M. R., W. W. Li, C. Zhao and R. J. Franklin (2006). "Myelin impairs CNS remyelination by inhibiting oligodendrocyte precursor cell differentiation." J Neurosci **26**(1): 328-332.

Kotter, M. R., C. Zhao, N. van Rooijen and R. J. Franklin (2005). "Macrophage-depletion induced impairment of experimental CNS remyelination is associated with a reduced oligodendrocyte progenitor cell response and altered growth factor expression." Neurobiol Dis **18**(1): 166-175.

Kucenas, S., H. Snell and B. Appel (2008). "nkx2.2a promotes specification and differentiation of a myelinating subset of oligodendrocyte lineage cells in zebrafish." Neuron Glia Biol **4**(2): 71-81.

Kuhlmann, T., V. Miron, Q. Cui, C. Wegner, J. Antel and W. Bruck (2008). "Differentiation block of oligodendroglial progenitor cells as a cause for remyelination failure in chronic multiple sclerosis." Brain **131**(Pt 7): 1749-1758.

Kunz, S., M. Spirig, C. Ginsburg, A. Buchstaller, P. Berger, R. Lanz, C. Rader, L. Vogt, B. Kunz and P. Sonderegger (1998). "Neurite fasciculation mediated by complexes of axonin-1 and Ng cell adhesion molecule." J Cell Biol **143**(6): 1673-1690.

Kutzelnigg, A., C. F. Lucchinetti, C. Stadelmann, W. Bruck, H. Rauschka, M. Bergmann, M. Schmidbauer, J. E. Parisi and H. Lassmann (2005). "Cortical demyelination and diffuse white matter injury in multiple sclerosis." Brain **128**(Pt 11): 2705-2712.

Kyriakopoulou, K., I. de Diego, M. Wassef and D. Karagogeos (2002). "A combination of chain and neurophilic migration involving the adhesion molecule TAG-1 in the caudal medulla." Development **129**(2): 287-296.

Labasque, M. and C. Faivre-Sarrailh (2010). "GPI-anchored proteins at the node of Ranvier." FEBS Lett **584**(9): 1787-1792.

Lassmann, H. (1998). "Neuropathology in multiple sclerosis: new concepts." Mult Scler **4**(3): 93-98.

Lassmann, H. (2011). "Review: the architecture of inflammatory demyelinating lesions: implications for studies on pathogenesis." Neuropathol Appl Neurobiol **37**(7): 698-710.

Lassmann, H. (2014). "Mechanisms of white matter damage in multiple sclerosis." Glia **62**(11): 1816-1830.

Lassmann, H., W. Bruck and C. F. Lucchinetti (2007). "The immunopathology of multiple sclerosis: an overview." Brain Pathol **17**(2): 210-218.

Lassmann, H., C. S. Raine, J. Antel and J. W. Prineas (1998). "Immunopathology of multiple sclerosis: report on an international meeting held at the Institute of Neurology of the University of Vienna." J Neuroimmunol **86**(2): 213-217.

Lassmann, H. and J. van Horssen (2011). "The molecular basis of neurodegeneration in multiple sclerosis." FEBS Lett **585**(23): 3715-3723.

Lassmann, H., J. van Horssen and D. Mahad (2012). "Progressive multiple sclerosis: pathology and pathogenesis." Nat Rev Neurol **8**(11): 647-656.

Lau, P., J. D. Verrier, J. A. Nielsen, K. R. Johnson, L. Notterpek and L. D. Hudson (2008). "Identification of dynamically regulated microRNA and mRNA networks in developing oligodendrocytes." J Neurosci **28**(45): 11720-11730.

Lauber, K., E. Bohn, S. M. Krober, Y. J. Xiao, S. G. Blumenthal, R. K. Lindemann, P. Marini, C. Wiedig, A. Zobywalski, S. Baksh, Y. Xu, I. B. Autenrieth, K. Schulze-Osthoff, C. Belka, G. Stuhler and S. Wesselborg (2003). "Apoptotic cells induce migration of phagocytes via caspase-3-mediated release of a lipid attraction signal." Cell **113**(6): 717-730.

Lee, S., S. Y. Chong, S. J. Tuck, J. M. Corey and J. R. Chan (2013). "A rapid and reproducible assay for modeling myelination by oligodendrocytes using engineered nanofibers." Nat Protoc **8**(4): 771-782.

Lee, S., M. K. Leach, S. A. Redmond, S. Y. Chong, S. H. Mellon, S. J. Tuck, Z. Q. Feng, J. M. Corey and J. R. Chan (2012). "A culture system to study oligodendrocyte myelination processes using engineered nanofibers." Nat Methods **9**(9): 917-922.

Lee, Y., B. M. Morrison, Y. Li, S. Lengacher, M. H. Farah, P. N. Hoffman, Y. Liu, A. Tsingalia, L. Jin, P. W. Zhang, L. Pellerin, P. J. Magistretti and J. D. Rothstein (2012). "Oligodendroglia metabolically support axons and contribute to neurodegeneration." Nature **487**(7408): 443-448.

Lieberoth, A., F. Splittstoesser, N. Katagihallimath, I. Jakovcevski, G. Loers, B. Ranscht, D. Karagogeos, M. Schachner and R. Kleene (2009). "Lewis(x) and alpha2,3-sialyl glycans and their receptors TAG-1, Contactin, and L1 mediate CD24-dependent neurite outgrowth." J Neurosci **29**(20): 6677-6690.

Lindner, M., J. K. Ng, S. Hochmeister, E. Meinl and C. Linington (2013). "Neurofascin 186 specific autoantibodies induce axonal injury and exacerbate disease severity in experimental autoimmune encephalomyelitis." Exp Neurol **247**: 259-266.

Liu, J., L. Magri, F. Zhang, N. O. Marsh, S. Albrecht, J. L. Huynh, J. Kaur, T. Kuhlmann, W. Zhang, P. A. Slesinger and P. Casaccia (2015). "Chromatin landscape defined by repressive histone methylation during oligodendrocyte differentiation." J Neurosci **35**(1): 352-365.

Liu, Y. and M. C. Halloran (2005). "Central and peripheral axon branches from one neuron are guided differentially by Semaphorin3D and transient axonal glycoprotein-1." J Neurosci **25**(45): 10556-10563.

Liu, Z., Y. Li, J. Zhang, S. Elias and M. Chopp (2008). "Evaluation of corticospinal axon loss by fluorescent dye tracing in mice with experimental autoimmune encephalomyelitis." J Neurosci Methods **167**(2): 191-197.

Lucchinetti, C., W. Bruck, J. Parisi, B. Scheithauer, M. Rodriguez and H. Lassmann (2000). "Heterogeneity of multiple sclerosis lesions: implications for the pathogenesis of demyelination." Ann Neurol **47**(6): 707-717.

Lucchinetti, C. F., W. Bruck, M. Rodriguez and H. Lassmann (1996). "Distinct patterns of multiple sclerosis pathology indicates heterogeneity on pathogenesis." Brain Pathol **6**(3): 259-274.

Ma, Q. H., T. Futagawa, W. L. Yang, X. D. Jiang, L. Zeng, Y. Takeda, R. X. Xu, D. Bagnard, M. Schachner, A. J. Furley, D. Karagogeos, K. Watanabe, G. S. Dawe and Z. C. Xiao (2008). "A TAG1-APP signalling pathway through Fe65 negatively modulates neurogenesis." Nat Cell Biol **10**(3): 283-294.

Mahad, D. H., B. D. Trapp and H. Lassmann (2015). "Pathological mechanisms in progressive multiple sclerosis." Lancet Neurol **14**(2): 183-193.

Maier, O., W. Baron and D. Hoekstra (2007). "Reduced raft-association of NF155 in active MS-lesions is accompanied by the disruption of the paranodal junction." Glia **55**(8): 885-895.

Marin-Husstege, M., M. Muggironi, A. Liu and P. Casaccia-Bonnefil (2002). "Histone deacetylase activity is necessary for oligodendrocyte lineage progression." J Neurosci **22**(23): 10333-10345.

Markoullis, K., I. Sargiannidou, C. Gardner, A. Hadjisavvas, R. Reynolds and K. A. Kleopa (2012). "Disruption of oligodendrocyte gap junctions in experimental autoimmune encephalomyelitis." Glia **60**(7): 1053-1066.

Markoullis, K., I. Sargiannidou, N. Schiza, A. Hadjisavvas, F. Roncaroli, R. Reynolds and K. A. Kleopa (2012). "Gap junction pathology in multiple sclerosis lesions and normal-appearing white matter." Acta Neuropathol **123**(6): 873-886.

Mason, J. L., C. Langaman, P. Morell, K. Suzuki and G. K. Matsushima (2001). "Episodic demyelination and subsequent remyelination within the murine central nervous system: changes in axonal calibre." Neuropathol Appl Neurobiol **27**(1): 50-58.

Menegoz, M., P. Gaspar, M. Le Bert, T. Galvez, F. Burgaya, C. Palfrey, P. Ezan, F. Arnos and J. A. Girault (1997). "Paranodin, a glycoprotein of neuronal paranodal membranes." Neuron **19**(2): 319-331.

Menn, B., J. M. Garcia-Verdugo, C. Yaschine, O. Gonzalez-Perez, D. Rowitch and A. Alvarez-Buylla (2006). "Origin of oligodendrocytes in the subventricular zone of the adult brain." J Neurosci **26**(30): 7907-7918.

Mensch, S., M. Baraban, R. Almeida, T. Czopka, J. Ausborn, A. El Manira and D. A. Lyons (2015). "Synaptic vesicle release regulates myelin sheath number of individual oligodendrocytes in vivo." Nat Neurosci **18**(5): 628-630.

Miller, D. J., T. Duka, C. D. Stimpson, S. J. Schapiro, W. B. Baze, M. J. McArthur, A. J. Fobbs, A. M. Sousa, N. Sestan, D. E. Wildman, L. Lipovich, C. W. Kuzawa, P. R. Hof and C. C. Sherwood (2012). "Prolonged myelination in human neocortical evolution." Proc Natl Acad Sci U S A **109**(41): 16480-16485.

Miller, R. H. and S. L. Fyffe-Maricich (2010). "Restoring the balance between disease and repair in multiple sclerosis: insights from mouse models." Dis Model Mech **3**(9-10): 535-539.

Miron, V. E., A. Boyd, J. W. Zhao, T. J. Yuen, J. M. Ruckh, J. L. Shadrach, P. van Wijngaarden, A. J. Wagers, A. Williams, R. J. Franklin and C. ffrench-Constant (2013). "M2 microglia and macrophages drive oligodendrocyte differentiation during CNS remyelination." Nat Neurosci **16**(9): 1211-1218.

Mirsky, R., J. Winter, E. R. Abney, R. M. Pruss, J. Gavrilovic and M. C. Raff (1980). "Myelin-specific proteins and glycolipids in rat Schwann cells and oligodendrocytes in culture." J Cell Biol **84**(3): 483-494.

Mitew, S., C. M. Hay, H. Peckham, J. Xiao, M. Koenning and B. Emery (2014). "Mechanisms regulating the development of oligodendrocytes and central nervous system myelin." Neuroscience **276**: 29-47.

Morgan, L., K. R. Jessen and R. Mirsky (1991). "The effects of cAMP on differentiation of cultured Schwann cells: progression from an early phenotype (04+) to a myelin phenotype (P0+, GFAP-, N-CAM-, NGF-receptor-) depends on growth inhibition." J Cell Biol **112**(3): 457-467.

Morrison, B. M., Y. Lee and J. D. Rothstein (2013). "Oligodendroglia: metabolic supporters of axons." Trends Cell Biol **23**(12): 644-651.

Mycko, M. P., R. Papoian, U. Boschert, C. S. Raine and K. W. Selmaj (2004). "Microarray gene expression profiling of chronic active and inactive lesions in multiple sclerosis." Clin Neurol Neurosurg **106**(3): 223-229.

Nave, K. A. and H. B. Werner (2014). "Myelination of the nervous system: mechanisms and functions." Annu Rev Cell Dev Biol **30**: 503-533.

Nikic, I., D. Merkler, C. Sorbara, M. Brinkoetter, M. Kreutzfeldt, F. M. Bareyre, W. Bruck, D. Bishop, T. Misgeld and M. Kerschensteiner (2011). "A reversible form of axon damage in experimental autoimmune encephalomyelitis and multiple sclerosis." Nat Med **17**(4): 495-499.

Novakovic, S. D., T. J. Deerinck, S. R. Levinson, P. Shrager and M. H. Ellisman (1996). "Clusters of axonal Na+ channels adjacent to remyelinating Schwann cells." J Neurocytol **25**(6): 403-412.

Ogawa, Y., J. Oses-Prieto, M. Y. Kim, I. Horresh, E. Peles, A. L. Burlingame, J. S. Trimmer, D. Meijer and M. N. Rasband (2010). "ADAM22, a Kv1 channel-interacting protein, recruits membrane-associated guanylate kinases to juxtaparanodes of myelinated axons." J Neurosci **30**(3): 1038-1048.

Okamoto, M., T. Namba, T. Shinoda, T. Kondo, T. Watanabe, Y. Inoue, K. Takeuchi, Y. Enomoto, K. Ota, K. Oda, Y. Wada, K. Sagou, K. Saito, A. Sakakibara, A. Kawaguchi, K. Nakajima, T. Adachi, T. Fujimori, M. Ueda, S. Hayashi, K. Kaibuchi and T. Miyata (2013). "TAG-1-assisted progenitor elongation streamlines nuclear migration to optimize subapical crowding." Nat Neurosci **16**(11): 1556-1566.

Olivier, C., I. Cobos, E. M. Perez Villegas, N. Spassky, B. Zalc, S. Martinez and J. L. Thomas (2001). "Monofocal origin of telencephalic oligodendrocytes in the anterior entopeduncular area of the chick embryo." Development **128**(10): 1757-1769.

Orentas, D. M., J. E. Hayes, K. L. Dyer and R. H. Miller (1999). "Sonic hedgehog signaling is required during the appearance of spinal cord oligodendrocyte precursors." Development **126**(11): 2419-2429.

Ozawa, K., G. Suchanek, H. Breitschopf, W. Bruck, H. Budka, K. Jellinger and H. Lassmann (1994). "Patterns of oligodendroglia pathology in multiple sclerosis." Brain **117 (Pt 6)**: 1311-1322.

Pan, Z., T. Kao, Z. Horvath, J. Lemos, J. Y. Sul, S. D. Cranstoun, V. Bennett, S. S. Scherer and E. C. Cooper (2006). "A common ankyrin-G-based mechanism retains KCNQ and NaV channels at electrically active domains of the axon." J Neurosci **26**(10): 2599-2613.

Patani, R., M. Balaratnam, A. Vora and R. Reynolds (2007). "Remyelination can be extensive in multiple sclerosis despite a long disease course." Neuropathol Appl Neurobiol **33**(3): 277-287.

Paterson, P. Y. and E. D. Day (1979). "Neuroimmunologic disease: experimental and clinical aspects." Hosp Pract **14**(7): 49-58.

Patrikios, P., C. Stadelmann, A. Kutzelnigg, H. Rauschka, M. Schmidbauer, H. Laursen, P. S. Sorensen, W. Bruck, C. Lucchinetti and H. Lassmann (2006). "Remyelination is extensive in a subset of multiple sclerosis patients." Brain **129**(Pt 12): 3165-3172.

Pavlou, O., K. Theodorakis, J. Falk, M. Kutsche, M. Schachner, C. Faivre-Sarrailh and D. Karagogeos (2002). "Analysis of interactions of the adhesion molecule TAG-1 and its domains with other immunoglobulin superfamily members." Mol Cell Neurosci **20**(3): 367-381.

Peles, E., M. Nativ, M. Lustig, M. Grumet, J. Schilling, R. Martinez, G. D. Plowman and J. Schlessinger (1997). "Identification of a novel contactin-associated transmembrane receptor with multiple domains implicated in protein-protein interactions." EMBO J **16**(5): 978-988.

Pfeiffer, S. E., A. E. Warrington and R. Bansal (1993). "The oligodendrocyte and its many cellular processes." Trends Cell Biol **3**(6): 191-197.

Plumb, J., S. McQuaid, M. Mirakhur and J. Kirk (2002). "Abnormal endothelial tight junctions in active lesions and normal-appearing white matter in multiple sclerosis." Brain Pathol **12**(2): 154-169.

Poliak, S. and E. Peles (2003). "The local differentiation of myelinated axons at nodes of Ranvier." Nat Rev Neurosci **4**(12): 968-980.

Poliak, S., D. Salomon, H. Elhanany, H. Sabanay, B. Kiernan, L. Pevny, C. L. Stewart, X. Xu, S. Y. Chiu, P. Shrager, A. J. Furley and E. Peles (2003). "Juxtaparanodal clustering of Shaker-like K+ channels in myelinated axons depends on Caspr2 and TAG-1." J Cell Biol **162**(6): 1149-1160.

Ponomarev, E. D., L. P. Shriver, K. Maresz and B. N. Dittel (2005). "Microglial cell activation and proliferation precedes the onset of CNS autoimmunity." J Neurosci Res **81**(3): 374-389.

Popescu, B. F. and C. F. Lucchinetti (2012). "Pathology of demyelinating diseases." Annu Rev Pathol **7**: 185-217.

Pourabdolhossein, F., S. Mozafari, G. Morvan-Dubois, J. Mirnajafi-Zadeh, A. Lopez-Juarez, J. Pierre-Simons, B. A. Demeneix and M. Javan (2014). "Nogo receptor inhibition enhances functional recovery following lysolecithin-induced demyelination in mouse optic chiasm." PLoS One **9**(9): e106378.

Prineas, J. W. and F. Connell (1979). "Remyelination in multiple sclerosis." Ann Neurol **5**(1): 22-31.

Prineas, J. W., E. E. Kwon, E. S. Cho, L. R. Sharer, M. H. Barnett, E. L. Oleszak, B. Hoffman and B. P. Morgan (2001). "Immunopathology of secondary-progressive multiple sclerosis." Ann Neurol **50**(5): 646-657.

Pringle, N. P. and W. D. Richardson (1993). "A singularity of PDGF alpha-receptor expression in the dorsoventral axis of the neural tube may define the origin of the oligodendrocyte lineage." Development **117**(2): 525-533.

Raine, C. S., L. Scheinberg and J. M. Waltz (1981). "Multiple sclerosis. Oligodendrocyte survival and proliferation in an active established lesion." Lab Invest **45**(6): 534-546.

Ransohoff, R. M. (2012). "Animal models of multiple sclerosis: the good, the bad and the bottom line." Nat Neurosci **15**(8): 1074-1077.

Rasband, M. N. (2004). "It's "juxta" potassium channel!" J Neurosci Res **76**(6): 749-757.

Rasband, M. N., T. Kagawa, E. W. Park, K. Ikenaka and J. S. Trimmer (2003). "Dysregulation of axonal sodium channel isoforms after adult-onset chronic demyelination." J Neurosci Res **73**(4): 465-470.

Rasband, M. N., E. W. Park, D. Zhen, M. I. Arbuckle, S. Poliak, E. Peles, S. G. Grant and J. S. Trimmer (2002). "Clustering of neuronal potassium channels is independent of their interaction with PSD-95." J Cell Biol **159**(4): 663-672.

Rasband, M. N., E. Peles, J. S. Trimmer, S. R. Levinson, S. E. Lux and P. Shrager (1999). "Dependence of nodal sodium channel clustering on paranodal axoglial contact in the developing CNS." J Neurosci **19**(17): 7516-7528.

Rasband, M. N., J. S. Trimmer, T. L. Schwarz, S. R. Levinson, M. H. Ellisman, M. Schachner and P. Shrager (1998). "Potassium channel distribution, clustering, and function in remyelinating rat axons." J Neurosci **18**(1): 36-47.

Recks, M. S., E. R. Stormanns, J. Bader, S. Arnhold, K. Addicks and S. Kuerten (2013). "Early axonal damage and progressive myelin pathology define the kinetics of CNS histopathology in a mouse model of multiple sclerosis." Clin Immunol **149**(1): 32-45.

Reynolds, R., F. Roncaroli, R. Nicholas, B. Radotra, D. Gveric and O. Howell (2011). "The neuropathological basis of clinical progression in multiple sclerosis." Acta Neuropathol **122**(2): 155-170.

Richardson, W. D., N. Kessaris and N. Pringle (2006). "Oligodendrocyte wars." Nat Rev Neurosci **7**(1): 11-18.

Richardson, W. D., H. K. Smith, T. Sun, N. P. Pringle, A. Hall and R. Woodruff (2000). "Oligodendrocyte lineage and the motor neuron connection." Glia **29**(2): 136-142.

Rios, J. C., C. V. Melendez-Vasquez, S. Einheber, M. Lustig, M. Grumet, J. Hemperly, E. Peles and J. L. Salzer (2000). "Contactin-associated protein (Caspr) and contactin form a complex that is targeted to the paranodal junctions during myelination." J Neurosci **20**(22): 8354-8364.

Rodriguez, E. G., C. Wegner, M. Kreutzfeldt, K. Neid, D. R. Thal, T. Jurgens, W. Bruck, C. Stadelmann and D. Merkler (2014). "Oligodendroglia in cortical multiple sclerosis lesions decrease with disease progression, but regenerate after repeated experimental demyelination." Acta Neuropathol **128**(2): 231-246.

Rosenberg, S. S., E. E. Kelland, E. Tokar, A. R. De la Torre and J. R. Chan (2008). "The geometric and spatial constraints of the microenvironment induce oligodendrocyte differentiation." Proc Natl Acad Sci U S A **105**(38): 14662-14667.

Rowitch, D. H. (2004). "Glial specification in the vertebrate neural tube." Nat Rev Neurosci **5**(5): 409-419.

Runmarker, B. and O. Andersen (1993). "Prognostic factors in a multiple sclerosis incidence cohort with twenty-five years of follow-up." Brain **116 (Pt 1)**: 117-134.

Sahel, A., F. C. Ortiz, C. Kerninon, P. P. Maldonado, M. C. Angulo and B. Nait-Oumesmar (2015). "Alteration of synaptic connectivity of oligodendrocyte precursor cells following demyelination." Front Cell Neurosci **9**: 77.

Sakaguchi, S., T. Yamaguchi, T. Nomura and M. Ono (2008). "Regulatory T cells and immune tolerance." Cell **133**(5): 775-787.

Samanta, J., E. M. Grund, H. M. Silva, J. J. Lafaille, G. Fishell and J. L. Salzer (2015). "Inhibition of Gli1 mobilizes endogenous neural stem cells for remyelination." Nature **526**(7573): 448-452.

Savvaki, M., T. Panagiotaropoulos, A. Stamatakis, I. Sargiannidou, P. Karatzioula, K. Watanabe, F. Stylianopoulou, D. Karagogeos and K. A. Kleopa (2008). "Impairment of learning and memory in TAG-1 deficient mice associated with shorter CNS internodes and disrupted juxtaparanodes." Mol Cell Neurosci **39**(3): 478-490.

Savvaki, M., K. Theodorakis, L. Zoupi, A. Stamatakis, S. Tivodar, K. Kyriacou, F. Stylianopoulou and D. Karagogeos (2010). "The expression of TAG-1 in glial cells is sufficient for the formation of the juxtaparanodal complex and the phenotypic rescue of tag-1 homozygous mutants in the CNS." J Neurosci **30**(42): 13943-13954.

Schneider, C. A., W. S. Rasband and K. W. Eliceiri (2012). "NIH Image to ImageJ: 25 years of image analysis." Nat Methods **9**(7): 671-675.

Scolding, N., R. Franklin, S. Stevens, C. H. Heldin, A. Compston and J. Newcombe (1998). "Oligodendrocyte progenitors are present in the normal adult human CNS and in the lesions of multiple sclerosis." Brain **121 (Pt 12)**: 2221-2228.

Serafini, B., B. Rosicarelli, R. Magliozzi, E. Stigliano and F. Aloisi (2004). "Detection of ectopic B-cell follicles with germinal centers in the meninges of patients with secondary progressive multiple sclerosis." Brain Pathol **14**(2): 164-174.

Sherman, D. L., S. Tait, S. Melrose, R. Johnson, B. Zonta, F. A. Court, W. B. Macklin, S. Meek, A. J. Smith, D. F. Cottrell and P. J. Brophy (2005). "Neurofascins are required to establish axonal domains for saltatory conduction." Neuron **48**(5): 737-742.

Sherratt, R. M., H. Bostock and T. A. Sears (1980). "Effects of 4-aminopyridine on normal and demyelinated mammalian nerve fibres." Nature **283**(5747): 570-572.

Smith, K. J., P. A. Felts and G. R. John (2000). "Effects of 4-aminopyridine on demyelinated axons, synapses and muscle tension." Brain **123 (Pt 1)**: 171-184.

Snaidero, N., W. Mobius, T. Czopka, L. H. Hekking, C. Mathisen, D. Verkleij, S. Goebbels, J. Edgar, D. Merkler, D. A. Lyons, K. A. Nave and M. Simons (2014). "Myelin membrane wrapping of CNS axons by PI(3,4,5)P3-dependent polarized growth at the inner tongue." Cell **156**(1-2): 277-290.

Soulika, A. M., E. Lee, E. McCauley, L. Miers, P. Bannerman and D. Pleasure (2009). "Initiation and progression of axonopathy in experimental autoimmune encephalomyelitis." J Neurosci **29**(47): 14965-14979.

Spassky, N., C. Goujet-Zalc, E. Parmantier, C. Olivier, S. Martinez, A. Ivanova, K. Ikenaka, W. Macklin, I. Cerruti, B. Zalc and J. L. Thomas (1998). "Multiple restricted origin of oligodendrocytes." J Neurosci **18**(20): 8331-8343.

Spassky, N., K. Heydon, A. Mangatal, A. Jankovski, C. Olivier, F. Queraud-Lesaux, C. Goujet-Zalc, J. L. Thomas and B. Zalc (2001). "Sonic hedgehog-dependent emergence of oligodendrocytes in the telencephalon: evidence for a source of oligodendrocytes in the olfactory bulb that is independent of PDGFRalpha signaling." Development **128**(24): 4993-5004.

Srinivasan, R., N. Sailasuta, R. Hurd, S. Nelson and D. Pelletier (2005). "Evidence of elevated glutamate in multiple sclerosis using magnetic resonance spectroscopy at 3 T." Brain **128**(Pt 5): 1016-1025.

Steinman, L. and S. S. Zamvil (2006). "How to successfully apply animal studies in experimental allergic encephalomyelitis to research on multiple sclerosis." Ann Neurol **60**(1): 12-21.

Stoeckli, E. T., T. B. Kuhn, C. O. Duc, M. A. Ruegg and P. Sonderegger (1991). "The axonally secreted protein axonin-1 is a potent substratum for neurite growth." J Cell Biol **112**(3): 449-455.

Sun, T., N. P. Pringle, A. P. Hardy, W. D. Richardson and H. K. Smith (1998). "Pax6 influences the time and site of origin of glial precursors in the ventral neural tube." Mol Cell Neurosci **12**(4-5): 228-239.

Susuki, K., K. J. Chang, D. R. Zollinger, Y. Liu, Y. Ogawa, Y. Eshed-Eisenbach, M. T. Dours-Zimmermann, J. A. Oses-Prieto, A. L. Burlingame, C. I. Seidenbecher, D. R. Zimmermann, T. Oohashi, E. Peles and M. N. Rasband (2013). "Three mechanisms assemble central nervous system nodes of Ranvier." Neuron **78**(3): 469-482.

Susuki, K. and M. N. Rasband (2008). "Molecular mechanisms of node of Ranvier formation." Curr Opin Cell Biol **20**(6): 616-623.

Susuki, K. and M. N. Rasband (2008). "Spectrin and ankyrin-based cytoskeletons at polarized domains in myelinated axons." Exp Biol Med (Maywood) **233**(4): 394-400.

Svaren, J. (2014). "MicroRNA and transcriptional crosstalk in myelinating glia." Neurochem Int **77**: 50-57.

Taveggia, C., M. L. Feltri and L. Wrabetz (2010). "Signals to promote myelin formation and repair." Nat Rev Neurol **6**(5): 276-287.

Tekki-Kessaris, N., R. Woodruff, A. C. Hall, W. Gaffield, S. Kimura, C. D. Stiles, D. H. Rowitch and W. D. Richardson (2001). "Hedgehog-dependent oligodendrocyte lineage specification in the telencephalon." Development **128**(13): 2545-2554.

Thaxton, C., A. M. Pillai, A. L. Pribisko, J. L. Dupree and M. A. Bhat (2011). "Nodes of Ranvier act as barriers to restrict invasion of flanking paranodal domains in myelinated axons." Neuron **69**(2): 244-257.

Tisell, A., O. D. Leinhard, J. B. Warntjes, A. Aalto, O. Smedby, A. M. Landtblom and P. Lundberg (2013). "Increased concentrations of glutamate and glutamine in normal-appearing white matter of patients with multiple sclerosis and normal MR imaging brain scans." PLoS One **8**(4): e61817.

Tomassy, G. S., L. B. Dershowitz and P. Arlotta (2015). "Diversity Matters: A Revised Guide to Myelination." Trends Cell Biol.

Tomassy, G. S. and V. Fossati (2014). "How big is the myelinating orchestra? Cellular diversity within the oligodendrocyte lineage: facts and hypotheses." Front Cell Neurosci **8**: 201.

Traka, M., J. L. Dupree, B. Popko and D. Karagogeos (2002). "The neuronal adhesion protein TAG-1 is expressed by Schwann cells and oligodendrocytes and is localized to the juxtaparanodal region of myelinated fibers." J Neurosci **22**(8): 3016-3024.

Traka, M., L. Goutebroze, N. Denisenko, M. Bessa, A. Nifli, S. Havaki, Y. Iwakura, F. Fukamauchi, K. Watanabe, B. Soliven, J. A. Girault and D. Karagogeos (2003). "Association of TAG-1 with Caspr2 is essential for the molecular organization of juxtaparanodal regions of myelinated fibers." J Cell Biol **162**(6): 1161-1172.

Trapp, B. D., A. Nishiyama, D. Cheng and W. Macklin (1997). "Differentiation and death of premyelinating oligodendrocytes in developing rodent brain." J Cell Biol **137**(2): 459-468.

Trapp, B. D., J. Peterson, R. M. Ransohoff, R. Rudick, S. Mork and L. Bo (1998). "Axonal transection in the lesions of multiple sclerosis." N Engl J Med **338**(5): 278-285.

Tripathi, R. B., L. E. Clarke, V. Burzomato, N. Kessaris, P. N. Anderson, D. Attwell and W. D. Richardson (2011). "Dorsally and ventrally derived oligodendrocytes have similar electrical properties but myelinate preferred tracts." J Neurosci **31**(18): 6809-6819.

Tzimourakas, A., S. Giasemi, M. Mouratidou and D. Karagogeos (2007). "Structure-function analysis of protein complexes involved in the molecular architecture of juxtaparanodal regions of myelinated fibers." Biotechnol J **2**(5): 577-583.

Vallstedt, A., J. M. Klos and J. Ericson (2005). "Multiple dorsoventral origins of oligodendrocyte generation in the spinal cord and hindbrain." Neuron **45**(1): 55-67.

Varea, O., M. D. Martin-de-Saavedra, K. J. Kopeikina, B. Schurmann, H. J. Fleming, J. M. Fawcett-Patel, A. Bach, S. Jang, E. Peles, E. Kim and P. Penzes (2015). "Synaptic abnormalities and cytoplasmic glutamate receptor aggregates in contactin associated protein-like 2/Caspr2 knockout neurons." Proc Natl Acad Sci U S A **112**(19): 6176-6181.

Voyvodic, J. T. (1989). "Target size regulates calibre and myelination of sympathetic axons." Nature **342**(6248): 430-433.

Wake, H., P. R. Lee and R. D. Fields (2011). "Control of local protein synthesis and initial events in myelination by action potentials." Science **333**(6049): 1647-1651.

Waksman, B. H. and R. D. Adams (1962). "A histologic study of the early lesion in experimental allergic encephalomyelitis in the guinea pig and rabbit." Am J Pathol **41**: 135-162.

Wang, S. Z., J. Dulin, H. Wu, E. Hurlock, S. E. Lee, K. Jansson and Q. R. Lu (2006). "An oligodendrocyte-specific zinc-finger transcription regulator cooperates with Olig2 to promote oligodendrocyte differentiation." Development **133**(17): 3389-3398.

Wang, W., D. Karagogeos and D. L. Kilpatrick (2011). "The effects of Tag-1 on the maturation of mouse cerebellar granule neurons." Cell Mol Neurobiol **31**(3): 351-356.

Warf, B. C., J. Fok-Seang and R. H. Miller (1991). "Evidence for the ventral origin of oligodendrocyte precursors in the rat spinal cord." J Neurosci **11**(8): 2477-2488.

Watanabe, I., J. Zhu, J. J. Sutachan, A. Gottschalk, E. Recio-Pinto and W. B. Thornhill (2007). "The glycosylation state of Kv1.2 potassium channels affects trafficking, gating, and simulated action potentials." Brain Res **1144**: 1-18.

Weiner, H. L. (2009). "The challenge of multiple sclerosis: how do we cure a chronic heterogeneous disease?" Ann Neurol **65**(3): 239-248.

Weinshenker, B. G., B. Bass, G. P. Rice, J. Noseworthy, W. Carriere, J. Baskerville and G. C. Ebers (1989). "The natural history of multiple sclerosis: a geographically based study. 2. Predictive value of the early clinical course." Brain **112 (Pt 6)**: 1419-1428.

Wolman, M. A., V. K. Sittaramane, J. J. Essner, H. J. Yost, A. Chandrasekhar and M. C. Halloran (2008). "Transient axonal glycoprotein-1 (TAG-1) and laminin-alpha1 regulate dynamic growth cone behaviors and initial axon direction in vivo." Neural Dev **3**: 6.

Wolswijk, G. (1998). "Chronic stage multiple sclerosis lesions contain a relatively quiescent population of oligodendrocyte precursor cells." J Neurosci **18**(2): 601-609.

Wolswijk, G. (1998). "Oligodendrocyte regeneration in the adult rodent CNS and the failure of this process in multiple sclerosis." Prog Brain Res **117**: 233-247.

Wolswijk, G. and R. Balesar (2003). "Changes in the expression and localization of the paranodal protein Caspr on axons in chronic multiple sclerosis." Brain **126**(Pt 7): 1638-1649.

Yasuda, T., T. Tsumita, Y. Nagai, E. Mitsuzawa and S. Ohtani (1975). "Experimental allergic encephalomyelitis (EAE) in mice. I. Induction of EAE with mouse spinal cord homogenate and myelin basic protein." Jpn J Exp Med **45**(5): 423-427.

Ye, F., Y. Chen, T. Hoang, R. L. Montgomery, X. H. Zhao, H. Bu, T. Hu, M. M. Taketo, J. H. van Es, H. Clevers, J. Hsieh, R. Bassel-Duby, E. N. Olson and Q. R. Lu (2009). "HDAC1 and HDAC2 regulate oligodendrocyte differentiation by disrupting the beta-catenin-TCF interaction." Nat Neurosci **12**(7): 829-838.

Yednock, T. A., C. Cannon, L. C. Fritz, F. Sanchez-Madrid, L. Steinman and N. Karin (1992). "Prevention of experimental autoimmune encephalomyelitis by antibodies against alpha 4 beta 1 integrin." Nature **356**(6364): 63-66.

Yeung, M. S., S. Zdunek, O. Bergmann, S. Bernard, M. Salehpour, K. Alkass, S. Perl, J. Tisdale, G. Possnert, L. Brundin, H. Druid and J. Frisen (2014). "Dynamics of oligodendrocyte generation and myelination in the human brain." Cell **159**(4): 766-774.

Young, K. M., K. Psachoulia, R. B. Tripathi, S. J. Dunn, L. Cossell, D. Attwell, K. Tohyama and W. D. Richardson (2013). "Oligodendrocyte dynamics in the healthy adult CNS: evidence for myelin remodeling." Neuron **77**(5): 873-885.

Yu, Y., Y. Chen, B. Kim, H. Wang, C. Zhao, X. He, L. Liu, W. Liu, L. M. Wu, M. Mao, J. R. Chan, J. Wu and Q. R. Lu (2013). "Olig2 targets chromatin remodelers to enhancers to initiate oligodendrocyte differentiation." Cell **152**(1-2): 248-261.

Zalc, B. and D. R. Colman (2000). "Origins of vertebrate success." Science **288**(5464): 271-272.

Zalc, B., D. Goujet and D. Colman (2008). "The origin of the myelination program in vertebrates." Curr Biol **18**(12): R511-512.

Zamvil, S. S. and L. Steinman (2003). "Diverse targets for intervention during inflammatory and neurodegenerative phases of multiple sclerosis." Neuron **38**(5): 685-688.

Zawadzka, M., L. E. Rivers, S. P. Fancy, C. Zhao, R. Tripathi, F. Jamen, K. Young, A. Goncharevich, H. Pohl, M. Rizzi, D. H. Rowitch, N. Kessaris, U. Suter, W. D. Richardson and R. J. Franklin (2010). "CNS-resident glial progenitor/stem cells produce Schwann cells as well as oligodendrocytes during repair of CNS demyelination." Cell Stem Cell **6**(6): 578-590.

Zhao, X., X. He, X. Han, Y. Yu, F. Ye, Y. Chen, T. Hoang, X. Xu, Q. S. Mi, M. Xin, F. Wang, B. Appel and Q. R. Lu (2010). "MicroRNA-mediated control of oligodendrocyte differentiation." Neuron **65**(5): 612-626.

Zhou, Q., G. Choi and D. J. Anderson (2001). "The bHLH transcription factor Olig2 promotes oligodendrocyte differentiation in collaboration with Nkx2.2." Neuron **31**(5): 791-807.

Zhu, Q., X. Zhao, K. Zheng, H. Li, H. Huang, Z. Zhang, T. Mastracci, M. Wegner, Y. Chen, L. Sussel and M. Qiu (2014). "Genetic evidence that Nkx2.2 and Pdgfra are major determinants of the timing of oligodendrocyte differentiation in the developing CNS." Development **141**(3): 548-555.

Zoupi, L., K. Markoullis, K. A. Kleopa and D. Karagogeos (2013). "Alterations of juxtaparanodal domains in two rodent models of CNS demyelination." Glia **61**(8): 1236-1249.

Zoupi, L., M. Savvaki and D. Karagogeos (2011). "Axons and myelinating glia: An intimate contact." IUBMB Life **63**(9): 730-735.

APPENDIX

Table 1. Primary antibodies used in the study

Antibody/Epitope	Source	Type	Directed against (species)	Working dilution	Application
TG2 (α-TAG-1)	Traka et al., 2002	Rabbit, polyclonal	Human, mouse, rat	1:2000	WB
α-TAG-1, clone 1c12	Developmental Studies Hybridoma Bank	Mouse, monoclonal	Human, rat	1:1000	IHC (HB)
α-CASPR2	Dr L. Goutebroze, Inserm UMR-S 839, Institut du Fer à Moulin, France	Rabbit, polyclonal	Human, mouse, rat	1:1000	WB
				1:100	IHC (HB)
				1:2000	IHC (MB)
α-CASPR	Dr L. Goutebroze	Rabbit, polyclonal	Human, mouse, rat	1:2000	WB
				1:500	IHC (HB)
				1:1000	IHC (MB)
α-CASPR	Dr E. Peles, Weizmann Institute of Science	Mouse, monoclonal	Human, mouse, rat	1:800	IHC (HB)
				1:1000	IHC (MB)

α-Kv1.1	Antibodies-online	Mouse, monoclonal		1:200	IHC (MB)
α-Kv1.2	Alomone Labs	Rabbit, polyclonal	Human, mouse, rat	1:800	WB
				1:100	IHC (HB)
α-MBP	Abcam	Mouse, monoclonal	Human, mouse, rat	1:2000	WB
				1:100	IHC (HB)
α-MBP	Serotec	Rat, monoclonal	Human, mouse, rat, rabbit	1:200	IHC (MB)
α-MOG	Dr S. Piddlesden, University of Cardiff, UK	Mouse, monoclonal		1:50	IHC (HB)
α-PLP (ab28488)	Abcam	Rabbit, polyclonal	Mouse, rat	1:1000	IHC (MB)
α-pN52	Sigma-Aldrich	Mouse, monoclonal		1:2000	WB
α-GAPDH	Santa Cruz Biotechnology Inc.	Mouse, monoclonal	Human, mouse, rat	1:3000	WB

α-IBA1	Wako Chemicals	Rabbit, polyclonal	Human, mouse, rat, rabbit	1:500	IHC (HB)
α-IBA1	Biocare Medical	Rabbit, polyclonal		1:500	IHC (MB)
α-RT97	Developmental Studies Hybridoma Bank	Mouse, monoclonal	Human, mouse, rat, chicken	1:1000	IHC (HB)
α-SMI32	Abcam	Mouse, monoclonal	Majority of mammalian species	1:300	IHC (HB)
α-NF200	Abcam	Chicken, polyclonal	Human, mouse, rat, chicken	1:15000	IHC (MB)
α-NeuN	Millipore	Mouse, monoclonal	Human, mouse, rat	1:500	IHC (MB)
α-APC (clone CC-1)	Calbiochem	Mouse, monoclonal	Human, mouse, rat	1:100	IHC (MB)
α-PDGFRa	Millipore	Rat, monoclonal	Mouse, rat	1:100	IHC (MB)

α-GFAP	Sigma	Mouse, monoclonal	Human, mouse, rat, pig	1:2000	IHC (MB)

WB: Western Blot; IHC: Immunohistochemistry; HB: Human Brain; MB: Mouse Brain

Table 2. Secondary antibodies and fluorescent-conjugated probes used in the study

Antibody/Epitope	Source	Working dilution	Application
α-rabbit IgG horseradish-conjugated	Jackson ImmunoResearch Laboratories	1:3000	WB
α-mouse IgG horseradish-conjugated	Jackson ImmunoResearch Laboratories	1:3000	WB
α-mouse IgG, biotinylated	Vector Laboratories	1:200	IHC
α-rabbit IgG, biotinylated	Vector Laboratories	1:200	IHC
α-mouse IgG-FITC	Jackson ImmunoResearch Laboratories	1:300	IHC
α-rabbit IgG-Texas Red	Jackson ImmunoResearch Laboratories	1:300	IHC
Streptavidin, FITC-conjugated	Dako, Agilent Technologies	1:800	IHC
Streptavidin, Texas Red-conjugated	Vector Laboratories	1:800	IHC
α-mouse IgG-Alexa Fluor® 488 or 555	Molecular Probes, Thermo Fisher Scientific	1:800	IHC
α-rabbit IgG-Cy3®	Jackson ImmunoResearch Laboratories	1:800	IHC
α-rat IgG- Alexa Fluor® 488 or 555	Molecular Probes, Thermo	1:800	IHC

	Fisher Scientific		
α-chicken IgG-FITC	Biotium	1:800	IHC

Table 3. Fluorescent-conjugated antibodies used in FACS

Antibody/Epitope	Source – Cat. No	Working dilution
α-CD4-APC (clone RM4-5)	BioLegend – 100516	1:200
α-CD8-PerCP (clone 53-67)	BioLegend – 100732	1:200
α-CD25-FITC (clone PC61)	BioLegend – 101907	1:200
α-FoxP3-PE	eBioscience (Affymetrix) – 12-5773	1:100
α-CD3-APC (clone 17A2)	BioLegend – 100236	1:200
α-CD19-PerCP (clone 6D5)	BioLegend – 115534	1:200
α-CD69-PE (clone H1.2F3)	BD Biosciences - 553237	1:200

Table 4. Clinico-pathological data of MS and control patients examined

Case	Age/ Sex	Cause of death	Disease Course/ duration	PMD (hours)	Type and number of tissue samples examined* and method in which used
MS58	51/F	Not known	SPMS/21	15	1 fixed block (1 CAL, 2 CILs); 1 unfixed block (1 CAL): IHC; RT-PCR
MS60	55/M	Aspiration pneumonia	SPMS/43	16	1 fixed block (1 CAL); 1 unfixed block (NAWM): IHC; WB
MS80	49/F	Aspiration pneumonia	SPMS/30	9	2 unfixed blocks (1 CAL; 1 CIL): RT-PCR; WB
MS88	54/F	Bronchopneumonia	SPMS/27	22	1 fixed block (NAWM); 3 unfixed blocks (NAWM, 1 CAL): IHC; RT-PCR; WB
MS100	46/M	Pneumonia	SPMS/8	7	2 unfixed blocks (2 CAL): RT-PCR
MS105	73/M	Pneumonia	SPMS/46	8	1 unfixed block (NAWM): RT-PCR; WB
MS111	92/M	Old age	PPMS/54	9	1 fixed block (NAWM): IHC

MS125	76/F	Not known	SPMS/30	13	2 fixed blocks (2 CALs); 2 unfixed blocks (NAWM): IHC; WB, RT-PCR
MS313	66/M	Gastrointestinal bleeding from ulcer	PPMS/29	16	2 unfixed block (NAWM, 1 CAL, 2 CIL): WB, RT-PCR
MS317	48/F	Aspiration Pneumonia	SPMS/29	21	1 unfixed block (NAWM): RT-PCR
C10	73/M	Cardiogenic shock	-	21	1 unfixed block (WM): RT-PCR
C16	92/M	cardiac failure/old age		13	1 unfixed block: IHC
C22	69/F	Lung cancer	-	33	1 fixed block; 2 unfixed blocks (WM): IHC; RT-PCR; WB
C25	35/M	Tongue Carcinoma	-	22	1 unfixed block WM: RT-PCR
C26	78/F	Myeloid leukaemia	-	33	1 fixed block; 1 unfixed block WM: RT-PCR; WB
C28	60/F	Ovarian cancer	-	13	1 fixed block; 1 unfixed block WM: IHC; RT-PCR
C36	68/M	Cor pulmonale, heart	-	30	2 fixed blocks: IHC

		failure			
C41	54/M	Lung cancer	-	20	1 unfixed block WM: RT-PCR
C51	68/M	Ischemic heart disease	-	24	1 unfixed block WM: RT-PCR; WB

MI: Myocardial Infarction; SPMS: Secondary Progressive Multiple Sclerosis; PPMS: Primary Progressive Multiple Sclerosis; PMD: Post-mortem Delay, NAWM: Normal Appearing White Matter; WM: White Matter; CAL: Chronic Active Lesion; CIL: Chronic Inactive Lesion; IHC: Immunohistochemistry; RT-PCR: Real-time PCR; WB: Western Blotting;

*All samples were characterized by IBA1/MOG immunohistochemistry and LFB/Haematoxylin staining (Markoullis et al., 2012).

Table 5. Primers used for Real-Time PCR

Target Gene	**Primer sequence (5' to 3')**
Human Gapdh	Forward: GAAGGTGAAGGTCGGAGTC
	Reverse: GAAGATGGTGATGGGATTTC
Human Tag-1	Forward: CAGTGGGCACCGTTGTCA
	Reverse: TTGAGGAGCCAGCGGTAG
Human Cntnap-1 (Caspr)	Forward: CTTGTATTTAGGGCGTGTGA
	Reverse: CGCAATTAGATTCGGACAGT
Human Cntnap2 (Caspr2)	Forward: GAAGGTCGCATTGGACTCA
	Reverse: TGCTGTCCTTCTCCGTGC